공학박사 학위 논문

Multi-Scale Approaches for Progressive Failure Analysis using Continuum Damage Mechanics Model

연속체 손상역학을 이용한 점진적 파손해석의 멀티스케일 접근방법

2015년 8월

서울대학교 대학원
기계항공공학부
우주항공공학전공
박국진

Multi-Scale Approaches for Progressive Failure Analysis using Continuum Damage Mechanics Model

연속체 손상역학을 이용한
점진적 파손해석의 멀티스케일 접근방법

지도 교수 김 승 조

이 논문을 공학박사 학위논문으로 제출함
2015년 6월

서울대학교 대학원
기계항공공학부
우주항공공학전공

박 국 진

박국진의 공학박사 학위 논문을 인준함
2015년 6월

위원장 _____(Seal)
부위원장 _____(Seal)
위 원 _____(Seal)
위 원 _____(Seal)
위 원 _____(Seal)

Abstract

In this paper, predictions of failure strength of carbon-fiber laminate composites are attempted using an improved continuum damage mechanics (CDM) model with emphasis on the material nonlinearity of the fiber, shear stiffness reductions, the damage contribution of matrix cracks in adjacent layers and the multi-scale approaches for PFA due to constituent material characteristic and fiber defects.

The Weibull parameter to establish a CDM model was extended to five parameters to satisfy multi-scale compatibility and inter-lamina effects. These five Weibull parameters, which serve as coefficients of a damage evolution function, were investigated using a statistical model of progressive tensile fiber failure in a composite laminate. The Newton-Raphson method was utilized to formulate a damage-estimation method via a progressive failure analysis (PFA) procedure. A continuum damage analysis based on the Matzenmiller-Lubliner-Taylor (MLT) model was revised to add the statistical characteristics of the material strength. The proposed CDM method was also used to solve laminate tension problems with various stacking sequences. The damage model, nonlinear shear model and nonlinear elastic model of fiber are implemented in IPSAP, which is a general structural analysis program developed at Seoul National University. An implicit integration procedure for the proposed material and degradation model also was developed. The Newton-Raphson method for equilibrium calculations was adopted in IPSAP.

Also, an improved continuum damage mechanics (CDM) model is proposed, which takes micro-scale phenomena into account. It

includes degradation due to the damage initiation and development, overloading on fibers in the neighbor of a broken fiber. Two-parameter Weibull distribution which is obtained through Kolmogorov-Smirnov test is used to find an approximate model of single fiber's strength distribution. A three-dimensional representative volume element model-based multi-scale approach is presented for applying degradation mechanism due to fiber defects. The present model reveals that composite failure which is controlled by defected fiber breakage and their clustering determines the post failure behavior after initial failure occurs. Macro-scale degradation factor for CDM is derived from the results.

Developed models for PFA were used to solve open-hole tension and compression problems about IM7/8552, AS8552 and CP150NS/K.015 materials. The results have been shown accurately predict the failure strength of the laminates under room temperature dry, cold temperature dry and elevated temperature wet condition.

Keyword : Progressive Failure Analysis, Continuum Damage Mechanics, Weibull distribution, Micro Mechanics of Failure, Multi-scale Analysis, Laminate Composite

Student Number : 2009-20679

Table of Contents

LIST OF FIGURES

LIST OF FIGURES

Chapter 1. Introduction

1.1. History of Progressive Failure Analysis

Carbon fiber-reinforced polymer plays an important role in fabricating light-weight structure in aerospace, military vehicles and in many other areas due to their high stiffness and high strength-to-weight ratio. However, it costs relatively much amount of expense and effort when one tries to obtain their mechanical properties empirically. For this reason, it is important to predict their mechanical properties accurately but also cheaply using computational approaches. But damage progression in composite materials and structures is in general very complicated because it involves various causes of failure mechanisms, like matrix cracking, fiber breakage, delamination, fiber-matrix debonding and so on. A progressive failure analysis (PFA) is a useful way to predict the mechanical behavior of composites. A common and practical approach to model damage is adopting the material property degradation methods (MPDM) in the analysis [1-3]. Ochoa and Reddy [4] presented an excellent discussion on the PFA methods. Their models were generally categorized into the following two groups: a ply-discounting material degradation approach [5-7] and a continuum damage mechanics (CDM) approach using internal state variables. The CDM approach is to

incorporate the statistical nature of the material into constitutive relationships, as proposed by Matzenmiller [8], to describe the accumulation of damage in composite materials.

The presently suggested method is based on the use of the Weibull function [9] which describes the distribution of the strength. A number of studies have been undertaken on the characterization of fiber strength distributions using the two-parameter Weibull distribution, the bimodal Weibull distribution and so on[10-13]. However, the state variables of the Weibull distribution, specifically the damage variables, were not measurable [14]. Because fiber strength and distribution depend on fiber fracture behavior of nanostructure, it is necessary to know the relationships between fiber bundle and fiber strength distribution. In order to predict the damage and fiber reinforced composite failure under mechanical loads, several modelling approaches will be available to analyze the load transfer and sharing between fibers in composites [15-17]. Recently, Yokozeki [18] investigated the key structural factors from micromechanics that control the fiber tensile strength. Wang [19] simulated the damage evolution, interaction between different damage mechanisms, and the effect of the phase and interface properties in unidirectional fiber reinforced composites under tension load.

In terms of nonlinear plastic deformation of polymeric composite materials, various ways to describe visco-elasticity and visco-plasticity was attempted by researches. The nonlinear model suggested by Ramberg [20] had a simple nonlinear mathematical

form in which the parameters were determined by fitting the test results. An alternative fitting model was suggested by Mohseni Shakib [21], who assumed a shear stress–strain relationship as linear at low strain values and a fourth–order polynomial at high strain values. The nonlinearity of the shear modulus was described by showing the nonlinear shear response as a combination of the elastic and plastic response [22–24]. Papanicolaou [25] analyzed nonlinear viscoelasticity in the transverse direction of a unidirectional composite using Schapery's model [26, 27] and the power law of viscoelastic compliance.

Polymeric matrix fiber reinforced composite materials have been modeled by means of macro–mechanical or micromechanical approaches. Sun [28, 29] developed a macro–mechanical approach to obtain transversely isotropic visco–plastic model to analyze the nonlinear deformation of polymeric composite materials. Kim and Oden [30] applied the ''unmixing–mixing'' method which was the micromechanical approach to account for visco–plastic behaviors, to the materials of type N using the modified Bodner–Partom model. Thereafter, the visco–plastic behavior of thermoplastic composite materials was predicted at elevated temperature and low strain rates by Kim and Cho [31].

1.2. Objectivities and Scope of the Thesis

In this paper, numerical continuum damage mechanics model will be developed and used to simulate the damage evolution of carbon fiber reinforced composites under tension and compression load.

First, nonlinear PFA is revised as iterative model by decoupling damage model from nonlinear material property. Nonlinear model of unidirectional composite is consists of viscosity, plasticity and damage model. In conventional approaches, those models should be considered at once but damage model is irreversible, then it is impossible to use nonlinear iterative procedure like Newton-Raphson method. Novel PFA procedure is proposed to overcome the weakness in usage of the procedure. New continuum damage mechanics model based on Weibull distribution without cumulated damage model like gradual selective stress degradation model in NASTRAN is developed. Novel damage model is based on Matzenmiler, Lubliner and Taylor's (MLT) model will be introduced but it uses stress vectors based failure criterion using intact fiber stress rather than strain vectors. Also, this algorithm uses non-cumulative damage method which gives robust solution independently of displacement increment or load increment.

Second, regression models for nonlinear material property are proposed. Predictions of the tensile strengths of carbon-fiber laminate composites are attempted using an improved CDM model with emphasis on the material nonlinearity of fiber, shear stiffness

reduction and the damage contribution of matrix cracks in adjacent layers. Constitutive equations of unidirectional composites are based on a regression model considering rational expressions to describe the shear stiffness precisely throughout the strain range. The CDM model will be revised to include the effect of matrix cracking of the adjacent layer.

Third, a way to determine degradation factor is proposed. A statistical approach is used to reveal the relationship between the meso-scale and macro-scale by determining damage variables using a generalized Weibull distribution. A Weibull location parameter is added to describe degradation induced by localized delamination. This value is investigated by means of cross-ply experimental results rather than inserting a cohesive-zone layer with interface properties and damage indicators which are associated with modes I~III. The revised CDM method will enable accurate predictions of the strength, with shell elements and without the use of cohesive zone layers. Because it is not necessary to determine additional material properties which come from the setting of a cohesive layer, this method can be used easily for any materials of which the ply-level properties and their distributions are known.

Fourth, a different way to set degradation factor using micro-scale PFA results which describes a statistical distribution of the fiber strength as caused by defects using fiber bundle model. Three-dimensional multi-fiber unit cells with random strength distribution will be simulated to provide degradation parameters based on

continuum damage mechanics. Statistical approaches like Kolmogorov-Smirnov test of Weibull distribution will be used to reveal the relationship between the micro- and macro-scale parameters. PFA procedure will be revised with the statistical distribution of tension strength caused by defect of fibers.

The PFA program is incorporated into IPSAP, which is a general structural analysis program developed in Seoul National University, and Newton-Raphson method is implemented in IPSAP to conduct the nonlinear computing process.

Chapter 2. Progressive Failure Analysis

2.1. Overview of Progressive Failure Analysis Procedure

Progressive Failure Analysis (PFA) is a one of major methodology that is applicable to laminated composite structures and focuses on implicit, quasi-static applications. Also, it is best way to describe damage of composite. In this chapter, PFA procedure and basic concept will be introduced.

There are numerous published failure theories about PFA. Especially, models for progressive failure of composite structures range from the fairly simple material property/stiffness degradation method (MPDM) like Sudden Degradation Method (SDM) and Ply-Discount Method (PDM) to much more sophisticated MPDM based on Continuum Damage Mechanics (CDM) and Fracture Mechanics (FM). Among them, CDM is most accurate way to predict failure strength. There are many way to determine failure using stress vector. In the PFA, MPDM methods are initiated by failure criteria, which is determine predict initial failure of material.

General procedure of PFA is described as following Figure 2.1. The idea of MPDM is that the damaged material post-initial failure behavior is modeled by reduced stiffness. But it does not mean that

nonlinear procedure is required describe the progressive failure. Even if the method includes degraded material to describe damage, stress/strain of next force/displacement step is obtained by static linear solver. Therefore, general stress/strain curve of each element is described as Figure 2.2. Unlike nonlinear iterative solver as Figure 2.3, even if the stiffness is degraded with damage variables, all of segments have zero y−intercept.

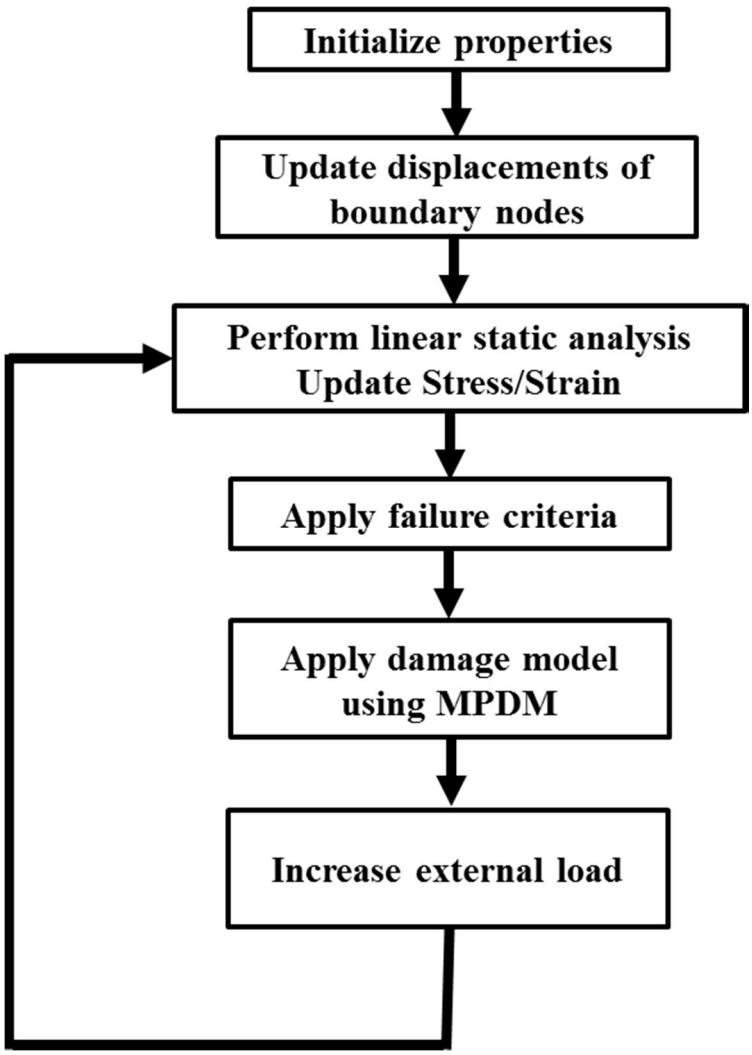

Figure 2.1 General PFA procedures using linear solver

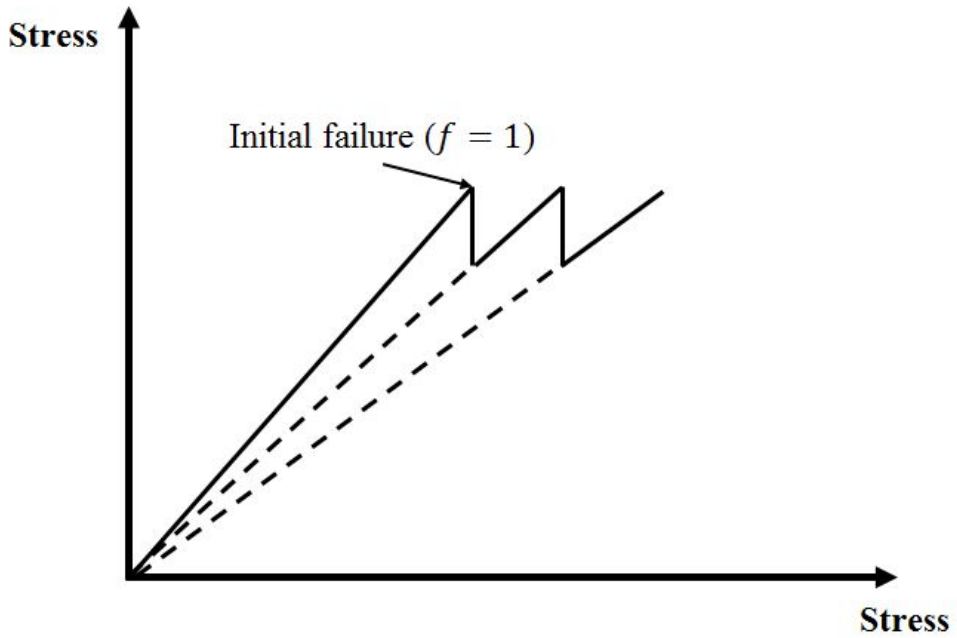

Figure 2.2 Typical pattern of stress/strain curve of element for PFA result using linear solver

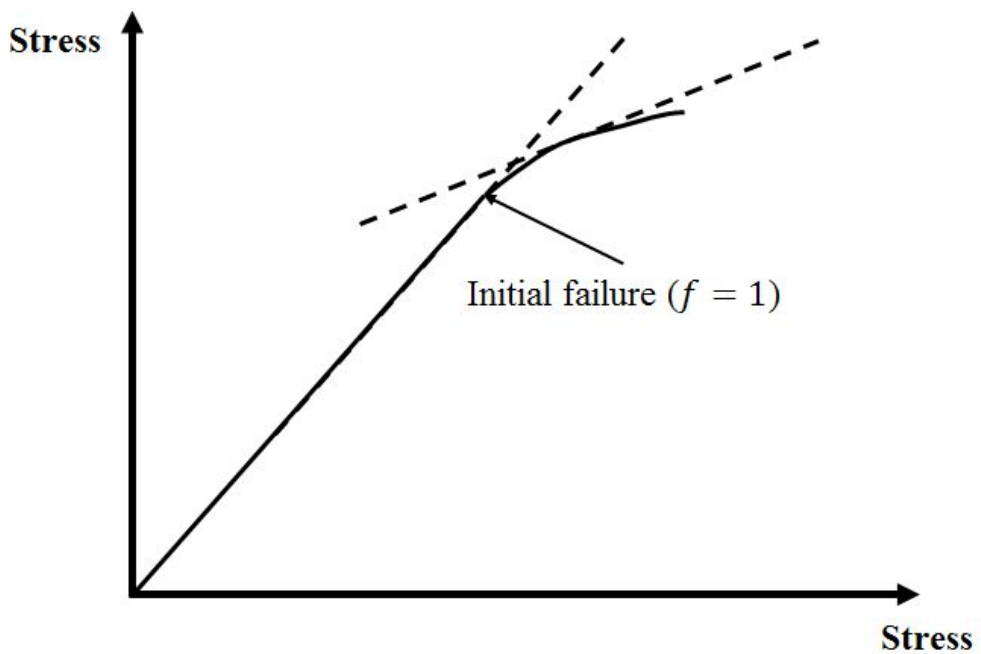

Figure 2.3 Typical pattern of stress/strain curve of element for PFA result using nonlinear solver

2.2 Macro-Scale Failure Criterion

There are numerous published papers about failure theories. Among them, some theories are effort to predict failure initiation by observing stress or strain immediately before failure. The earlier approaches such as maximum stress/strain, Hashin, Tsai-Hill and Tsai-Wu are still widely used. Those failure theories are based on macro-scale state variables. Because those criteria have second order term of stress components, it can be called as quadric form of failure. All of term will be described for shell elements.

Tsai-Wu model is one of model emphasis interaction between stress component, and it gives fairly good results of strength prediction for laminate composite. According to Tsai-Wu failure criterion, failure occurs under this following condition.

$$F_i\sigma_i + F_{ij}\sigma_i\sigma_j = \begin{cases} \geq 1\ failure \\ < 1\ no\ failure \end{cases} \tag{2.1}$$

Where F_i, F_{ij} are parameters from experiments. In this case, F_i indicate contribution for failure of i-th direction while F_{ij} means correlation factor coming from two different component of stress. σ_i means element-averaged stress which is obtained by finite element methods, and elements are defined in macro-scale domain. It is special form of generalized Hill yield criterion.

If we assume $F_{ij} = F_{ji}$, then there are no coupling term from shear stresses. Then it can be described as follow.

$$F_1\sigma_{11} + F_2\sigma_{22} + F_6\sigma_{12} + F_{12}\sigma_{11}\sigma_{22} + F_{11}\sigma_{11}^2 + F_{22}\sigma_{22}^2 = \begin{cases} \geq 1\ failure \\ < 1\ no\ failure \end{cases} \quad (2.2)$$

Where

$$F_1 = \frac{1}{X_t} - \frac{1}{X_c}$$

$$F_2 = \frac{1}{Y_t} - \frac{1}{Y_c}$$

$$F_{11} = \frac{1}{X_t X_c}$$

$$F_{22} = \frac{1}{Y_t Y_c}$$

$$F_6 = \frac{1}{S_{12}^2}$$

Where X_t is longitudinal tension failure strength, X_c is compressive failure strength, Y_t and Y_c are transverse direction' s failure strength. Only value of F_{12} cannot be determined with physical definition. The term can be obtained by experimental approaches. However, the criterion is not adequate to predict failure initiation of many case of fiber-reinforce composite material because it doesn' t define failure mode of fiber/matrix separately. There are several researches try separating predictions of fiber-dominated and matrix-dominate failure. Hashin' s and Puck' s failure criterions are representative advance failure criterion using macro-scale stress vector. Hashin 's failure criterion can be described as follow.

– Tensile fiber failure mode (σ_{11} >0)

$$\left(\frac{\sigma_{11}}{X_t}\right)^2 + \frac{\sigma_{12}^2+\sigma_{13}^2}{X_t^2} = \begin{cases} \geq 1\ failure \\ < 1\ no\ failure \end{cases} \quad (2.3)$$

– Compressive fiber failure mode (σ_{11} <0)

$$\left(\frac{\sigma_{11}}{X_c}\right)^2 = \begin{cases} \geq 1\ failure \\ < 1\ no\ failure \end{cases} \quad (2.4)$$

– Tensile matrix failure mode (σ_{22} >0)

$$\left(\frac{\sigma_{22}}{Y_t}\right)^2 + \frac{\sigma_{12}^2+\sigma_{13}^2}{S_{12}^2} = \begin{cases} \geq 1\ failure \\ < 1\ no\ failure \end{cases} \quad (2.5)$$

– Compressive matrix failure mode (σ_{22} <0)

$$\left[\left(\frac{Y_C}{2S_{23}}\right)^2 - 1\right]\left(\frac{\sigma_{22}}{Y_t}\right)^2 + \frac{\sigma_{22}^2}{4S_{23}^2} + \frac{\sigma_{23}^2}{S_{23}^2} + \frac{\sigma_{12}^2+\sigma_{13}^2}{S_{12}^2} = \begin{cases} \geq 1\ failure \\ < 1\ no\ failure \end{cases} \quad (2.6)$$

Where σ_{33} is negligible.

The stress vectors for above failure criterion can be obtained by classical laminated theory. Energy equation of lamina can be described as follow.

$$\mathrm{U} = \frac{1}{2}\int_A \int_{-h/2}^{h/2} \sigma^T \varepsilon \, dz dA = \frac{1}{2}\int_A [N \quad M]\begin{bmatrix}\varepsilon^0 \\ \kappa\end{bmatrix} + [V_1 \quad V_2]\begin{bmatrix}\gamma_1 \\ \gamma_2\end{bmatrix} dA \quad (2.7)$$

And stress/strain relationship can be described as follow

$$\sigma_{ij} = C_{ijkl}\varepsilon_{kl} \tag{2.8}$$

where $\mathbf{C}$ is stiffness matrix, ε_{kl} is strain vector and σ_{ij} is stress tensor. It can be reduced by assuming two dimensional orthotropic and expressed as following matrix form

$$\begin{bmatrix}\sigma_{11}\\ \sigma_{22}\\ \sigma_{12}\end{bmatrix} = \frac{1}{1-\nu_{21}\nu_{12}}\begin{bmatrix} E_1 & \nu_{21}E_1 & 0\\ \nu_{12}E_2 & E_2 & 0\\ 0 & 0 & G_{12}\end{bmatrix}\begin{bmatrix}\varepsilon_{11}\\ \varepsilon_{22}\\ \varepsilon_{12}\end{bmatrix} \tag{2.9}$$

Also, stress/moment resultant vector can be expressed as follow.

$$\begin{bmatrix}N\\ M\end{bmatrix} = \int_T \begin{bmatrix}\sigma\\ z\sigma\end{bmatrix} dz = \begin{bmatrix}A & B\\ B^T & D\end{bmatrix}\begin{bmatrix}\varepsilon^0\\ \kappa\end{bmatrix} \tag{2.9}$$

$$\mathrm{A} = \int_T Cdz$$

$$\mathrm{B} = \int_T zCdz$$

$$\mathrm{D} = \int_T z^2Cdz$$

After solving linear equation from formulating structural analysis, strain vector can be obtained by displacement vectors. For the small strain, two dimensional strain–displacement relations can be expressed as follow.

$$\varepsilon_{ij} = \frac{1}{2}\left(\frac{\partial u_i}{\partial x_j} + \frac{\partial u_j}{\partial x_i}\right) \tag{2.10}$$

Where u_i is displacement tensor.

However, there are only three stress component, therefore it is not enough to get compressive failure mode. The transverse shear stress and strain components can be obtained by the other terms.

In equation (2.6), because σ_{13} and σ_{23} doesn't exist in two-dimensional elements, those transverse shear stress and strain should be obtained by following equations

$$\gamma_{i3} = G_{ij}^{-1}\sigma_{j3} = D_{ij}\sigma_{j3} \tag{2.11}$$

Shear strain energy per unit area of reference plane as follow

$$\mathrm{U} = \int \sigma_{i3}\gamma_{i3}dz = \int \sigma_{i3}D_{ij}\sigma_{j3}dz \tag{2.12}$$

$$\mathrm{U} = \int \sigma_{i3}\gamma_{i3}dz = \frac{(\int \sigma_{i3}dz)(\bar{D}_{ij})(\int \sigma_{j3}dz)}{(\int dz)} = V^T\bar{D}V/T \tag{2.13}$$

Then it can be summarized as follow

$$V^T\bar{D}V = T\int \sigma_{i3}D_{ij}\sigma_{j3}dz \tag{2.14}$$

From equilibrium equations, transverse shear stress formula of i-th laminate plate can be obtained.

$$\sigma_{c3}^i = E_{cc}^i\kappa_{c,c}z^2 + c_c^i \tag{2.15}$$

Where

$$c_{c3}^{i} = -\sum_{j=1}^{i}\left(E_{cc}^{j} - E_{cc}^{j-1}\right)z_{j-1}^{2}\kappa_{c,c} \tag{2.16}$$

σ_{23} and σ_{13} can be obtained by equation (2.15)

Even if there is many other various form of failure criterion, only Hashin and Tsai-Wu failure criterion will be discussed in this research because there are several shortcomings to use as failure initiation of PFA.

2.3 Material Property Degradation Method

Most of MPDM is applied to degrade Young's moduli and shear modulus as follow

$$\begin{aligned} E_1 &= d_1 E_1^0 \\ E_2 &= d_2 E_2^0 \\ G_{12} &= d_6 G_{12}^0 \end{aligned} \tag{2.17}$$

Where E_1, E_2 and G_{12} are the effective material properties of the damaged ply while E_1^0, E_2^0 and G_{12}^0 are the material properties of the undamaged ply. Actually, the damage progression patterns agreed with experiment results, but the predicted ultimate strength is not because it is very sensitively affected by damage variables (or degradation factors). For this reason, the way to determine the damage variables becomes important part to set MPDM models.

The continuum damage mechanics (CDM) model was used to describe post-failures of laminated, unidirectional, orthotropic, polymeric composites, with the statistical distribution of the strength. The ply-discount method, the gradual selective stiffness degradation (GSSD) model and the Matzenmiller-Lubliner-Taylor (MLT) model are well-known damage models based on the use of a Weibull function to describe the statistical nature of internal defects and the ultimate strength of a fiber bundle within a composite lamina.

2.3.1 Ply-Discount Method

An elementary way to determine the degradation factor gives specific value of degradation factor. It is called as sudden degradation method. For examples, about Hashin failure criterion, if failure occurred about some failure mode, then degradation factor can be given as some value. Using the notation in Equation (2.17), sudden degradation of Hashin failure mode can be described. Following equation is one of the examples.

- Tensile fiber failure mode ($d_1 = 0.07$)
- Compressive fiber failure mode ($d_1 = 0.14$) (2.18)
- Tensile matrix failure mode ($d_2 = d_6 = 0.2$)
- Compressive matrix failure mode ($d_2 = d_6 = 0.4$)

The value of d_i is obtained by empirical ways. Therefore it should be surveyed again if another material is used. Mainly, constant degradation factor of 0.1 are widely used because of simplicity and convenience. It the value is too small, then computational problem can be occurred from zero value of stiffness matrix (9). The stiffness matrix is assembled in ply-level, then progressive failure can be appeared in laminate cases. In this case, this method can be called as ply-discount method. If internal load immediately before failure cannot be sustained by adjacent elements, then it will suddenly reach to ultimate strength. This model has advantage for unnotched problems which don't have stress concentrated position.

If stress is concentrated as Figure 2.4, typical pattern of stress/strain curve of open-hole tension test is described such as Figure 2.5 (a)~(c), when ply-discount method is applied. Actually, this method return non-continuous curve locally as Figure 5-(b) because each layer doesn't carry the load anymore after failure initiated as Figure 2.5-(a). Therefore, Failure mode can be distinguished in element scale. In macro-scale which have stress concentration, failed element's internal load will be redistributed to the other layer or adjacent element. It enables to coupon can endure a certain load after initial failure is occurred as Figure 2.5-(c). Because this method has very small residual stiffness, the difference of initial failure strength and ultimate strength is also small.

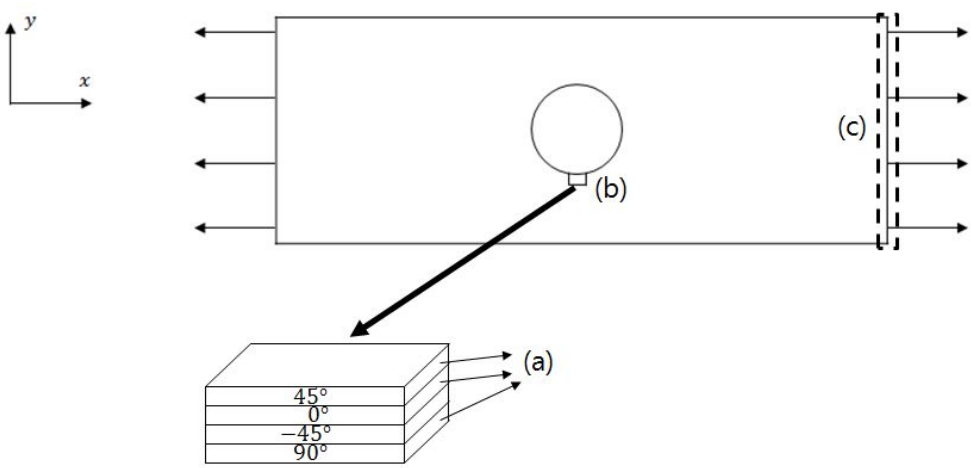

Figure 2.1 Typical description of stress concentrated problem. (a) ply (b) element (c) nodes receiving external loads.

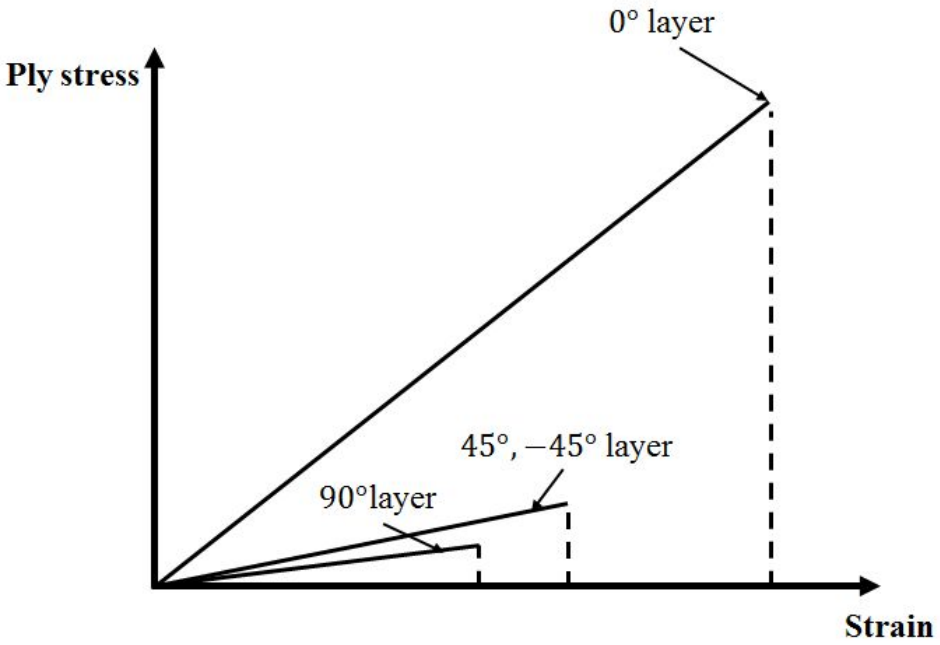

Figure 2.5-(a) Stress/strain curve of each plies (PDM)

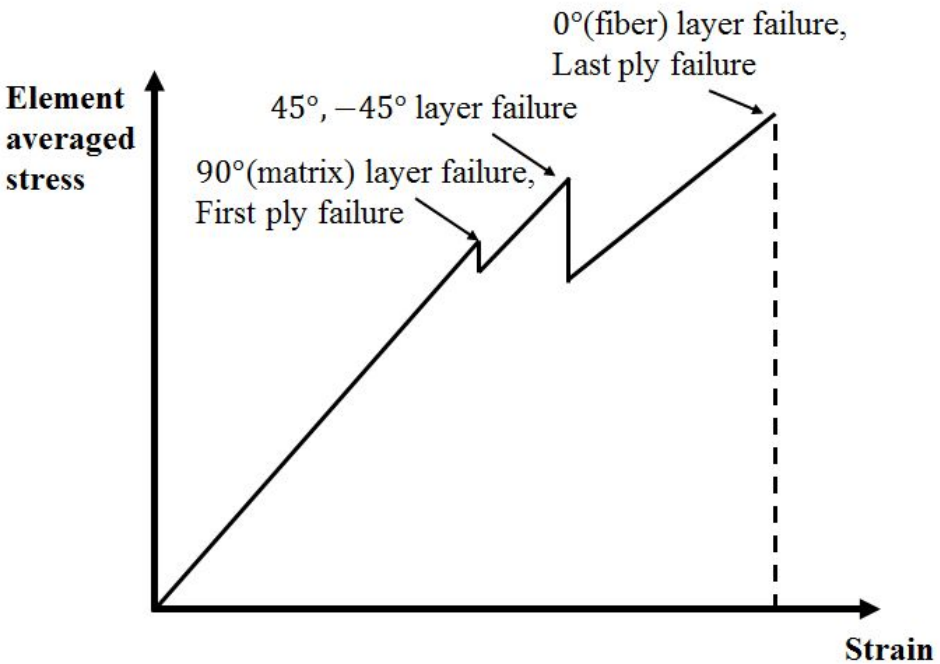

Figure 2.5-(b) Element averaged stress/strain curve (PDM)

2.3.2 Gradual Selective Stiffness Degradation Method

Gradual selective stiffness degradation (GSSD) method is scheme to study the failure of composite laminates under tensile and bending load. The stiffness of element is gradually degraded only to a level at which the failure criterion is no longer satisfied. GSSD method is one of most widely used form of continuum damage mechanics.

In the GSSD model, damage initiation and evolution are predicted by a stress tensor. Before a failure occurs, the degradation factor is determined through a unity value. If the failure index exceeds unity, an additional degradation factor is then determined via the following equation.

$$d_{I,GSSD}^{1} = 0,\ d_{I,GSSD}^{n+1} = d_{I,GSSD}^{n} + \left(1 - \mathrm{e}^{1-F_I(\sigma)}\right)\ if\ F_I(\sigma) > 1 \qquad (2.19)$$

$$I = \{1t, 1c, 2t, 2c\}$$

The damage variable $d_{I,GSSD}^{n}$ is cumulated damage variable by failure criterion. $F_I(\sigma)$ is failure criterion from the nominal stress tensor of I−th failure mode. The stress vector σ is in−plane stress vector obtained in previous section. If Tsai−Wu failure criterion is used, every mode of failure is shared while it is separated when Hashin failure criterion is used.

GSSD method returns relatively larger failure strain comparing to PDM method because it has larger residual internal force after initial failure. It makes a difference of ultimate strength in open−

hole cases which have stress concentration.

Figure 2.6 describes the typical pattern of GSSD method. If local element reaches at unit failure index from each failure criterion, then degradation factor in Equation (2.19) is updated until the factor reached at minimum boundary value which has typically 0.01. This method has a merit defining nonlinear shear that has high nonlinearity coming from damage, viscosity and plasticity. As Figure 2.6-(a), each element has potential to endure certain load until degradation factor reaches 0.01. It affects to ply-level averaged stress and therefore it becomes soft curve contrary to the result from PDM method. As a result of residual internal load of failed elements, laminate failure strength become higher. In macro-scale, predicted failure strength also higher than PDM's result.

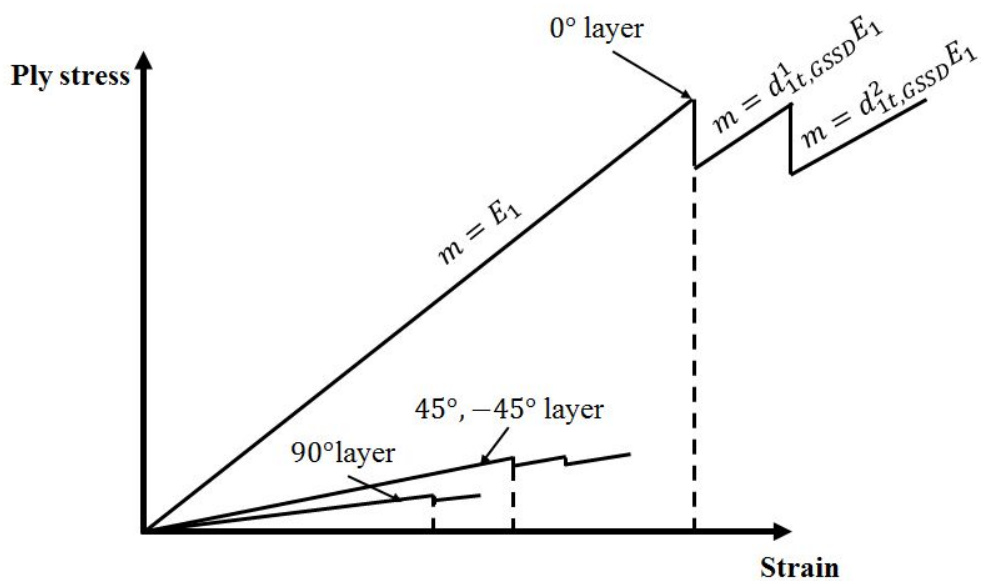

Figure 6-(a) Stress/strain curve of each plies (GSSD)

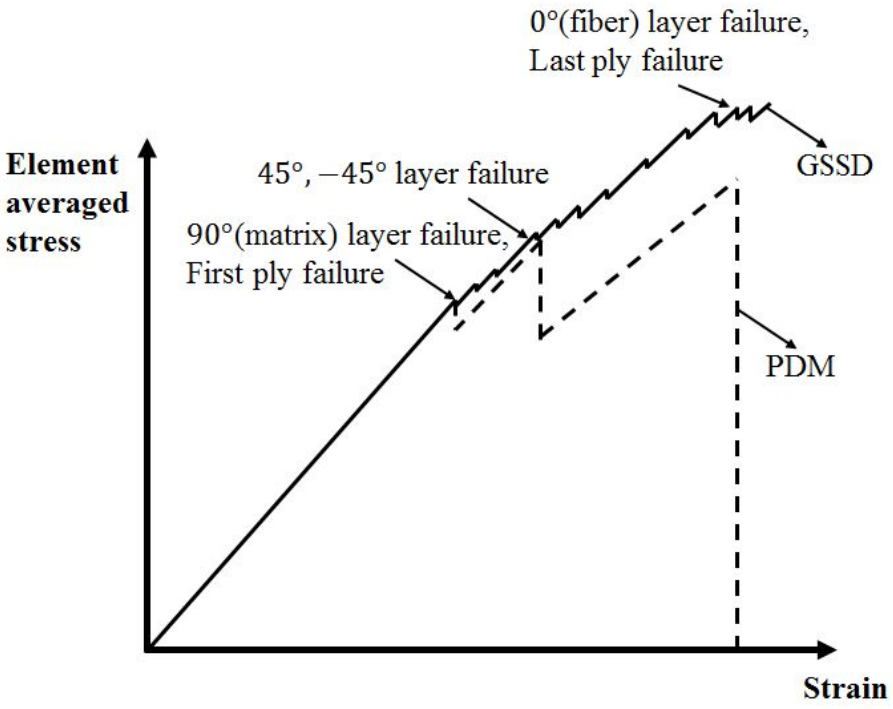

Figure 2.6-(b) Element averaged stress/strain curve (GSSD)

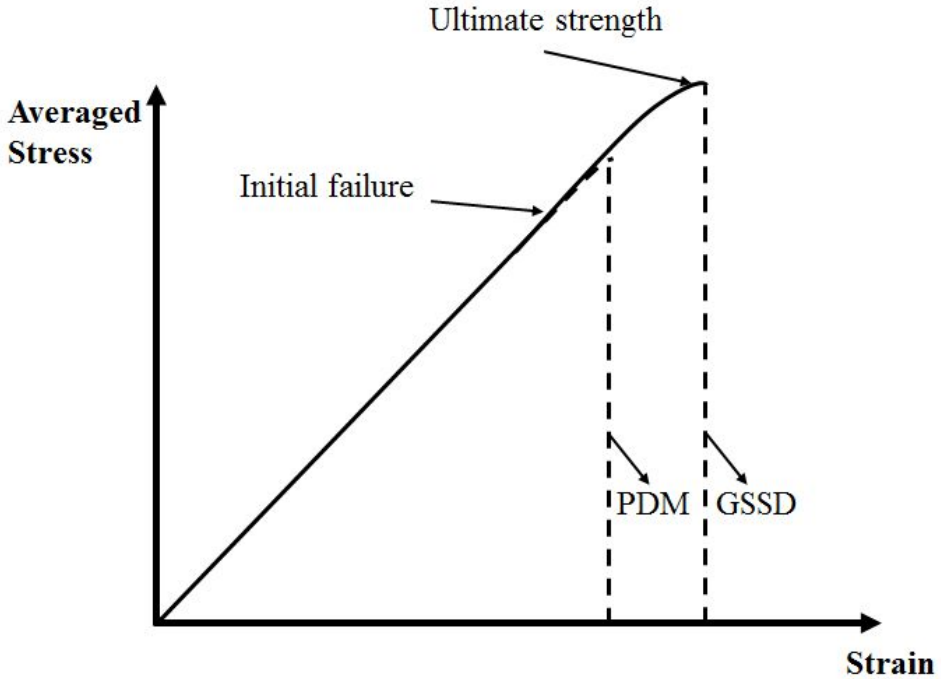

Figure 2.6-(c) Averaged stress/strain curve (GSSD/PDM)

2.3.3 Matzenmiller, Lubliner, Taylor (MLT) Method

Both of GSSD and PD methods have several shortcomings. It has discontinuous points of a function whenever failure index reaches unity. It is influenced by load increment steps. Also, non-linear iterative procedure cannot be applied in the PFA procedure because of degraded stiffness definition. Because the cumulative function is just numerical setting to maintain internal load of failed elements, there are no reliability.

On the other hands, the degradation factor of the MLT model is based on a strain tensor which describes a post-failure continuously. Accordingly, the failure criteria should be replaced by the loading criteria. The damage variable in the MLT model is described as shown below,

$$d_{I,MLT} = 1 - \mathrm{e}^{-\frac{1}{me}\left(\frac{\varepsilon_I}{\varepsilon_{f,I}}\right)^m} \qquad I = \{1t, 1c, 2t, 2c\} \tag{2.20}$$

where m is the stress-strain curve shape control factor, which is referred to as the m factor. $\varepsilon_{f,I}$ is the failure strain of the I-th component. Figures 2.7 and 2.8 show graphical representations of the damage variable of d_i; the stress vs strain which are normalized with respect to the strength X_t. And the nominal failure strain ε_f in the constitutive law for loading cases. For the MLT model, m values of 1,2,4,8,100 were used.

Figure 2.9 shows the typical force-displacement curves of the GSSD and MLT degradation models used for longitudinal tensile

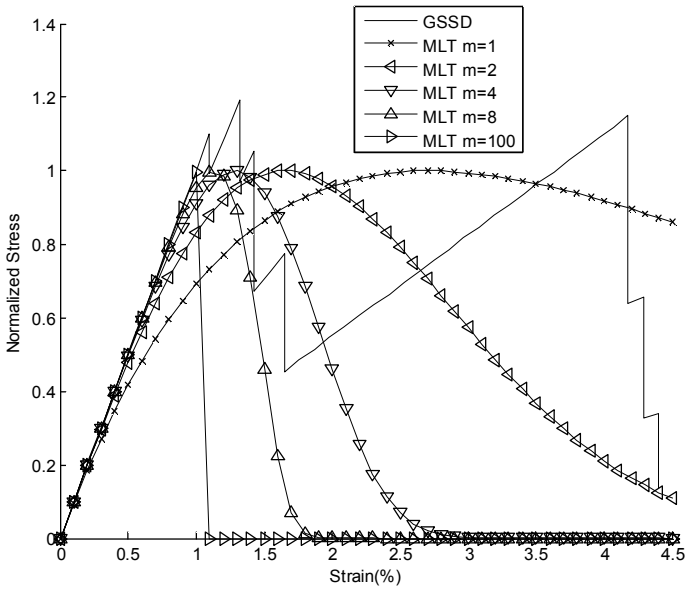

Figure 2.7 Normalized stress vs strain curve of the GSSD model and the MLT model with Weibull parameters when m=1, 2, 4, 8, and 100

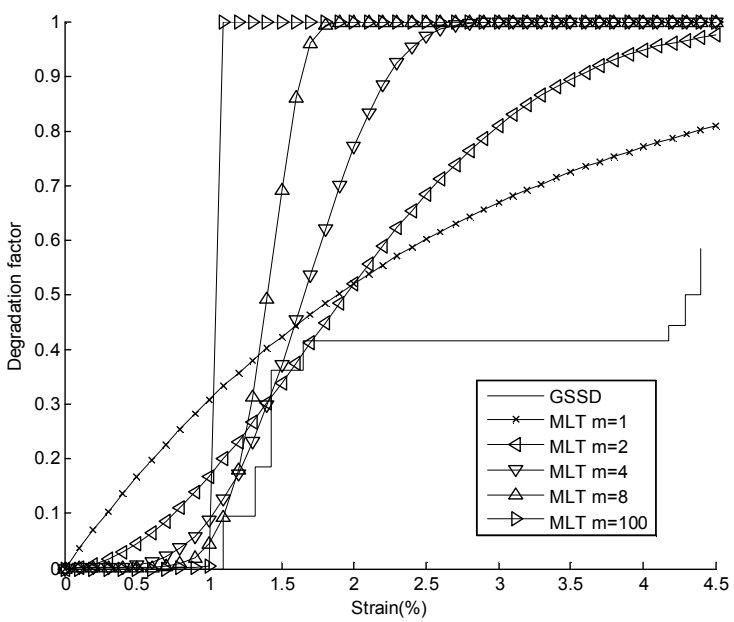

Figure 2.8 Degradation factors of the GSSD model and MLT model with the Weibull parameter when $\mathbf{m = 1, 2, 4, 8, 100}$

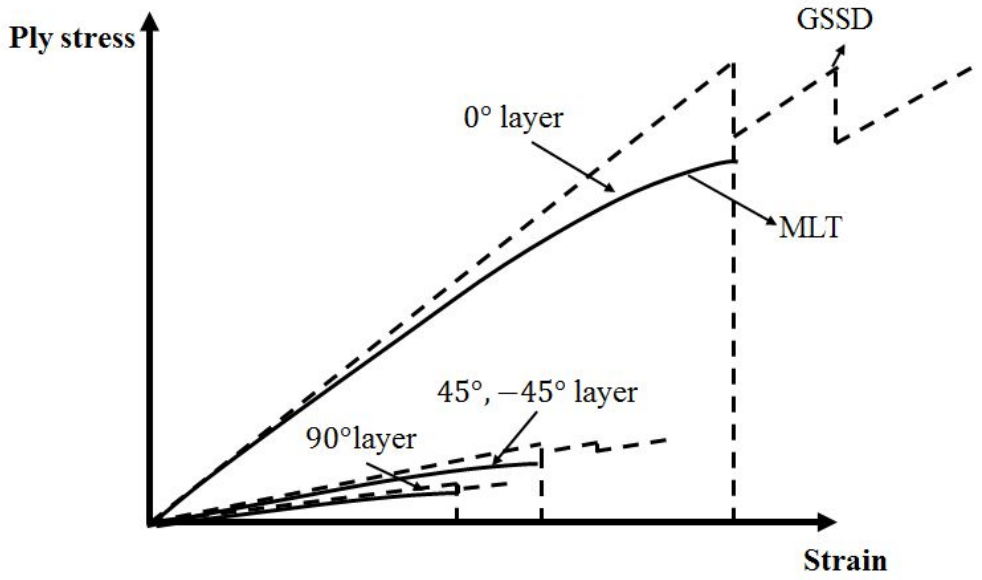

Figure 2.9-(a) Stress/strain curve of each plies (MLT)

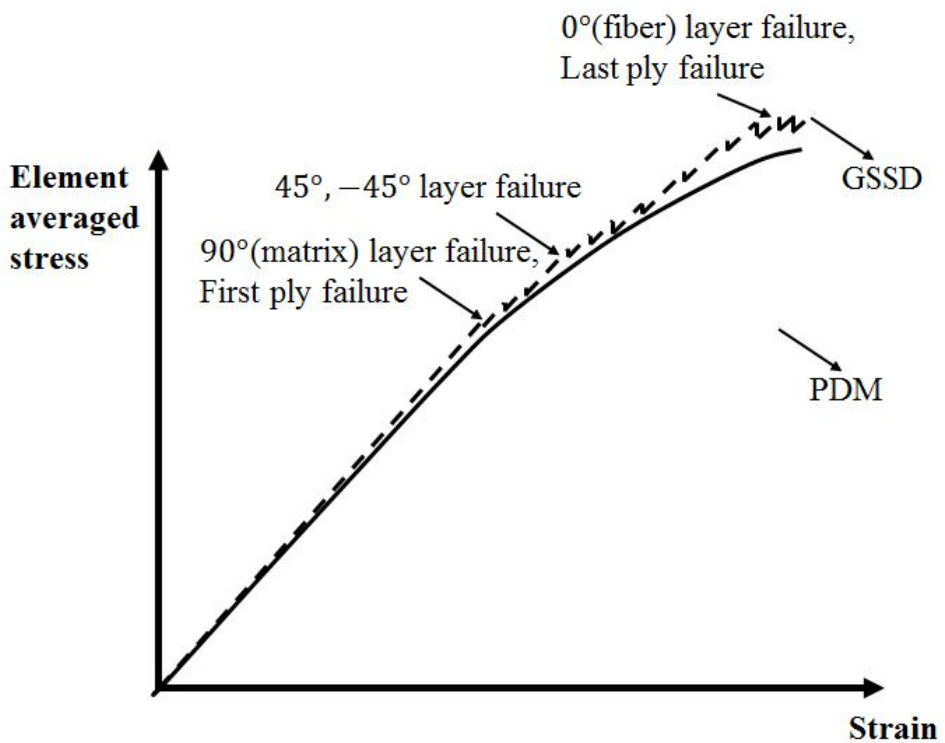

Figure 2.9-(b) Element averaged stress/strain curve (MLT)

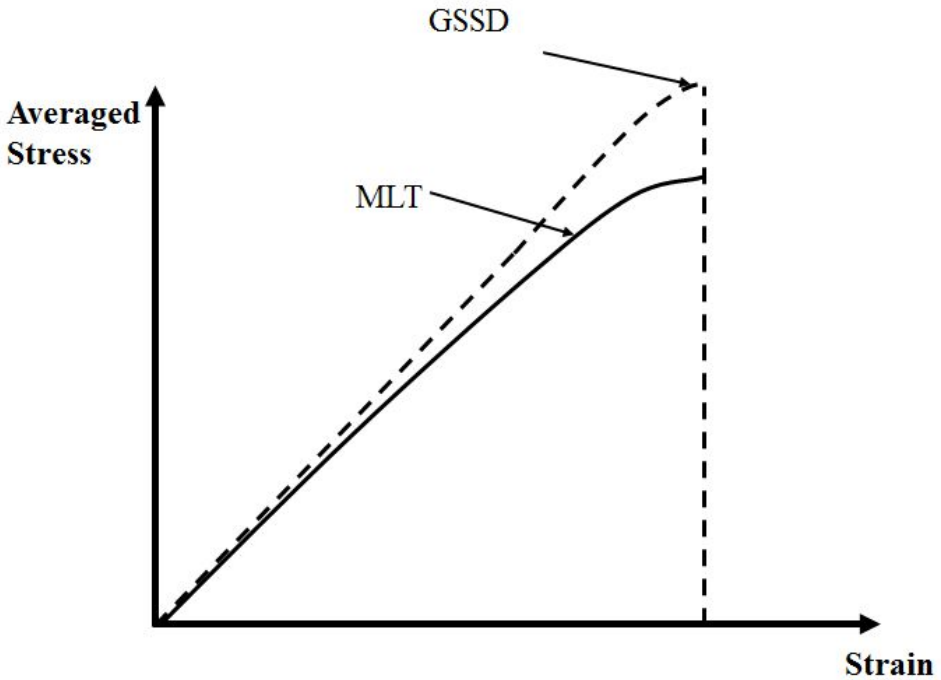

Figure 2.9-(c) Averaged stress/strain curve (MLT/GSSD)

testing. The stress was normalized by the longitudinal tensile strength X_t. The GSSD model has the advantage of preserving the initial modulus until failure initiation, and it shows good reproducibility of the lamina properties in the elastic range. However, because its degradation factor was added discretely, the stress-strain curve also has a jump discontinuity.

In the MLT model, in contrast, when increasing damage continuously up to the point of fracture, the stress-strain curve shows post-failure region. However, the selection of the m factor is difficult because it depends on the material used. The most significant limitation of the MLT constitutive model is the coupling of the initial modulus to the post deformation. As shown in Figure 2.8, the use of a high value for the m factor provided a linear elastic material with little post-failure stiffness, but it was difficult to

estimate the initial material accurately. On the other hand, a low value of the m factor caused a more ductile response, but the elastic modulus deviated grossly from the initial modulus prior to failure. This suggests that the m factor is required to have a relatively high value of m to preserve the modulus, but this causes an inaccurate post-failure response of the laminate.

MLT method is not only simple to apply for composite laminate but also intuitive way to determine degradation factors, all the more so because it uses only one additional parameter. It can be one off solution to consider fiber bundle model. Especially, because it uses strain vector to obtain the degradation factors instead of stress vector, it retains continuum state of damage until the degradation factor reaches minimum boundary value, namely it isn't the cumulative damage model but continuum damage model. It is reason why it can be combined with non-linear iterative solvers.

However, MLT model also have several problem. Because the model should make adjustment to balance between ductility and brittleness, it cannot realize fiber behavior exactly due to their characteristics. Even if fiber's strength which measured from tensile/compressive tests doesn't have ductility, the failure strength has distribution with 3~10% of coefficient of variables. Therefore, UD composite behavior should be considered as brittle material over stiffness degradation occurs continuously. In this sense, it has limitation to use for composite laminate because MLT method uses strain vector without failure criterion.

2.3.4 Noncumulative Stress based Continuum Damage Mechanics

In this research, noncumulative stress based continuum damage mechanics model will be suggested. A failure index is used to obtain not only the failure initiation point but also the continuum damage post failure. For this purpose, the internal state variable $d_{i,j}$ was determined by a failure criterion obtained by the effective stress after measuring the damage evolution. The damage evolution function of the MLT model can be revised as follows,

$$d_{I,1} = f\left(F_{1,I}, F_{2,I-1}, F_{2,I+1}\right) = 1 - e^{-A_2\left(F_{1,I}(\hat{\sigma}_{11},\hat{\sigma}_{12}) - h\left(F_{2,I-1},F_{2,I+1}\right)\right)^{A_1}}$$
$$: F_{1,I} > h,\ \mathrm{I} = 1\mathrm{t}, 1\mathrm{c}$$
$$d_{I,2} = f\left(F_{2,I}, F_{2,I-1}, F_{2,I+1}\right) = 1 - e^{-A_2\left(F_{2,I}(\hat{\sigma}_{22},\hat{\sigma}_{12}) - h\left(F_{2,I-1},F_{2,I+1}\right)\right)^{A_1}}$$
$$: F_{2,I} > h,\ \mathrm{I} = 2\mathrm{t}, 2\mathrm{c} \qquad (2.21)$$

where $d_{I,i}$ is the internal state variable of the I−th layer. $F_{i,I}$ is obtained from the effective stress, as calculated by intact fibers. A_1 and A_2 are the primary and secondary m factors of the Weibull distribution, and $\hbar$ is a location parameter of the strength distribution as obtained by the statistical conditions and the adjacent layer. Unlike the MLT model, it includes the effective shear stress $\bar{\sigma}_{12}$ as a variable. By initiating failure using failure criteria rather than with the loading criteria of MLT, the damage model can preserve the stiffness before it reaches the initiation

point. The Weibull parameters A_1, A_2 and $\hbar$ can be tuned via a longitudinal tensile test for $[0]$ (LT) and in an unnotched tensile test for $[0/90]_{2s}$ (UNT0), respectively.

The determination of $F_{i,I}$ and Weibull parameters are derived from test. It will be discussed at next section.

The relationship between the adjacent layers is described in Figure 2.10. The damage variables are correlated with adjacent layers. Some layer's damage variable are depends on adjacent layer's failure mode, especially matrix failure mode. The location parameter $\hbar$ is affected by the matrix failure mode, thus it can be expressed as function of own failure index and the adjacent layers.

Fiber direction failure index depends on $\bar{\sigma}_{11}$, $\bar{\sigma}_{12}$ of the layer while matrix dominated failure index is obtained by $\bar{\sigma}_{22}$, $\bar{\sigma}_{12}$. The stress tensor $\bar{\sigma}_{ij}$ is intact fiber' s stress. In Figure 2.11, the relation of intact fiber area's averaged stress $\hat{\sigma}_{ij}$ and total area-averaged stress tensor σ_{ij}. In here, Hatched area of fiber is failed fiber while white fiber is not failed yet. If matrix stiffness of fiber direction is negligible, damaged and intact area can be defined as follow

$$\hat{\sigma}_{11} = \frac{A_{intact}+A_{damaged}}{A_{intact}}\sigma_{11} \qquad (2.22\text{-a})$$

Above relationship is formed by the other direction also. From equation (2.21) and (2.22-a),

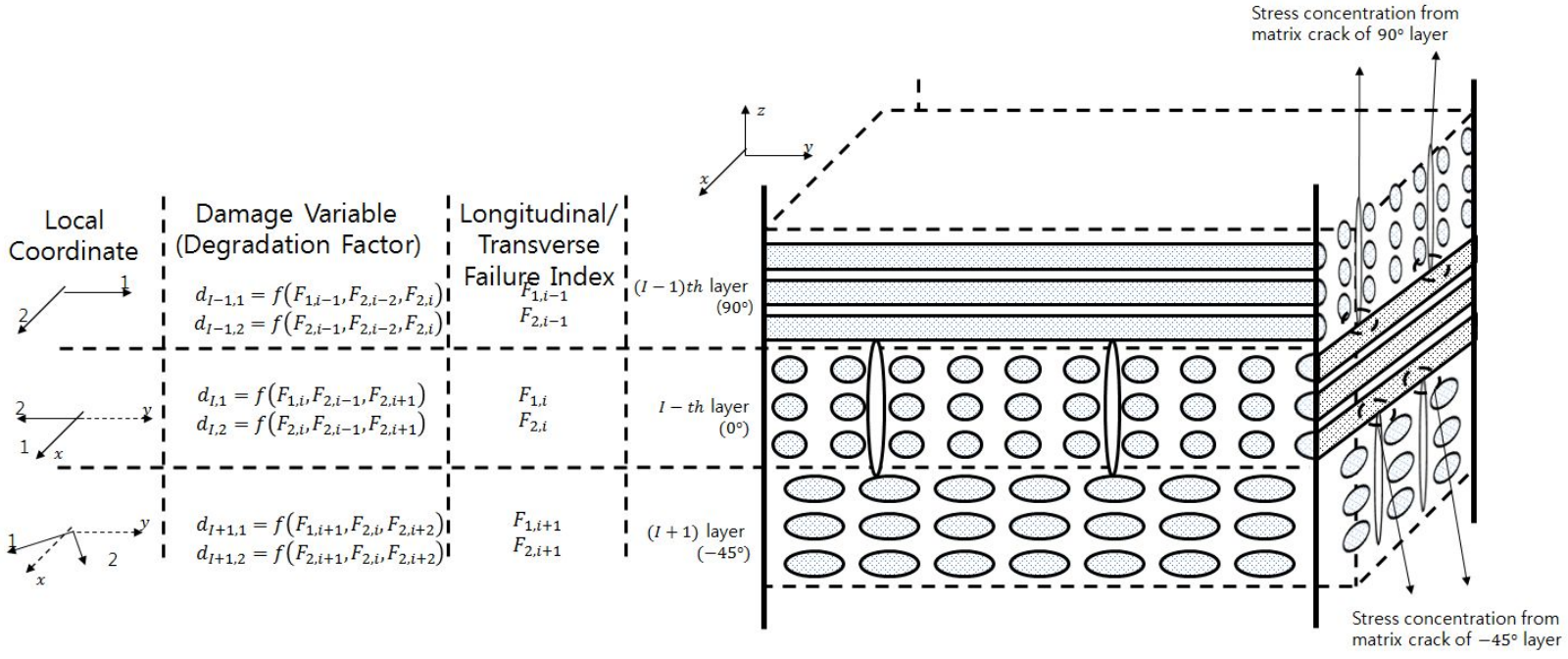

Figure 2.10 Damage variable functions from adjacent layers in a laminate composite

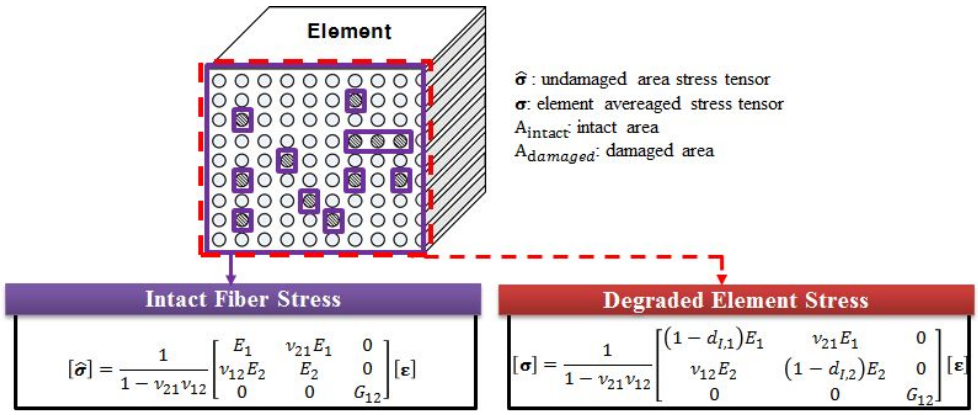

Figure 2.11 Intact fiber's stiffness matrix and degraded element-averaged stiffness matrix

$$d_{I,1} = \frac{A_{intact}}{A_{intact}+A_{damaged}} \qquad (2.22-b)$$

Therefore, the damage variables can be obtained by counting the number of failed and intact fibers. The failure index of equation (2.21) is defined as function of intact fiber's stress.

– Intact fiber' s tensile failure mode ($\hat{\sigma}_{11} > 0$)

$$\left(\frac{\hat{\sigma}_{11}}{X_t}\right)^2 + \frac{\hat{\sigma}_{12}^2+\hat{\sigma}_{13}^2}{X_t^2} = \begin{cases} \geq 1\ failure \\ < 1\ no\ failure \end{cases} \qquad (2.23)$$

– Intact fiber' s Compressive failure mode ($\hat{\sigma}_{11} < 0$)

$$\left(\frac{\hat{\sigma}_{11}}{X_c}\right)^2 = \begin{cases} \geq 1\ failure \\ < 1\ no\ failure \end{cases} \qquad (2.24)$$

– Intact matrix’ s Tensile failure mode (σ_{22} >0)

$$\left(\frac{\hat{\sigma}_{22}}{Y_t}\right)^2 + \frac{\hat{\sigma}_{12}^2+\hat{\sigma}_{13}^2}{S_{12}^2} = \begin{cases} \geq 1\, failure \\ < 1\, no\, failure \end{cases} \tag{2.25}$$

– Intact matrix’ s Compressive failure mode (σ_{22} <0)

$$\left[\left(\frac{Y_c}{2S_{23}}\right)^2 - 1\right]\left(\frac{\hat{\sigma}_{22}}{Y_t}\right)^2 + \frac{\hat{\sigma}_{22}^2}{4S_{23}^2} + \frac{\hat{\sigma}_{23}^2}{S_{23}^2} + \frac{\hat{\sigma}_{12}^2+\hat{\sigma}_{13}^2}{S_{12}^2} = \begin{cases} \geq 1\, failure \\ < 1\, no\, failure \end{cases} \tag{2.26}$$

Even if material properties are degraded, intact fiber is increasing until stiffness matrix approaching zero. Therefore, $\boldsymbol{d_{I,j}}$ of equation (2.21) will be increased continuously until it has unity value. How to determine the Weibull parameter $\boldsymbol{A_1}$, $\boldsymbol{A_2}$ and **h** will be discussed using two method. It can be derived from test results in the chapter 2.6 and from micro mechanics approaches in the chapter 3.

2.4 Separating Method for Nonlinearity and Damage of Composites

The damage models discussed previous chapters only consider damage from failure, which is independent to material nonlinearity like nonlinearity behaviour, plasticity and viscosity.

One of the reason why nonlinear material properties cannot be used with damage model is degradation models don't allow iterative procedure, namely PFA is defined as forward integral. Especially, cumulative damage model such as gradual selective stiffness degradation method is clearly limited to use non-linear iteration. To adapt implicit method such as Newton-Raphson method, stiffness matrix is defined as function of stress tensor. Then stiffness matrix in Figure 2.11 can be revised as follow

$$\boldsymbol{\sigma} = \left(\mathbf{D}(\mathbf{d}) \circ \mathbf{C}(\boldsymbol{\varepsilon})\right) : \boldsymbol{\varepsilon}; \quad \hat{\boldsymbol{\sigma}} = \mathbf{C}(\boldsymbol{\varepsilon}) : \boldsymbol{\varepsilon} \tag{2.27}$$

If it is obtained by the corresponding complementary energy density function, it also can be summerized as follow

$$\boldsymbol{\sigma} = \left(\mathbf{D}(\mathbf{d}) \circ \mathbf{C}(\hat{\boldsymbol{\sigma}})\right) : \boldsymbol{\varepsilon}; \quad \hat{\boldsymbol{\sigma}} = \mathbf{C}(\hat{\boldsymbol{\sigma}}) : \boldsymbol{\varepsilon} \tag{2.28}$$

Where the symbols shown in the boldface represent the tensor, ":" denotes the inner product of two tensors, and "∘" denotes the Hadamard product of two tensors. $\boldsymbol{\sigma}$ is the Cauchy nominal stress tensor and $\hat{\boldsymbol{\sigma}}$ is the effective stress tensor, respectively. $\mathbf{D}(\mathbf{w})$ is the stiffness degradation matrix, whereas $\mathbf{C}(\boldsymbol{\sigma})$ denotes the material nonlinearity model. $\mathbf{D}(\mathbf{w})$ and $\mathbf{C}(\boldsymbol{\sigma})$ are presented below for each layer.

$$\mathbf{D}(\boldsymbol{d}) = \frac{1}{D}\begin{bmatrix} (1-d_{I,1}) & (1-d_{I,1})(1-d_{I,2}) & 0 \\ (1-d_{I,1})(1-d_{I,2}) & (1-d_{I,2}) & 0 \\ 0 & 0 & 1 \end{bmatrix} \tag{2.29}$$

$$\mathbf{C}(\boldsymbol{\sigma}) = \begin{bmatrix} E_1(\sigma_{11}) & \nu_{21}(\sigma_{11})E_1(\sigma_{11}) & 0 \\ \nu_{12}E_2^0 & E_2^0 & 0 \\ 0 & 0 & G_{12}(\sigma_{12}) \end{bmatrix} \tag{2.30}$$

where $D = 1-(1-d_{I,1})(1-d_{I,2})\nu_{21}(\sigma_{11})\nu_{12}$; parameters w_1 and w_2 denote damage developed in the fiber and transverse direction. $E_1(\sigma_{11})$ is the nonlinear elastic modulus curve depending on the strain, and E_2^0 denotes the transverse modulus. In FEM procedure, $E_1(\sigma_{11})$ can be replaced by $E_1(\varepsilon_{11})$ having same function.

ν_{12} and ν_{21} are the Poisson's ratios of the unidirectional composite laminate. $G_{12}(\sigma_{12})$ is the shear deformation curve, which includes material nonlinearity which mainly stems from the elasto-plasticity. As expected, E_1 was virtually independent of the crack density parameter for those cracks parallel to the fiber. Some degree of thermodynamic potential was assumed to exist if the

deformation was nonlinear elastic under certain conditions[5]. Consequently, the following equality would remain valid not only for an intact material, but also for a degraded material. A similar assumption was established for which cracks orthogonal to the fiber did not affect Poisson's ratio ν_{12}. In other words, ν_{12} was independent of the normal strain ε_1. To preserve the following relationship, ν_{21} would be dependent on ε_1. This assumption was in good agreement with the result by Nuismer.

$$\frac{\nu_{12}}{E_1(\varepsilon_1)} = \frac{\nu_{21}(\varepsilon_1)}{E_2} \tag{2.31}$$

Unlike MLT Method, shear stress condition is directly obtained by shear stress-strain curve obtained from experiment. Therefore, shear direction degradation factor is not used. Instead of that, $G_{12}(\sigma_{12})$ is used to get nonlinear solution. When $\mathbf{D(d)}$ is unity matrix, it can be summarized as typical nonlinear form of stress/strain relationship.

Each ply has unique degradation factor, and thus it should be stored individually. The degradation factor is obtained by modified Weibull distribution. MLT method, which is used in CDM model in order to find Weibull distribution, defines the distribution using strain components as strain is continuously increased after initial failure occurs.

The damage variables and fiber material nonlinearity provided different values according to whether they received tensile or

compressive loads. The following variables were introduced.

$$d_1 = \begin{cases} d_{1t} \; if \;\; \hat{\sigma}_{11} \geq 0 \\ d_{1c} \; if \;\; \hat{\sigma}_{11} < 0, \end{cases} \quad d_2 = \begin{cases} d_{2t} \; if \; \hat{\sigma}_{22} \geq 0 \\ d_{2c} \; if \; \hat{\sigma}_{22} < 0 \end{cases} \tag{2.32}$$

$$E_1(\varepsilon_{11}) = \begin{cases} E_{1,t}(\varepsilon_{11}) \; if \;\; \hat{\sigma}_{11} \geq 0 \\ E_{1,c}(\varepsilon_{11}) \; if \;\; \hat{\sigma}_{22} < 0 \end{cases} \tag{2.33}$$

2.4.1 Nonlinear elasticity behaviours of Composite

In general, unidirectional composites exhibit nonlinear elasticity only in the fiber direction due to their fiber misalignment and kink band as Figure 2.12. It makes the stress–strain response of the carbon fibers non–Hookean. Such behavior has been observed for carbon fibers themselves, as well as for their unidirectional composites. The non–Hookean stress–strain response of the carbon fiber is reversible and is unaffected by loading and unloading cycles up to at least 40% of the tensile strength.

A regression model in the curve equation of the modulus E_1 is derived from experimental results of Curtis, as follows,

$$E_{1,t\,or\,c}(\varepsilon_{11}) = E_{1,0}\{1 \pm \gamma\} = E_{1,0}\left\{1 \pm a_1\left(\frac{\varepsilon_{11}}{\varepsilon_{f,t\,or\,c}}\right)^{a_2}\right\} \tag{2.34}$$

where $\varepsilon_{f,t\,or\,c}$ is the failure strain under a tensile or a compressive load. The slope coefficients a_1 and a_2 are defined based on experimental observations of the evolution of γ under increasing tensile or compressive loads. In fact, the value of γ was correlated

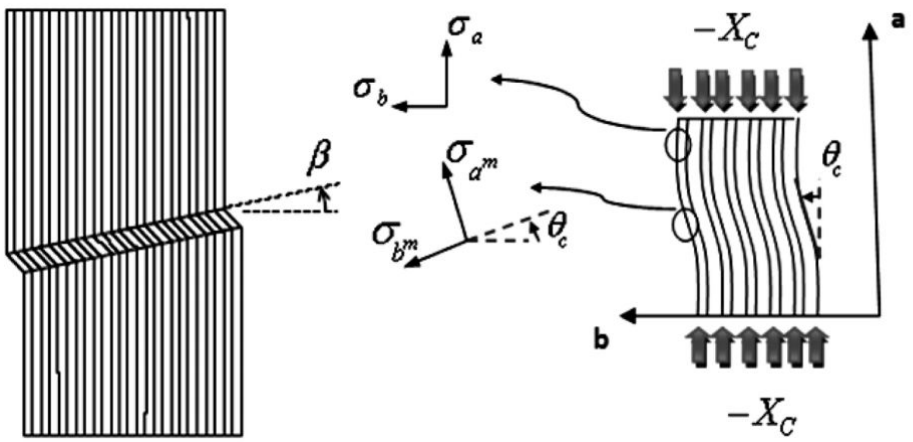

(a) (b)

Figure 2.12 (a) Kink band, (b) fiber misalignment

with the values of the mean modulus of the fibers and to characteristics of the fiber crystallite structures. For a standard axial test, the $E_1 - \varepsilon_{11}$ dependences were derived for the tensile strength by choosing alternative a_1 and a_2 values.

Generally, the longitudinal elastic modulus E_1 of each material was obtained by averaging the strain between 0.1%~0.3%. Therefore, the initial elastic modulus $E_{1,0}$ was obtained using an integrating equation (2.34).

$$E_{1,avg} = \frac{E_{1,0}}{0.3\%-0.1\%} \int_{0.1\%}^{0.3\%} \left\{1 + a_1 \left(\frac{\varepsilon_1}{\varepsilon_f}\right)^{a_2}\right\} d\varepsilon_1 \qquad (2.35)$$

Figure 2.13 is the example of setting of a_1 and a_2 values to make nonlinear elasticity behavior of fiber

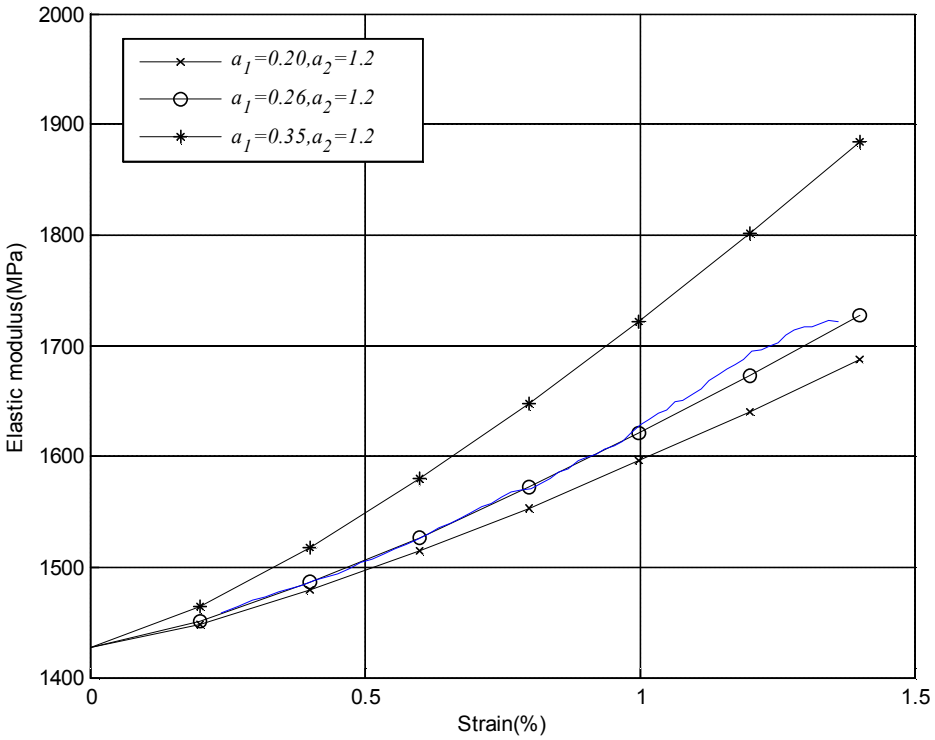

Figure 2.13 Stiffness hardening of the T700/M015 lamina

2.4.2 Shear Nonlinearities based on Damage and Elasto-Plasticity

The formation of a matrix crack influences the degradation of the material capacity to carry a load, measured as the elastic properties change as a function of the damage state. Stress in the fiber direction does not have a large effect on the shear viscoelasticity, and the effect of shear damage is lower with slow loading, as the level of stress reached is lower. Therefore, even if nonlinearity in the in-plane shear direction is a combination of nonlinear elasticity, viscosity and plasticity with significant strain hardening, a one-parameter analysis, which expresses nonlinearity functions using the shear stress (or strain), would be valuable. For this reason, in this work, only a one-parameter analysis was conducted to determine the nonlinear shear behavior. For quasi-static situations, a curve fitting equation was selected by examining the experimental results. This was obtained from shear modulus reduction data. The shear modulus was approximated as an analytic function of high order term of energy density function.

Before yielding occurs, the complementary energy density function can be expressed linear stress-strain relationship which is derived as follow.

$$W^* = \frac{1}{2}S_{11}\sigma_{11}^2 + S_{12}\sigma_{11}\sigma_{22} + \frac{1}{2}S_{22}\sigma_{22}^2 \tag{2.36}$$

After yielding, it can be expressed as follow.

$$W^* = \frac{1}{2}S_{11}\sigma_{11}^2 + S_{12}\sigma_{11}\sigma_{22} + \frac{1}{2}S_{22}\sigma_{22}^2 + \frac{1}{4}S_{661}\sigma_{12}^4 + \frac{1}{2}S_{662}\sigma_{12}^2 + S_{663} \quad (2.37)$$

First order term of σ_{12} is required to satisfy continuous of stress/strain curve at yield. The fourth order terms of shear stress are considered.

Where the strains are calculated as :

$$\varepsilon_{11} = \frac{\partial W^*}{\partial \sigma_{11}} = S_{11}\sigma_{11} + S_{12}\sigma_{22} \quad (2.38)$$

$$\varepsilon_{22} = \frac{\partial W^*}{\partial \sigma_{22}} = S_{12}\sigma_{11} + S_{22}\sigma_{22} \quad (2.39)$$

$$\gamma_{12} = \frac{\partial W^*}{\partial \sigma_{12}} = S_{661}\sigma_{12}^3 + S_{662}\sigma_{11} + S_{663} \quad (2.40)$$

Where S_{661} is fourth order compliance coefficient and S_{663} is zero order compliance. This relationship can be written in the matrix form as :

$$\begin{bmatrix}\varepsilon_{11}\\ \varepsilon_{22}\\ \gamma_{12}\end{bmatrix} = \begin{bmatrix}S_{11} & S_{12} & 0\\ S_{12} & S_{22} & 0\\ 0 & 0 & S_{662}\end{bmatrix}\begin{bmatrix}\sigma_{11}\\ \sigma_{22}\\ \sigma_{12}\end{bmatrix} + \begin{bmatrix}0 & 0 & 0\\ 0 & 0 & 0\\ 0 & 0 & S_{661}\sigma_{12}^2 + S_{663}\end{bmatrix}\begin{bmatrix}\sigma_{11}\\ \sigma_{22}\\ \sigma_{12}\end{bmatrix} \quad (2.41)$$

In this equation, shear nonlinearity from plasticity, damage and viscosity can be involved by choosing $S_{661} \sim S_{663}$. Stress/strain relationship can be integrated as follow.

$$\gamma_{12} = \begin{cases} \sigma_{12}/G_{12}^{0} & \tau_{12} \le S_y \\ S_{661}{\sigma_{12}}^3 + S_{662}\sigma_{12} + S_{663} & S_y < \tau_{12} < S_f \end{cases} \quad (2.42)$$

The parameter C_{661}~C_{663} is determined from an empirical way or experiment, as follows:

$$\begin{bmatrix} S_{661} \\ S_{662} \\ S_{663} \end{bmatrix} = \begin{bmatrix} {S_y}^3 & S_y & 1 \\ {S_f}^3 & S_f & 1 \\ 3{S_y}^2 & 1 & 0 \end{bmatrix}^{-1} \begin{bmatrix} \gamma_y \\ \gamma_f \\ 1/G_{12}^{0} \end{bmatrix} \quad (2.43)$$

In this equation, G_{12}^{0} is the elastic shear modulus, shear yield strength is S_y, failure strength is S_f, and the yield strain is γ_y. These material constants were acquired through a static tensile coupon test on $[45/-45]_s$. It contained elastic and plastic components. The effective shear modulus depending on the shear strain was valid only for a layer in this particular laminate. Figure 2.14 shows the tensile coupon analysis result using a curve-fitting function. The stress-strain curves were in good agreement with the experimental results.

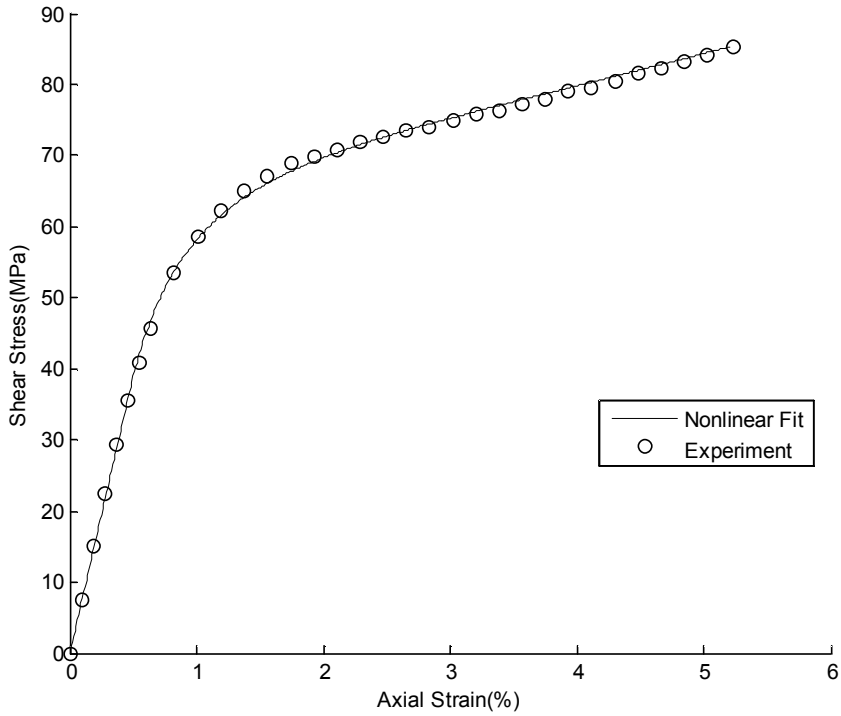

Figure 2.14. Stress-strain curve of the T700/M015 $[\mathbf{45}/-\mathbf{45}]_{4s}$ composite laminate

2.5 Nonlinear Progressive Failure Analysis Procedure

The present nonlinear inelastic equations were solved by an incremental approach. Driven by the displacement increment instead of the load increment, a discrete problem in the context of the Newton–Raphson method for a combined material nonlinearity and damage model was formulated. The updated stresses obtained by damage variables and a material model were stored at the end of the $(i+1)$th increment and then passed onto beginning of the next increment. The variable set used here was established as the following vector: $\left\{U_n^{(i)}, \boldsymbol{\varepsilon_n}, \boldsymbol{\sigma_n}, \bar{\boldsymbol{\sigma}}_{\boldsymbol{n}}, \boldsymbol{W_i}\right\}$. Figure 2.15 shows a flow chart of the present PFA. The PFA consisted of the determination of the load increment, the calculation of the effective stress, the detection of any material failures, the calculation of the damage variable, and Newton Raphson iteration.

Time was removed from the calculation. Instead of time, the initial displacement at every load–increment step was given, and this was updated by means of Newton Raphson iteration. Therefore, the strain rate effect was completely excluded from the present PFA procedure; therefore, the solving of the problem was restricted to a quasi–static analysis. The initial stiffness matrix was described as follow

$$K_0 = \int B^T C_0 B d\Omega. \tag{2.44}$$

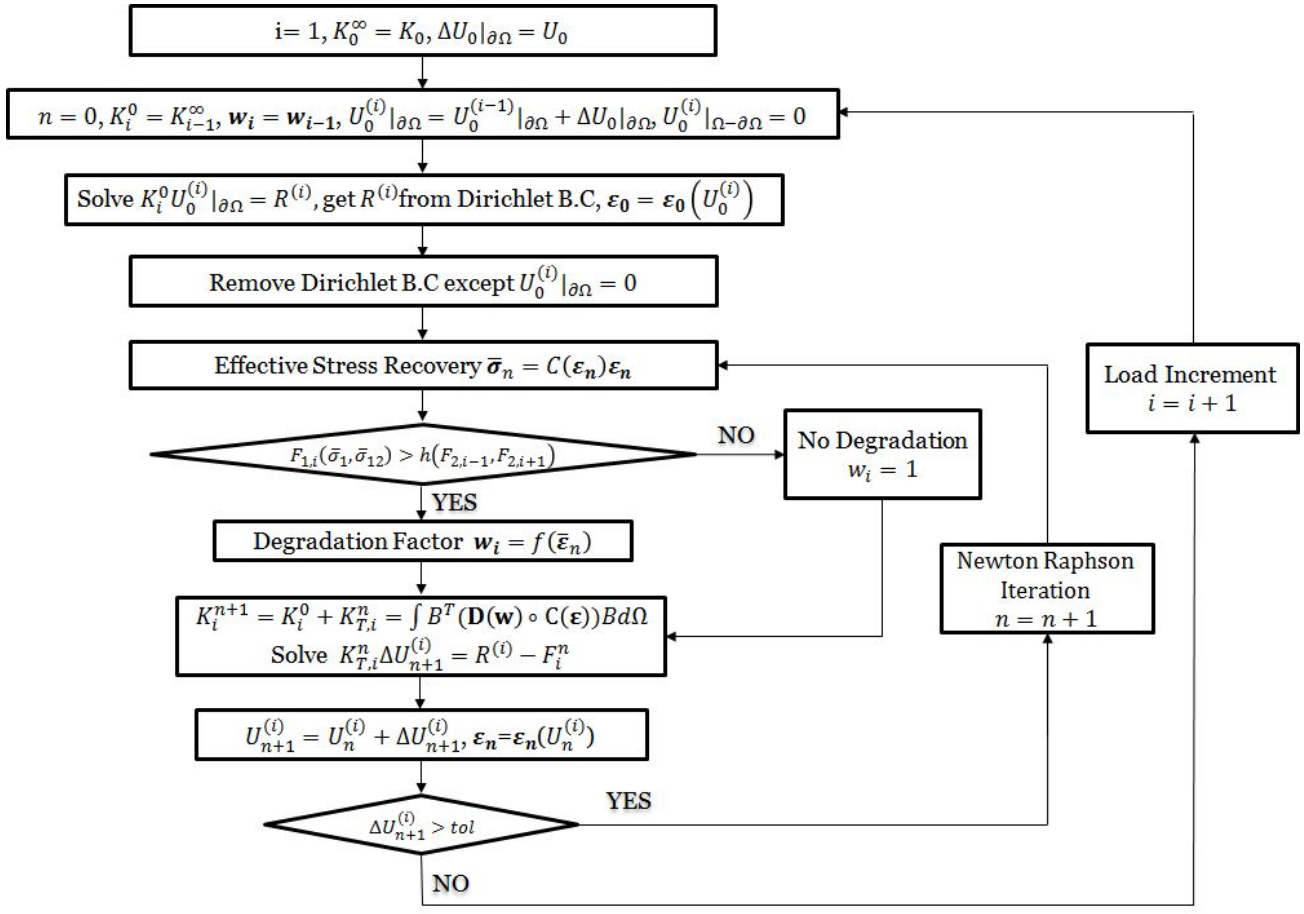

Figure 2.15 Flow chart of the progressive failure analysis with separation of nonlinear material property and degradation

In the present problem, Dirichlet boundary conditions were prescribed, and the target reaction force $R^{(i)}$ was estimated as shown below.

$$R^{(i)} = K_i^0 U_0^{(i)}|_{\partial\Omega} \tag{2.45}$$

In the stiffness matrix K_i^0 at the start of the $(\mathrm{i}+1)$th increment, degradation of the previous step was reflected. Within Newton–Raphson iteration, the Dirichlet boundary was not applied at fixed degrees of freedom. The present nonlinear equation was linearized using a tangent stiffness matrix considering degradation and material nonlinearity. It was solved iteratively until the final set of the state variables in the $(\mathrm{n}+1)$th iteration fulfilled the criterion below.

$$\left|\Delta U_{n+1}^{(i)}\right| \leq tol \tag{2.46}$$

Here, tol was set to 1×10^{-9}. The effective stress tensor $\bar{\boldsymbol{\sigma}}_{\boldsymbol{n}}$ was used for the damage model, while the stress tensor $\boldsymbol{\sigma}_{\boldsymbol{n}}$ was used to obtain the tangent stiffness matrix.

2.6 Weibull Parameters from Lamina Test Results

In this chapter, how to determine the Weibull parameter of novel CDM method will be discussed.

2.6.1 Determination of Weibull shape and scale parameter by meso and macro-scale correlation

The basic idea of the present degradation methods the classical fiber bundle model is presented here. For localized load sharing, the load of a broken fiber is equally redistributed over its nearest intact neighboring fibers. The construction of the fiber bundle models (FBMs) is based on several simplifying assumptions. FBMs consider the longitudinal component of the composite as a discrete set of parallel fibers of number organized on a regular lattice. Also, these several fibers are assumed to have perfectly brittle behavior with either linear or nonlinear elastic properties, until they break under a failure load. Finally, after a fiber failure occurs, the load should be shared by the intact fibers. FBM will be discussed in Chapter 3 in detail.

With a meso-scale finite element model considering the statistical distribution of the fiber strength, the degradation factors will be obtained. Figure 2.16 describes the relationships among the macro-, meso-scale models of a laminate composite. $\bar{\sigma}_{T,micro}$ is averaged stress at failure and $X_{T,meso}$ is meso-scale strength of each element. Because fiber defect exists, it can be assumed every

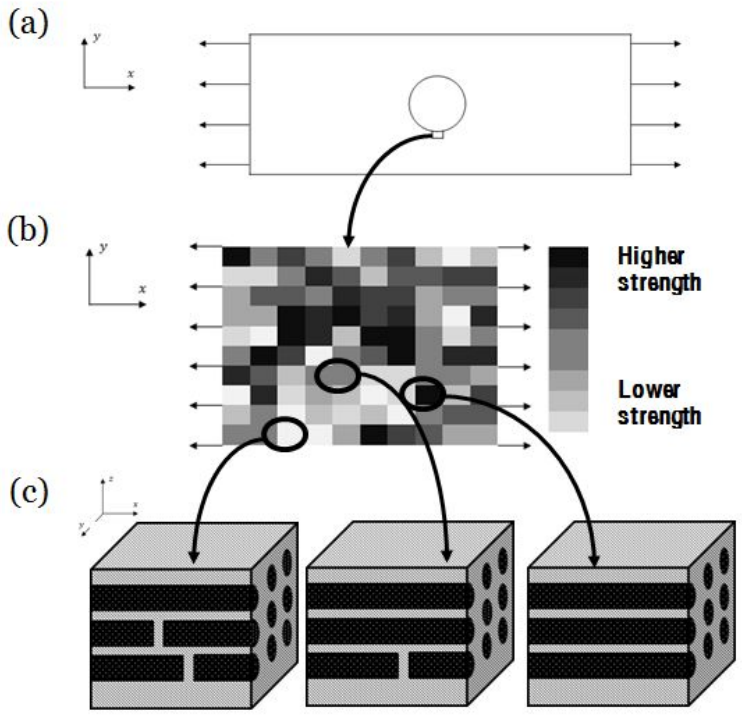

I. Average strength :

$$X_T = Constant$$

II. Damage variable(Continuum damage) :

$$w_{I,i} = \frac{n}{N} = 1 - f(F_{1,i}, F_{2,i-1}, F_{2,i+1})$$

n: number of intact fiber

N: number of total fiber

I. Average strength:

$\bar{X}_{T,meso}=X_T \quad (\bar{X}_{T,meso} = \frac{\sum X_{T,meso}}{N_{meso}})$

II. Damage variable(Ply-discount) :

$D_{I,i} = 1$ (intact)

$D_{I,i} = 0$ (failed)

III. Strength distribution:

$$g(X_{T,meso}, 0,0) = 1 - e^{-\left(\frac{X_{T,meso}-\sigma_0}{\lambda}\right)^k}$$

I. Longitudinal tensile strength of cell :

$$\bar{\sigma}_{T,micro} = X_{T,meso}$$

Figure 2.16 Description of the strength relationship between macro-scale, meso-scale and micro-scale models: (a) Strength assumption of the CDM model in macro-scale problems, (b) meso-scale heuristic degradation model using the ply-discount method, and (c) micro-scale multi-fiber unit-cell model

element in the meso-scale model have different strength value. A coupon test of the laminate to estimate the stiffness or strength can be considered as a macro-scale experiment. It describes an open-hole tensile test of a laminate with a stress concentration that exists near a hole.

When a macro-scale analysis is used, the strength of each layer will be determined by the relevant properties, in this case X_t, X_c, Y_t, Y_c and S_{12f}, which have the same value for every element. However, the degradation factor of each element is obtained from a statistical distribution of the fiber strength. We can derive the constants A_1 and A_2 from this. The strength of each fiber has a different stress threshold $X_{T,meso}$, which has an average of $\bar{X}_{T,meso}$ and unknown Weibull parameters on the meso-scale, as follows.

$$g(X_{T,meso}) = 1 - e^{-\left(\frac{X_{T,meso} - \min(X_{T,meso})}{\lambda}\right)^k} \tag{2.47}$$

Here, $X_{T,meso}$ is the meso-scale strength of each element, and $\min(X_{T,meso})$ is the failure strength of the weakest meso-scale element. Additionally, λ is the scale parameter, k is the shape parameter. Because the degradation factor is defined by the ratio of the intact area to the failed area of a fiber as referred previous chapter, the function f in equation (2.21) should have the same shape and scale parameters to function g when there are no adjacent layer, as follows,

$$f\left(X_{T,meso}/X_T, 0,0\right) = g\left(X_{T,meso}\right) \tag{2.48}$$

where f is the macro-level damage evolution function, and where the failure index is substituted for the meso-scale and macro-scale strength. Above equation is assumed in order to remove mesh size sensitivity on strength distribution. It means element-averaged strength distribution in macro-scale and meso-scale should be same.

$$f\left(X_{T,meso}/X_T, 0,0\right) = 1 - e^{-A_2\left(X_{T,meso}/X_T - h_{meso}\right)^{A_1}} \text{ if } X_{T,meso} \geq h_{meso} \tag{2.49}$$

On the other hand, g is the distribution of the meso-scale strength $X_{T,meso}$

$$g\left(X_{T,meso}\right) = 1 - e^{-\left(\frac{X_{T,meso} - \min(X_{T,meso})}{\lambda}\right)^k} \tag{2.50}$$

When the meso-scale strength $X_{T,meso}$ of elements is given randomly, $\min\left(X_{T,meso}\right)$ will not be zero if there are no initial defects in the fiber. Equation (2.50) is given below.

$$g\left(X_{T,meso}\right) = 1 - e^{-\frac{\bar{X}_{T,meso}{}^k}{\lambda^k}\left(\frac{X_{T,meso} - \min(X_{T,meso})}{\bar{X}_{T,meso}}\right)^k} = 1 - e^{-\frac{\bar{X}_{T,meso}{}^k}{\lambda^k}\left(F_1 - h_{0,meso}\right)^k}$$
$$= 1 - e^{-A_2\left(X_{T,meso}/\bar{X}_{T,meso} - h_{0,meso}\right)^{A_1}} = f\left(X_{T,meso}/X_T, 0,0\right) \tag{2.51}$$

Therefore, the meso- and macro-scale Weibull parameters can be

correlated as follows.

$$A_1 = k$$
$$A_2 = \frac{\bar{X}_{T,meso}{}^{k}}{\lambda^{k}} \tag{2.52}$$
$$\bar{X}_{T,meso} = X_T$$
$$h_{0,meso} = \frac{\min(X_{T,meso})}{\bar{X}_{T,meso}}$$

Note that $h_{0,meso}$ is defined on the meso-scale. All of the elements have the same strength on the macro-scale, while the elements on the meso-scale are assigned a random strength. The element average of the strength on the meso-scale is expressed as

$$\bar{X}_{T,meso} = X_T = \frac{\sum X_{T,meso}}{n_{meso}} = \lambda\Gamma(1 + 1/k) + \bar{X}_{T,meso} h_{0,meso} \tag{2.53}$$

where Γ is the Gamma function. Pairs of $(\lambda, k, h_{0,meso})$ determine the distribution. X_t should be considered as the strength of each element on the macro-scale. It is possible to assume $h_{0,meso} = 0$ because an initial defect exists in the fiber bundle. Then, λ will depend on k and X_t, as follows.

$$\lambda = \frac{X_T}{\Gamma(1+1/k)} \tag{2.54}$$

This is summarized below.

$$A_1 = k,\ A_2 = \frac{{X_T}^k}{\lambda^k} = \left(\Gamma(1+1/k)\right)^k \tag{2.55}$$

Macro-scale Weibull parameter can be analyzed by statistical analysis results in the meso-scale. In order to obtain proper degradation factors, meso-scale analysis was simulated under the condition of the ASTM D3039 0° tension test. Figure 2.17 is an example of the meso-scale FE model for which micro-level strength is generated randomly. It will clearly have another average strength, as they have different damage shapes according to the k value. Because the strength of each element $X_{T,meso}$ determined randomly, the meso-scale strength will have a different value every time. However, when increasing the number of iterations, it should converge to a certain value.

Meso-scale mesh domain should be provided to construct the meso-scale FE model. Because mesh density in the meso-scale model affects the distribution of $X_{T,meso}$, it should be chosen carefully. From the micro-scale standpoint, because defected fiber cannot carry any load, the loads should be shared with neighboring fibers. If the fiber bundle has only one live fiber, the element will not be able to carry any loads. Mainly, it will be redistributed to neighboring elements. However, if the fiber bundle has two fibers, it may carry certain loads even after defected fiber is completely broken. By increasing the number of fibers in the bundle, degraded stiffness will also be increased, as shown in Figure 2.18, especially when ply-discount method concept is used for the meso-scale

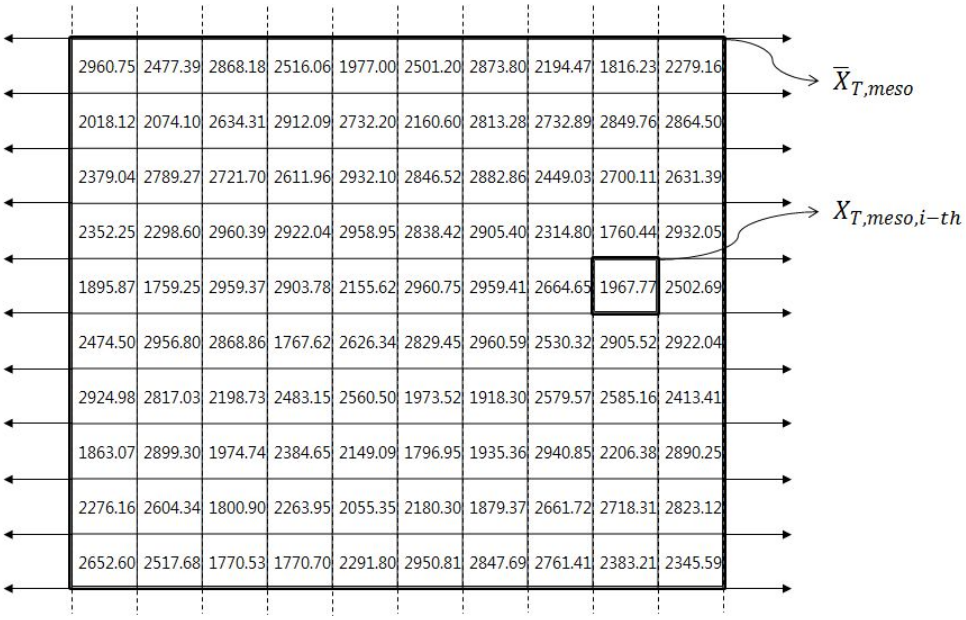

Figure 2.17 Example of a meso-scale FEM model with random $\boldsymbol{X_{T,meso}}$ values for IM7/8552

analysis. In Figure 2.18-(a), sum of the number of the defected fibers n_{defect} and that of the intact fibers n_{intact} equals to total number of fiber bundles n_f. $X_{T,micro}$ is the defected fiber strength and $\bar{X}_{T,micro}$ is the intact fiber strength in Figure 2.18-(b). Because the fiber diameter is fixed, the degradation ratio after initial failure of the micro-scale model depends on mesh size of the meso-scale model. From the typical fiber diameter and representative mesh size of the target example, it is possible to choose suitable size of mesh. Because of the numerical complexity, lower bound of the degraded stiffness should be established in advance. Residual stiffness after the ultimate strength is set to be 1% in this paper.

If the fiber diameter D_f is given, the meso- and micro-scale length can be related as follows.

$$L_{unit} = \sqrt{\frac{\pi\left(D_f^2/4\right)}{v_f}} \tag{2.56}$$

where L_{unit} is the length of one side of a square unit-cell. v_f is the fiber volume fraction. Then meso-scale element size can be obtained as follows.

$$L_{meso} = \sqrt{n_f} L_{unit} \tag{2.57}$$

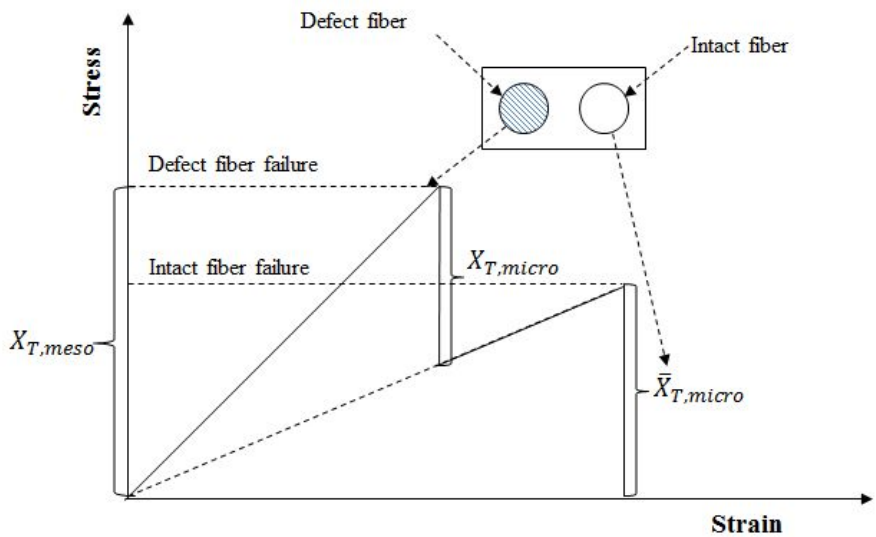

(a)

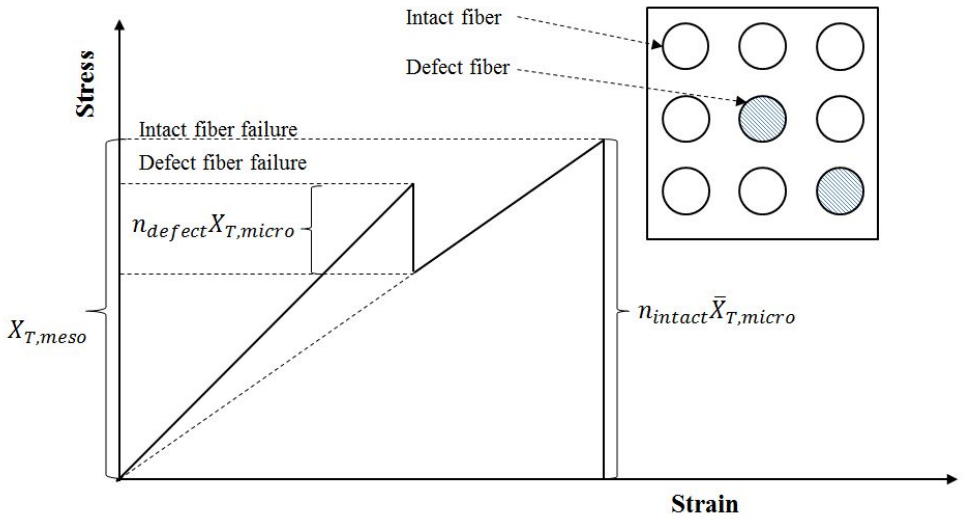

(b)

Figure 2.18 Concept of multi-cell model considering defect fiber when (a) 50% fiber defect model of2 strands (b) 22% fiber defect model of 9 strands

where L_{meso} is the meso-scale element size. n_f is the number of the fiber strands. If the meso-scale model size is equal to the macro-scale element size, it can be expressed as follows.

$$L_{macro} = \sqrt{n_{meso}} L_{meso} \tag{2.58}$$

where L_{macro} is the macro-scale element size, and n_{meso} is the number of elements. D_f, v_f are obtained by the experimental method. The number of the meso-scale elements can be obtained as follows.

$$n_{meso} = \frac{v_f}{\pi\left(D_f^2/4\right)}\left(\frac{L_{macro}}{\sqrt{n_f}}\right)^2 \tag{2.59}$$

For the square mesh domains, square root of n_{meso} can be chosen as the number of divisions. Figure 2.19 shows 512 results of the progressive failure analysis with k=1,2,3,4,5 using the meso-scale approach. Among these, when k was set to 10, it could predict the strength accurately within 3.16% of the coefficient of variation (C.V.). According to the experimental results of a carbon fiber composite performed by NCAMP, the longitudinal tension strength at room temperature has 4.43% of the C.V. for 18 counts. Figure 2.20 shows the results from an experiment and from a PFA analysis with randomly-generated strength.

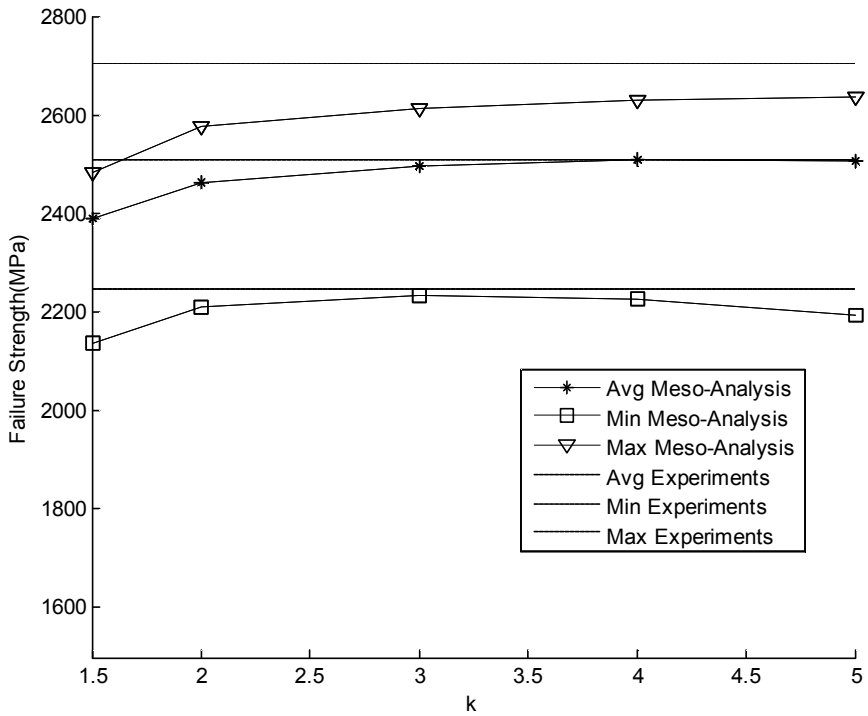

(a)

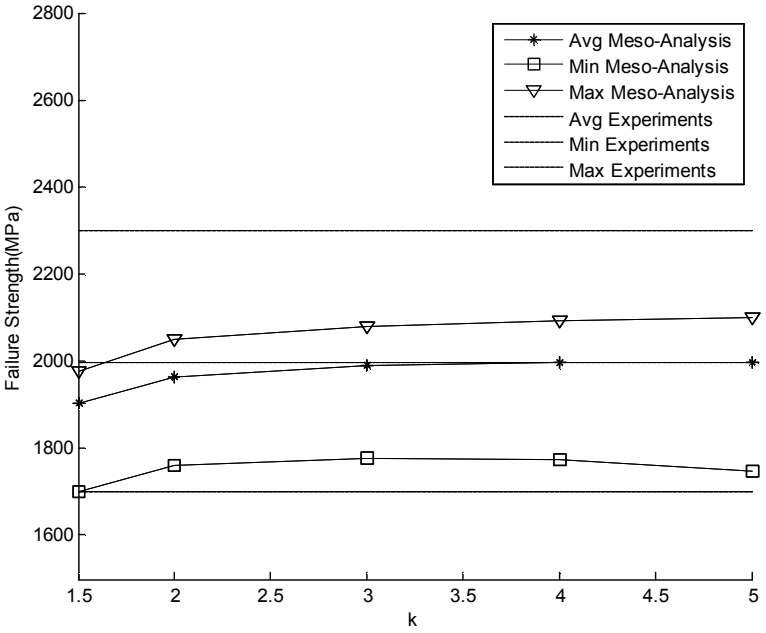

(b)

Figure 2.19 Meso-scale strength analysis results of 512 cases for simulation and 18 cases for experimental tests of (a) IM7/8552 (b) AS4/8552

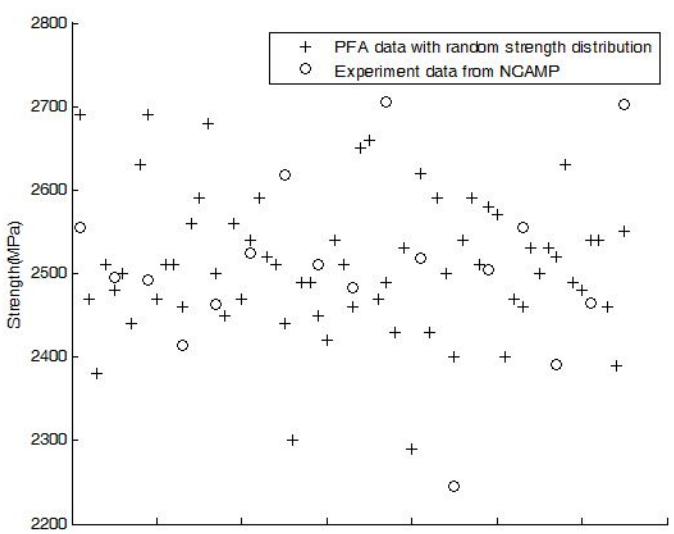

Figure 2.20 IM7/8552 longitudinal tensile strength specimen data from the experiments and PFA

2.6.2 Determination of the macro-scale location parameter

The Weibull location parameters of macro-scale h and meso-scale h_{meso} are greater than zero, and they are smaller than the unity value according to their definition. In the absence of a meso-scale strength distribution, both h_{meso} and h will become unity. Otherwise, h_{meso} will be zero if an initial defect exists. In contrast, h will remain unknown because it is uncertain whether a meso-scale defect is critical with regard to macro-scale elements. Even if the entire load of the failed fiber is redistributed equally over its local neighborhood in the lattice consider to leading to stress concentrations in failure regions by ply-discounting approaches, as shown in Figures 2.16 and Figure 2.17, the strength of the lattice will exceed the minimum strength of the local elements. In the macroscopic approach, the strength X_T is constant for every element without any distribution, while the damage evolution model replaces the statistical distribution of the fiber strength. If there is no stress concentration, a failure will be induced by defects in the fiber. In this case, h should be zero on the meso-scale. Otherwise, as the failure is initiated in the region where the stress is concentrated, h should also fit to satisfy the statistical results. When replacing ply-discounting degradation with stress-based continuum degradation, the location parameter should also be replaced by h_0. A macro-scale PFA analysis was performed, as shown in Figure 2.21, by changing h_0 from zero to unity. When $h_0 = 0.60$, the CDM and ply-discounting methods provide analogous

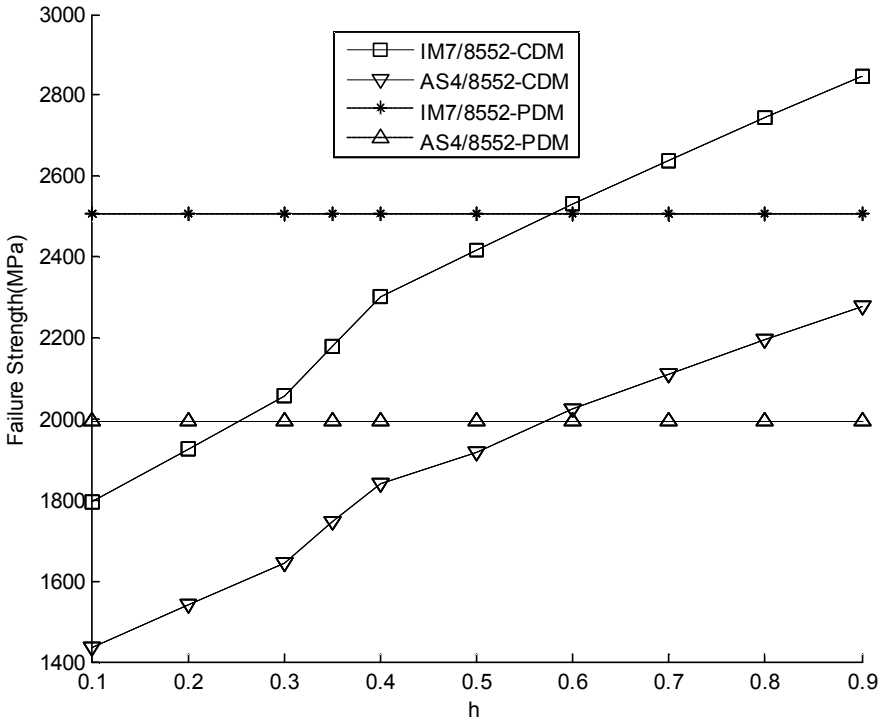

Figure 2.21 Macro-scale strength analysis results of IM7/8552 and AS4/8552, with Present CDM model and equivalent PDM model from different Weibull location parameters of $\boldsymbol{h_0}$

results.

Additionally, matrix cracks from adjacent layers can be accounted for in the parameter$\boldsymbol{h}$, as follows,

$$h\left(F_{2,I-1}, F_{2,I+1}\right) = h_0 - A_3 max\left(d_{I-1,2}, d_{I+1,2}\right):\ F_{2,i-1} > 1\ or\ F_{2,i-1} > 1 \quad (2.60)$$

where A_3 is an adjacent layer factor which is determined by the stress concentration factor from the adjacent layers. $d_{I-1,2}$ and $d_{I+1,2}$ denote damage from the matrix cracks. Matrix cracks offset the stress concentration of the fiber in the outer boundaries of

adjacent layers. Localized delamination is caused by the stress concentration at the tips of transverse matrix cracks, as the crack spacing of the matrix also has an approximate Weibull distribution when it is proportional to the matrix strength,

This leads to early failure of the fiber by the factor h instead of h_0. The adjacent layer factor can be obtained from the experimental data of the ASTM D3039 $0°$ tension test of a layup $[0/90]_{2s}$. The $0°$ lamina tensile strength can be obtained by testing cross-ply laminates under tension and then backing out the unidirectional composite. Cross-ply laminates do not contain plies other than $0°$ and $90°$ plies. Therefore, the shear stiffness properties of unidirectional plies of these types of laminates do not enter the calculation. Nevertheless, the unidirectional composite strength from the measured cross-ply strength is not compatible with results of unidirectional tensile tests, even if there is no observed buckling or delamination. In terms of the average strength, cross-ply tests show a longitudinal tensile strength of approximately 2,250MPa, while unidirectional tests show a value of 2,500MPa for IM7/8552. Adjacent layer factors enable each layup to have the same amounts of strength by shifting back the failure initiation.

For layup $[0/90]_{2s}$, failure of the $0°$ lamina is influenced by a matrix crack at $90°$ lamina. The Weibull location parameter h can be expressed as

$$h\left(F_{2,90°}\right) = h_0 - \left(1 - e^{-A_3\left(F_{2,90°}-1\right)^{A_4}}\right) \tag{2.61}$$

where $F_{2,90°}$ is the matrix failure index of the $90°$ layer. If matrix cracks induce fiber breakage immediately, h should be 0 on the meso-scale. The critical matrix failure index can be determined as follows.

$$F_{2,cr} = 1 + \frac{1}{A_3}\left(log\frac{1}{1-h_0}\right)^{1/A_4} \quad 0 \le h_0 < 1 \tag{2.62}$$

A_3 and A_4 are determined by comparing the $[0/90]_{2s}$ layup (UNT0) of the experimental results. When A_3 is set to 0.5 and A_4 is set to 1.41, the average strength of longitudinal tensile case is similar to the strength obtained from the UNT0 layup calculations. Several pairs of A_3 and A_4 are described in Figure 2.22 with PFA results under a tensile load for a cross-ply sample.

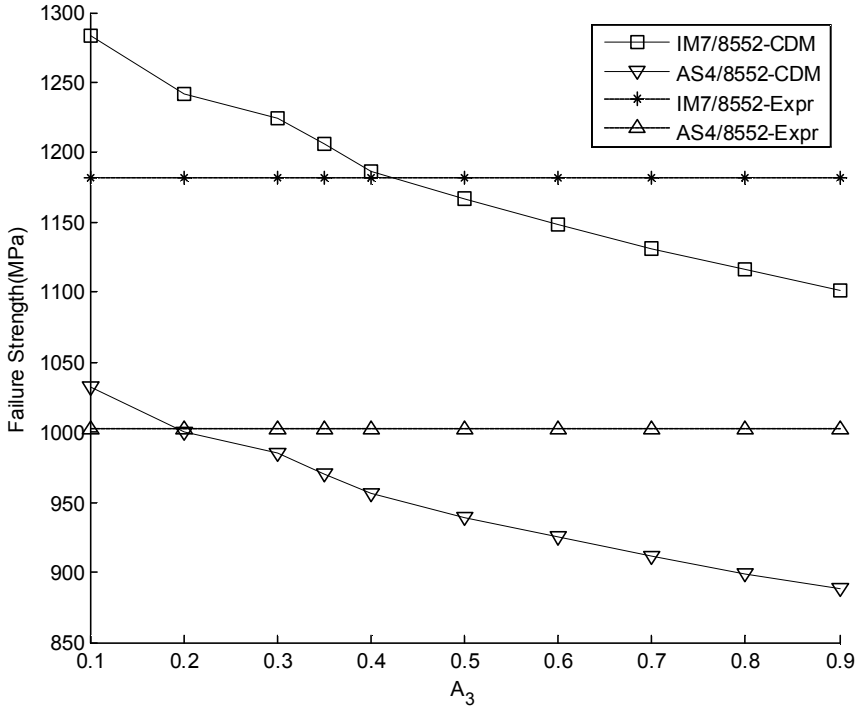

Figure 2.22 Cross-ply strength analysis results of IM7/8552 and AS4/8552 from different adjacent layer factors of $\boldsymbol{A_3}$

2.7 Unnotched Tension Results

The developed PFA procedure will be validated using unnotched tension(UNT) tests. The rectangular laminates from the first group which is described in Figure 2.23 are the unnotched coupon test type ASTM D3039 with various combinations of stacking sequences and materials, including the length in mm, the thickness of each layer in mm, and the width in mm. After choosing the ply-level properties and the CDM parameters A_1, A_2, A_3, A_4 and h_0 from the experiment result of longitudinal tension (LT) for $[0]_6$, transverse tension for $[90]_{11}$, in-plane shear (IPS) for $[45/-45]_{3s}$ and unnotched tension (UNT0) for the $[0/90]_{2s}$ layup, a strength analysis for laminate was performed. "quasi-isotropic", "soft" and "hard" layups were designated as layup number 1, 2, and 3, respectively. The simulations were performed for three materials: IM7/8552, AS4/8552 and T700/M015. The ply-properties are described in Table 1~ Table 4. The analysis results are compared with the

experimental results from earlier work on IM7/8552 and AS4/8552 and from the experiments which were carried out using a MTS 810

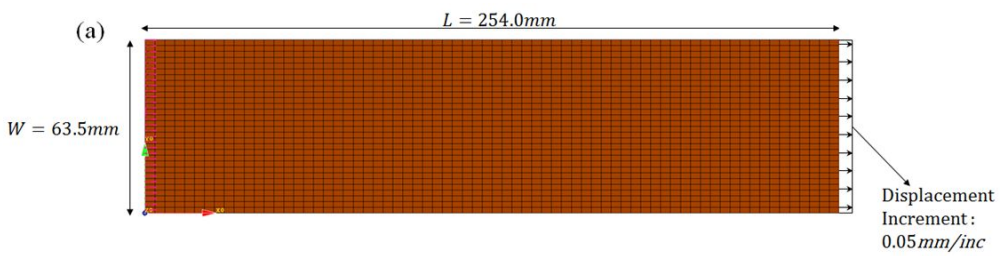

Figure 2.23 Problem description of ASTMD3039 unnotched tensile (UNT) test

Table 2.1 Mechanical properties of the lamina

Material	Longitudinal elastic modulus $\boldsymbol{E_1}$ [GPa]	Transverse elastic modulus $\boldsymbol{E_2}$ [GPa]	Poisson's ratio, ν_{12}	Initial shear modulus [GPa] $\boldsymbol{G_{12}}$
IM7/8552	159	8.96	0.316	4.69
T700/M015	147	8.43	0.290	4.90
AS4/8552	127	9.24	0.302	4.83

Table 2.2 Failure strength of lamina

Material	Strength [MPa]				
	X_t	X_c	Y_t	Y_c	S_f
IM7/8552	2500	1716	64.05	286.00	91.15
T700/M015	2460	1500	61.30	280.00	75.00
AS4/8552	2000	1870	63.90	268.00	91.60

Table 2.3 Nonlinear parameters for each material

Material	$\boldsymbol{E_{1,0}}$ (GPa)	$\boldsymbol{a_1}$	$\boldsymbol{a_2}$	$\boldsymbol{S_{661}}$	$\boldsymbol{S_{662}}$	$\boldsymbol{S_{663}}$
IM7/8552	1.21	1.12	0.48	4.500E-3	5.00E-2	2.041E-4
T700/M015	1.40	1.30	0.26	5.900E-3	5.00E-2	2.132E-4
AS4/8552	1.24	1.02	0.11	5.217E-3	5.00E-2	2.070E-4

Table 2.4. Parameters to determine meso-scale mesh size

Material	v_f	$D_f(\mu m)$	$L_{macro}(mm)$	N_f	n_{mesh}
IM7/8552	0.6	5.2	5.00	6000	118
AS4/8552	0.6	7.1	5.00	6000	63

hydraulic testing machine for T700/M015. The test machine is described in Figure 2.24.

To validate the phenomenological maturity and the improvement of the present CDM, analyses with the GSSD model were performed and the results were compared with the experimental results. The set of plastic model parameters is determined by the experimental result of the $[45/-45]_{3s}$ layup. The appropriateness of the parameters is verified by a comparison of the shear stress strain curve predicted using these parameters for the material under consideration.

Three layups $[45/0/-45/90]_{2S}$, $[45/-45/0/45/-45/90/45/-45/45/-45]_S$, and $[0/45/0/90/0/-45/0/45/0/-45]_S$, were considered for the UNT group. The problems were solved by five methods: the GSSD method of NASTRAN with Hashin or Tsai-Wu failure criteria, the ply-discounting method, experiments, and the presented CDM approach with a Weibull distribution of the longitudinal tensile strength. The results of the simulations are shown in Table 2.5 and Figure 2.24. The tensile strengths of the laminates $X_{lam} = P_{max}/(WT)$ can be obtained by the failure loadP_{max}.

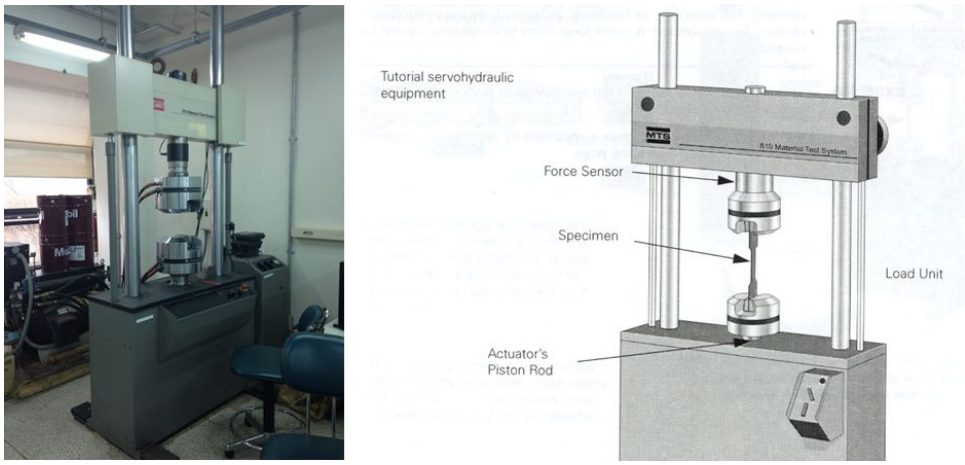

Figure 2.24 810 Material Test System (MTS)

The aim of this paper is to obtain accurate strength and stress–strain curves of composites including nonlinearity characteristics with high accuracy using the statistical distribution of the lamina level test results. To establish confidence, it is initially necessary to verify the ability of the proposed method to predict the curves and strength levels in a displacement–controlled test. The results from the proposed CDM method were more accurate compared to predictions using other methods. The stress–strain curve graph is compared with the experiment results and with other numerical methods for laminates in Figure 2.24. The strength and stiffness predicted by the proposed model are in good agreement with the experimental and computational results for all stacking sequences, as shown in Table 2.5.

UNTB and UNTC denote the PFA results using the GSSD method in NASTRAN. These methods were less accurate than the proposed method in most cases. UNTB, in which the Hashin failure criteria was used with the GSSD model, gives better results than the Tsai–

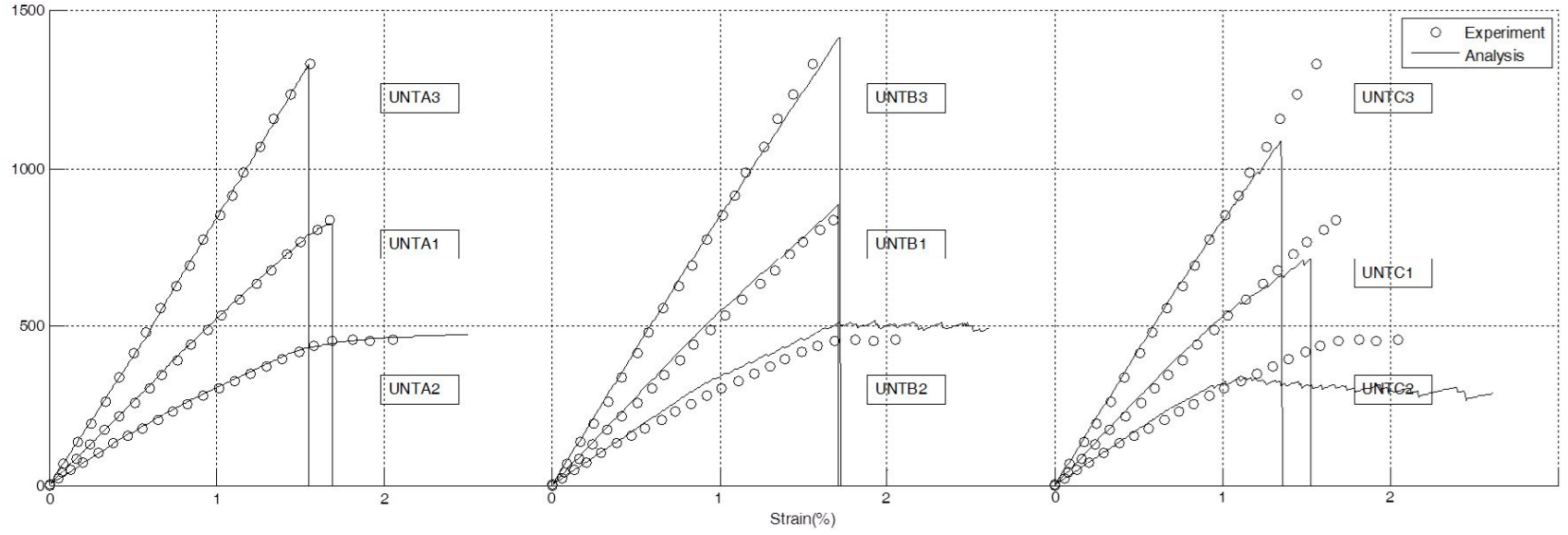

Figure 2.24-(a) Stress-strain curves of unnotched tension tests of T700/M015

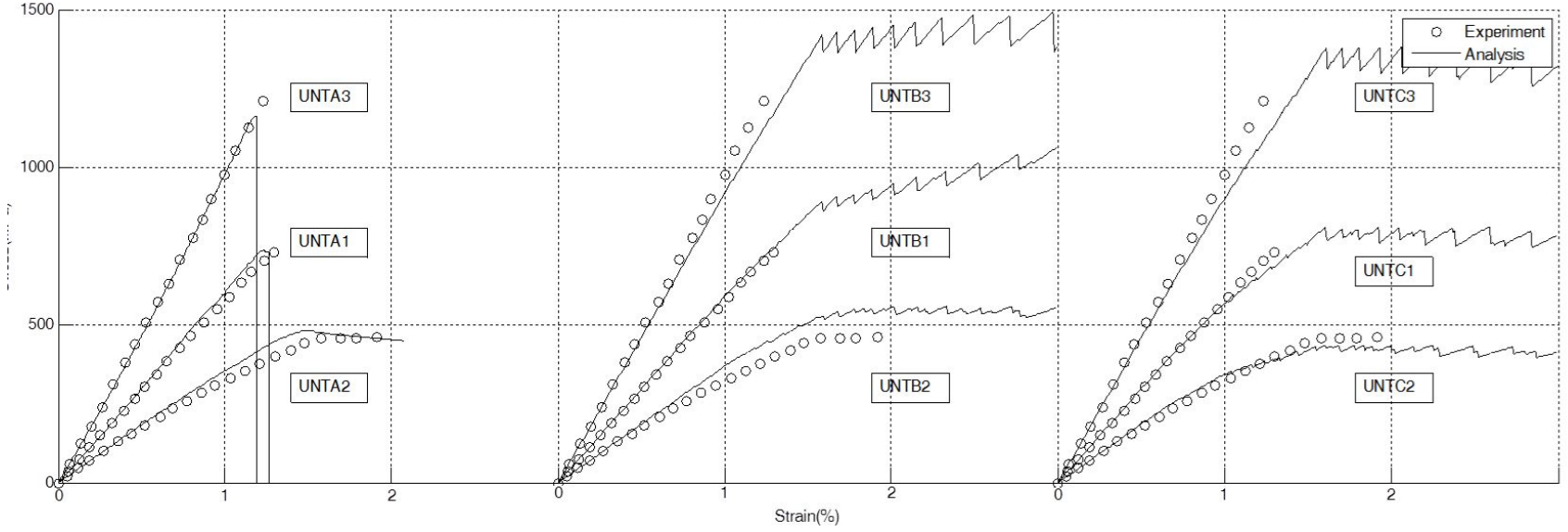

Figure 2.24-(b) Stress-strain curves of unnotched tension tests of IM7/8552

Table 2.5 Calculated and experimental strength values of the unnotched laminates

Mat Name	Layup	Failure Stress σ_u(MPa)				Difference (%)		
		UNTA (Present CDM	UNTB (GSSD Hashin)	UNTC (GSSD Tsai-Wu)	Experiment	UNTA (Present CDM	UNTB (GSSD Hashin)	UNTC (GSSD Tsai-Wu)
T700 /M015	[45/0/-45/90/45/0/-45/90/45/0/-45/90]s	828.63	887.15	714.49	838.13	-1.13	5.85	-14.75
	[45/-45/90/45/-45/45/-45/0/45/-45]s	475.12	517.93	338.84	458.74	3.57	12.90	-26.14
	[45/0/-45/90/0/0/45/0/-45/0]s	1329.41	1413.44	1088.67	1328.39	0.08	6.40	-18.05
IM7 /8552	[45/0/-45/90]2s	737.02	1062.94	812.93	729.74	1.00	45.66	11.40
	[45/-45/0/45/-45/90/45/-45/45/-45]s	482.94	560.89	437.22	462.02	4.53	21.40	-5.37
	[0/45/0/90/0/45/0/-45]s	1159.69	1494.70	1381.43	1210.92	-4.23	23.43	14.08
AS4 /8552	[45/0/-45/90]2s	642.56	868.16	658.16	610.94	-1.37	42.10	7.73
	[45/-45/0/45/-45/90/45/-45/45/-45]s	369.92	479.84	372.46	438.64	-15.67	9.39	-15.09
	[0/45/0/90/0/45/0/-45]s	947.24	1209.16	1111.46	1050.21	-9.80	15.14	5.83

Wu criteria for T700/M015, while the UNTC model gives better results when the IM7/8552 or the AS4/8552 material is used. In most cases, GSSD-based CDM models give inaccurate results for the failure stress, as these methods overestimate the stress after failure, when the specimens have no stress concentration. On the other hand, the UNTD model, which uses the ply-discount method, has high accuracy compared to conventional CDM methods, except in several cases showing nonlinearity of the material. In comparison, the presented CDM results are in good agreement with the experimental data compared to the other methods for every material and for most stacking sequences within 5% error of the strength.

The "soft" layup UNT2 and the "hard" layup UNT3 have different nonlinear characteristics; UNT2 has elasto-plasticity in the 45° and -45° layers, while UNT3 has nonlinear-elastic characteristics in the 0° layer. For UNT2, over 90% of the internal force comes from the 0° layer, even if it uses 50% of the space of the laminates. Thus, the behavior in the longitudinal fiber direction strongly contributes to determining the strength. It was noted that the nonlinear elasticity of the fiber direction has significant effects on the predicted tensile strength. UNT3 is affected by the nonlinearity of the in-plane shear, as 80% of the layer consists of $[45/-45]_{3s}$; thus, it is clear that UNT3 is a shear-stress-dominant stacking sequence rather than having normal stress in the fiber direction. With regard to the UNT tests, every result with the

present CDM was in good agreement with the experimental results reported in the literature. On the other hand, the results of the GSSD model show good agreement with UNTB (quasi-isotropic) cases, whereas the strength stress-strain curve prediction results of UNTA and UNTB have larger differences from the experimental results.

Nonlinearity effects in this research are classified with a material nonlinear model and a degradation model. Most of the nonlinearity of the laminates results from shear dominant layers, while their critical point (i.e., the strength) is determined by the degradation model and failure criteria. This is why this novel method has the virtue of good accuracy compared to conventional methods which consider degradation only. It is possible to redistribute the internal force based on the shear nonlinearity, as the degradation history does not influence the nonlinearity of shear stress. For example, in the result of an analysis with the GSSD model, which considers only the degradation, the material nonlinearity function is obtained via the degradation factor. Because the factors are accumulated at every step, it causes the stiffness matrix to change at every step. Thus, the maximum stress as the strain increases can be affected by the load increment step, as can other numerical environment variables.

2.8 Open Hole Tension(OHT) Test

Results In this subsection, open-hole strength predictions are made for quasi-isotropic (OHT1), soft (OHT2) and hard (OHT3) layups which is described in Figure 2.25. The strength values associated with every material parameter set are reported and discussed. In the experimental results, a pull-out type of failure mode without delamination was noted, as every specimen consists of thin plies. This shows agreement with results in the literature38. Thus, these coupon tests show the fiber-breakage-dominated failure mode as opposed to delamination. Therefore, only the local delamination effect caused by the stress concentration from adjacent layer matrix cracks is considered.

A comparison of the experimental results and the simulation results is presented in Table 2.6 for the tensile strength. Compared to the UNT cases, GSSD methods also show fair agreement between the experimental and numerical predictions, as post behavior after failure plays an important

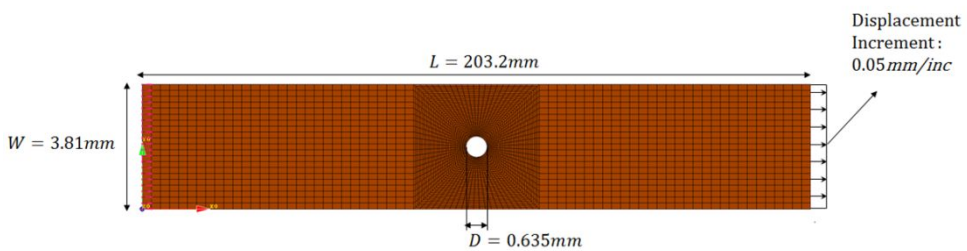

Figure 2.25. Open-hole specimen tensile test descriptions

role in cases in which a stress concentration exists. OHTD denotes the results for which the ply-discount approach was used, with the internal force of each layer after failure set to zero. In this case, it is difficult to determine the exact strength, as overall failure occurs immediately after the initial failure. Therefore, the laminate strength, also predicted, was lower than it was in the experimental results. CDM also has an advantage over the ply-discount approach when OHT problems are considered. For the OHTB and OHTC cases, for which the Hashin and Tsai-Wu conditions were used to determine the failure index, high accuracy was noted due to the gradual degradation contribution.

Table 5. Calculated and experimental strength values of the open-hole laminates

Mat Name	Layup	Failure Stress σ_u(MPa)				Difference (%)		
		UNTA (Present CDM	UNTB (GSSD Hashin)	UNTC (GSSD Tsai-Wu)	Experiment	UNTA (Present CDM	UNTB (GSSD Hashin)	UNTC (GSSD Tsai-Wu)
T700 /M015	[45/0/-45/90/45/0/-45/90/45/0/-45/90]s	563.63	324.99	415.52	567.10	0.61	-14.0	-9.91
IM7 /8552	[0/45/0/90/0/45/0/-45]s	580.09	470.07	636.59	597.01	-2.83	-21.26	6.63
	[45/0/-45/90]2s	405.39	396.33	427.93	406.79	-0.35	-2.57	5.20
	[45/-45/0/45/-45/90/45/-45/45/-45]s	314.39	327.03	303.17	300.96	4.47	8.67	0.73
AS4 /8552	[0/45/0/90/0/45/0/-45]s	462.06	381.55	526.52	472.63	-2.24	-19.27	11.4
	[45/0/-45/90]2s	327.44	316.20	345.69	328.40	-0.29	-3.71	5.26
	[45/-45/0/45/-45/90/45/-45/45/-45]s	261.70	265.67	248.38	270.07	-3.10	-1.63	-8.03

2.9 Chapter Summary

In this chapter, a PFA solver was developed to predict the nonlinear mechanical behavior of carbon/epoxy laminates under tensile loading by considering the material nonlinearity with a novel CDM model from the statistical results of experiments. A numerical analysis was conducted under unnotched tensile test.

Material nonlinearity was associated with the nonlinear elastic behavior of the fiber direction and the viscoelasticity of the in-plane shear. The shear nonlinearity of fiber-reinforced composites was considered with a quasi-static loading condition. It was also assumed that the nonlinear response depends on the shear nonlinearity, localized delamination, and nonlinear elasticity of the longitudinal stiffness.

Generalized Weibull distribution parameters were configured to determine the damage evolution of a laminate composite. The amount of stiffness degradation was quantified by developing a multi-scale model to determine the parameters. We used open-hole tensile tests and unnotched tensile tests in order to validate the damage variables from a meso-model of laminates. The scale, shape and location parameters of the Weibull distribution of damage evolution were effective when used to obtain the strength and load-displacement curves pertaining to UNT problems. Through validation of the present CDM-associated damage variables with a meso-scale model, it was confirmed that the approach proposed here precisely captures the nonlinearity of the stress-strain curves

and predicts the strength with various combinations of layups with a lower computational cost. Not only the strength of "quasi-isotropic" laminates, but also the strength of "soft" and "hard" layups were predicted accurately compared to a conventional damage evolution approaches such as the ply-discount model and the GSSD model.

Chapter 3. Multi-Scale Progressive Failure Analysis

In this chapter, the PFA solver will be revised using micro-mechanics of failure. There are two way to improve PFA algorithm as referred, revising the procedure by developing novel damage evolution methods and improving failure criterion. In this chapter, both methods will be revised as multi-scale method.

In conventional multi-scale approaches to predict material properties are focused on the failure criterion. Micro Mechanics of Failure (MMF) and Strain Invariant Failure Theory (SIFT) are representative multi-scale model of composites.

After MMF-based multi-scale approaches are introduced, PFA procedure also will be reconstructed using the multi-scale adaption in terms of failure criterion and material property degradation method.

3.1 Micro Mechanics of Failure

Micro mechanics of failure (MMF) is a method considering non-uniform micro-stresses at the constituent level develop due to mechanical loadings. It divides domain as three regions, the fiber, the matrix and the fiber-matrix interface. In this section, failure initiation mechanism in micro-scale is discussed.

3.1.1 Stress/Strain Amplficiation Factors

To define the failure criterion in micro-scale, it is required to obtain micro-level stress due to macro-scale stress is used in macro-scale. Using unit-cell representative volume element (RVE) model, micro-macro stress relationship can be defined as follow.

$$\boldsymbol{\sigma}^{(i)} = M_{\boldsymbol{\sigma}^{(i)}}\boldsymbol{\sigma} + A_{\boldsymbol{\sigma}^{(i)}}\Delta\mathbf{T} \tag{3.1}$$

$$\boldsymbol{t}^{(i)} = M_{\boldsymbol{t}}\boldsymbol{\sigma} + A_{\boldsymbol{t}}\Delta\mathbf{T} \tag{3.2}$$

Where $\boldsymbol{\sigma}^{(i)}$ and $t^{(i)}$ denote micro-scale stress and interfacial traction, $\boldsymbol{\sigma}$ and $\Delta\mathbf{T}$ are macro-scale stress and temperature increment. $M_{\boldsymbol{\sigma}^{(i)}}$ and $M_{\boldsymbol{t}}$ represent the stress amplification factor for macro-scale stress, interfacial traction amplification factor for macro stress while $A_{\boldsymbol{\sigma}^{(i)}}$ and $A_{\boldsymbol{t}}$ denote amplification factors for the temperature increment.

Equation (3.1) and (3.2) has many-to-one mapping cardinality. The representative volume element is required the relationship. When the microscopic model is assumed as well aligned arrangements, then square and hexagonal array can be chosen as representative model because the periodicity exists. Square array and hexagonal array are the model frequently used. As Figure 3.1, fibers in square model are arranged 90 degrees apart whereas they are 60 degrees apart in the hexagonal model. Each model has

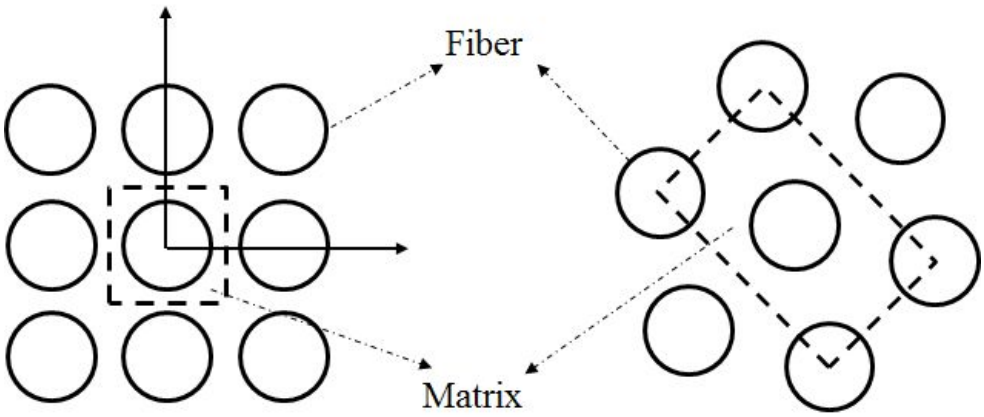

Figure 3.1 Square array (left) and hexagonal array (right) of RVE model

different number of neighbor fiber, thus their mechanical response under external load also can be different, especially when RVE model receives transverse and inter-lamina direction external loads.

Figure 3.2 and Figure 3.3 describes the finite element model of square array and hexagonal array of fiber. As referred, micro- and macro-scale stress should be connected using the stress amplification factor matrix, about several points. Because each failure is initiated in the node which has highest stress state, it is possible to pick representative points to obtain the matrix. In the Figure 3.2 and Figure 3.3, the points which pick the micro-scale stress are marked. Thirty to forty points usually used to construct stress amplification factors. Then the number of failure criterion for that model is the number of stress amplification factor.

The coefficients of stress amplification factor matrix can be obtained by results of RVE model's linear static analysis. The amplification factor coefficient can be described as follow when there are no temperature increments.

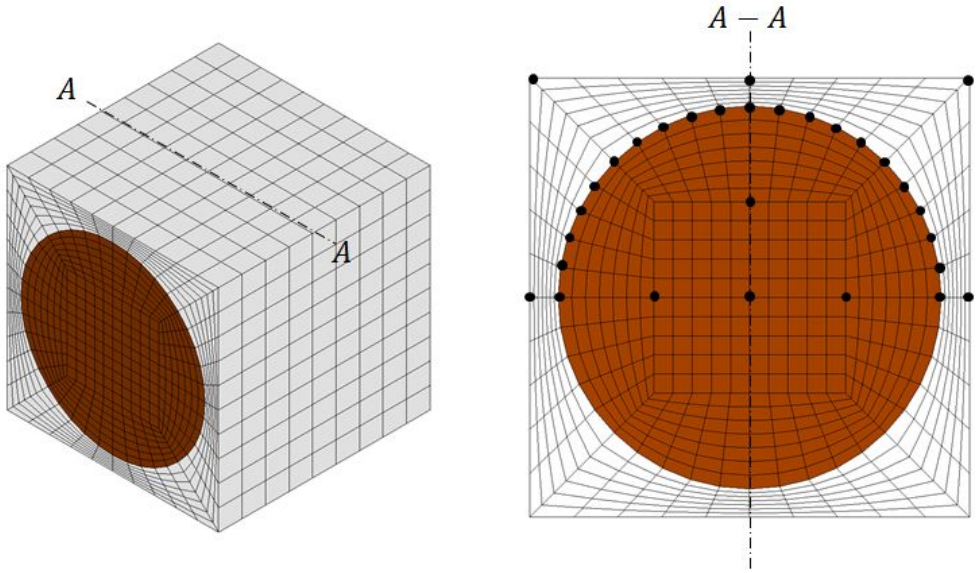

Figure 3.2 Finite elements and amplification factor acquisition points of square array RVE model

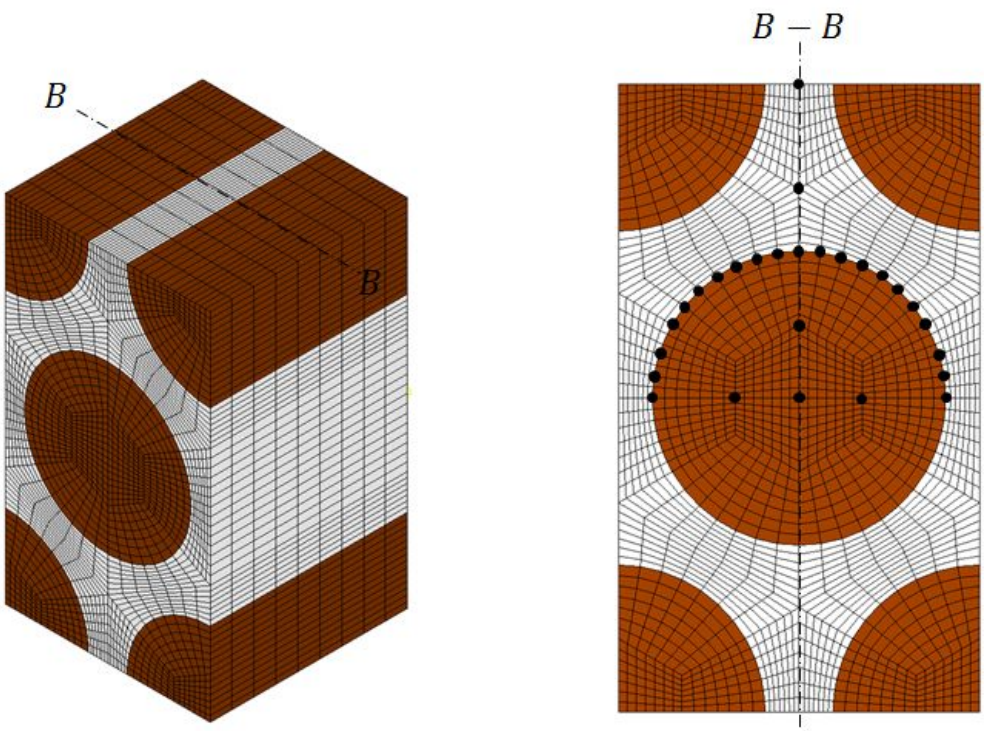

Figure 3.3 Finite elements and amplification factor acquisition points of hexagonal array RVE model

$$\begin{bmatrix}\sigma_{11}^{(i)}\\ \sigma_{22}^{(i)}\\ \sigma_{33}^{(i)}\\ \sigma_{23}^{(i)}\\ \sigma_{31}^{(i)}\\ \sigma_{12}^{(i)}\end{bmatrix}=\begin{bmatrix}M_{11} & M_{12} & M_{13} & M_{14} & 0 & 0\\ M_{21} & M_{22} & M_{23} & M_{24} & 0 & 0\\ M_{31} & M_{32} & M_{33} & M_{34} & 0 & 0\\ M_{41} & M_{42} & M_{43} & M_{44} & 0 & 0\\ 0 & 0 & 0 & 0 & M_{55} & M_{56}\\ 0 & 0 & 0 & 0 & M_{65} & M_{66}\end{bmatrix}\begin{bmatrix}\sigma_{11}\\ \sigma_{22}\\ \sigma_{33}\\ \sigma_{23}\\ \sigma_{31}\\ \sigma_{12}\end{bmatrix} \tag{3.3}$$

Stress tensor σ_{ij} of Equation (3.3) is face-averaged stress of the unit cell model. Because the unit cell model's characteristics depends on not only fiber and matrix mechanical properties, but also fiber volume fraction. Therefore amplification factor is not mechanical properties, but the specific ply that volume fraction is given. To obtain the coefficient of matrix, six problems with external loads are solved by linear static solver.

Boundary conditions should be given as periodic boundary condition. In the linear static solver, periodic boundary conditions are given as following form

$$U|_{s1} - U|_{s2} = U|_{n1} - U|_{n2} \tag{3.4}$$

where U is displacement vector in the boundary, $S1$ is nodes on dependent surface of periodic boundary condition, $S2$ is nodes on independent surface, $n1$ is a node on $S1$, and $n2$ is the node corresponding with $n1$. Figure 3.4 describes the node set of square array. In this case, $NSET_1$ and $NSET_2$ become $S1$ in equation (3.4)

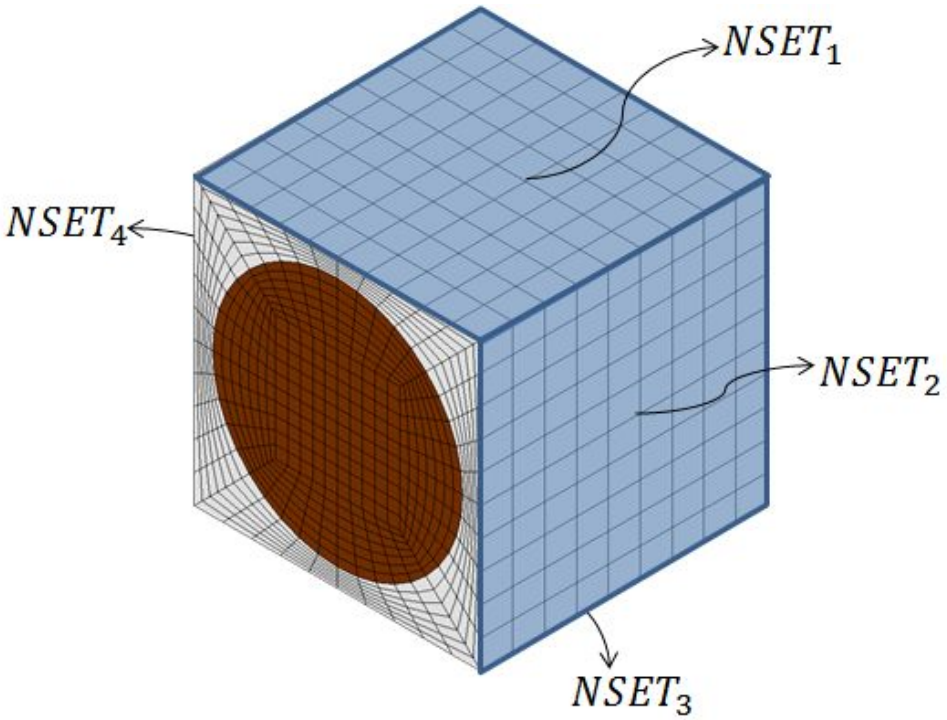

Figure 3.4 Node set for periodic boundary conditions

while $NSET_3$ and $NSET_4$ are$S2$. Any node can be chosen as $n1$ and $n2$ in here.

Figure 3.5 load conditions of the square array model. Longitudinal normal and shear direction force, and transverse normal and shear direction force are given as external loads.

From the longitudinal tension load, M_{i1} component values are attained because stress σ_{11} can be normalized and the other components are zero. In the same way, the other components are obtained. It should be repeated by all points which chosen stress amplification factor.

Figure 3.6 (a)~(d) are the results of linear static analysis by each load condition. Using the stress components of the results, coefficients matrix of equation (3.3) can be obtained. Because of its

symmetry, z-direction coefficient is calculated from y-direction components.

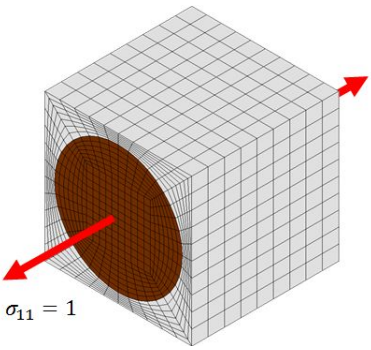

(a) Longitudinal tensile unit load

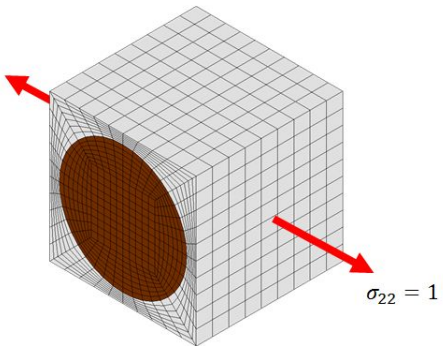

(b) Transverse tensile unit load

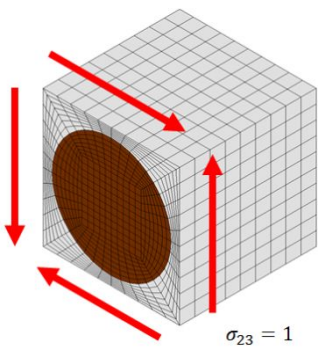

(b) Transverse shear unit load

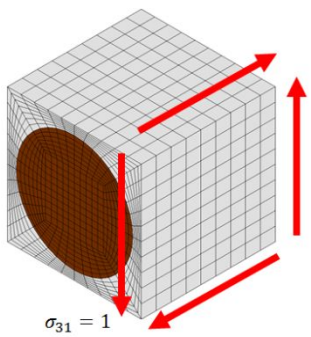

(d) Longitudinal shear unit load

Figure 3.5. Unit loads for unit cell model to obtain stress amplification factors

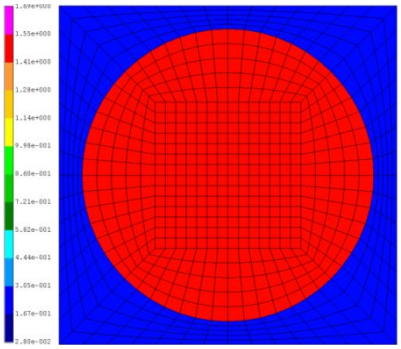

(a) Longitudinal normal stress $\boldsymbol{\sigma_{11}}$

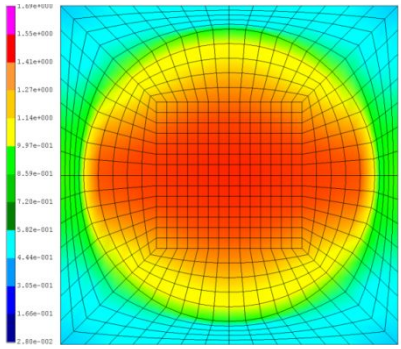

(b) Transverse normal stress $\boldsymbol{\sigma_{22}}$

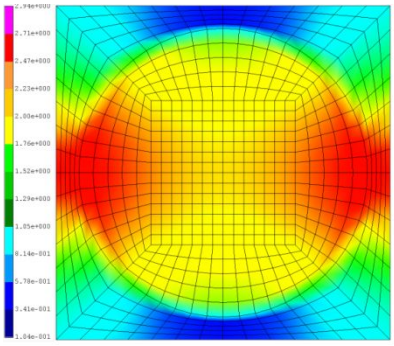

(c) Longitudinal shear stress $\boldsymbol{\sigma_{12}}$(or $\boldsymbol{\sigma_{31}}$)

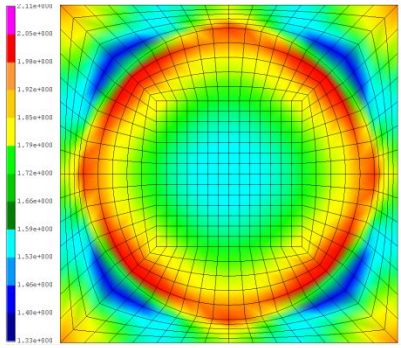

(d) Transverse shear stress $\boldsymbol{\sigma_{23}}$

Figure 3.6. Linear static analysis results of unit cell under unit loads

3.1.2 Fiber Failure Criterion

In general, fiber reinforced composite materials are considered as transversely isotropic material. It means longitudinal and transverse direction strength can be defined differently. Moreover, tensile and compressive strength also will be different. To describe failure criterion of fiber, let"s assume it has a quadric failure criterion which is refered in the chapter 2.

Then general failure criteion can be expressed using the first order and second order stress as follow.

$$\sum_{j=1}^{6}\sum_{k=1}^{6} F_{ik}\sigma_i^{(i)}\sigma_k^{(i)} + \sum_{k=1}^{6} F_k\sigma_k^{(i)} \begin{cases} \geq 1\ failure \\ < 1\ no\ failure \end{cases} \tag{3.5}$$

Where coefficients F_{ik} and F_k are determined and summarized as follows.

$$\begin{aligned} F_{11} &= \frac{1}{T_{f1}C_{f1}},\ F_{22} = F_{33} = \frac{1}{T_{f2}C_{f2}} \\ F_{44} &= \frac{1}{S_{f4}^2},\ F_{55} = F_{66} = \frac{1}{S_{f6}^2} \\ F_1 &= \frac{1}{T_{f1}} - \frac{1}{C_{f1}},\ F_2 = F_3 = \frac{1}{T_{f2}} - \frac{1}{C_{f2}} \end{aligned} \tag{3.6}$$

$$\begin{aligned} F_{12} = F_{21} = F_{13} = F_{31} &= -\frac{1}{2\sqrt{T_{f1}C_{f1}T_{f2}C_{f2}}} \\ F_{23} = F_{32} &= -\frac{1}{2T_{f2}C_{f2}} \end{aligned} \tag{3.7}$$

Where T_{f1} and C_{f1} are longitudinal tensile and compressive strength, T_{f2} and C_{f2} are transverse tensile and compressive strength, and S_{f4} and S_{f6} are transverse–transverse shear and longitudinal shear strength. Above failure criterion can be assumed as more simple form from the fact which matrix failure dominate the failure behavior under transverse and shear loads because fiber strength much larger than in general fiber reinforced materials. Because stress distribution of fiber under longitudinal tensile load nearly constants, initial failure of fiber induce overall failure of unit cell model. Also, it is hard to adopt the failure strength of transverse and shear direction by experiments. For these reasons, the failure criterion of fiber can be summarized as follow

$$-C_{f1} < \sigma_{11}^{(i)} < T_{f1} \tag{3.8}$$

Then longitudinal tensile and compressive strength is required to evaluate initial failure and ultimate strength of RVE model under longitudinal tensile load. For this reason, fiber breakage under longitudinal tensile and compressive can be considered a brittle behavior, and thus no material property degradation model is needed. However, MMF fiber failure model cannot explain strength incompatibility of macro and micro scale. Therefore, it is required using micro mechanics modification (MMM) to solve laminates problems. MMM and the other methods to overcome the drawback is explained in the fiber bundle model chapter.

3.1.3 Matrix Failure Criterion

Unlike fiber model, matrix material model can be assumed as isotropic material in terms of modulus. However, it also has different tensile and compressive strength because their failure mode can be change according to the load conditions. the von-Mises equivalent stress σ_{VM} and stress invariant I_1, I_2 of matrix can be expressed as follow.

$$\begin{aligned} I_1 &= \sigma_{11}^{(i)} + \sigma_{22}^{(i)} + \sigma_{33}^{(i)} \\ I_2 &= \sigma_{11}^{(i)}\sigma_{22}^{(i)} + \sigma_{22}^{(i)}\sigma_{33}^{(i)} + \sigma_{33}^{(i)}\sigma_{11}^{(i)} - (\sigma_{12}^2 + \sigma_{23}^2 + \sigma_{31}^2) \\ \sigma_{VM} &= \sqrt{I_1^2 - 3I_2} \end{aligned} \tag{3.9}$$

Using the modified vertion of the von Mises failure criterion, generalized form of failure criterion can be expressed as follow.

$$\left(\frac{\sigma_{VM}}{\sigma_{VM}^{cr}}\right)^{n_p} + \left(\frac{I_1}{I_1^{cr}}\right) = 1 \tag{3.10}$$

Where critical value σ_{VM}^{cr} and I_1^{cr} can be expressed as function of T_m, C_m and n_p:

$$\begin{aligned} \sigma_{VM}^{cr} &= T_m \left(\frac{\alpha^{n_p}+\alpha}{\alpha+1}\right)^{1/n_p} \\ I_1^{cr} &= T_m \frac{\alpha^{n_p}+\alpha}{\alpha+1} \end{aligned} \tag{3.11}$$

Where $\alpha = T_m/C_m$, T_m is tensile strength of matrix and C_m is compressive strength.

3.1.3 Fiber/Matrix Interface Failure Criterion

There are an interfacial failure which come from debonding and detachment between fiber and matrix. It is caused by normal and tangential traction force. A quadric form of failure criterion is used to take into account the interaction between the tractions.

$$\left(\frac{\langle t_n \rangle}{Y_n}\right)^2 + \left(\frac{t_t}{Y_t}\right)^2 + \left(\frac{t_x}{Y_x}\right)^2 = 1 \qquad (3.12)$$

Where bracket <> stand for the Macaulay brackets, which return the argument if positive and zero otherwise. In means interfacial failure induced by normal traction t_n is occurred under tensile load only. Tangential traction to the circumference t_t and longitudinal direction traction t_x also should be considered.

3.1.4 Micro Mechanics Modification(MMM)

Micro mechanics of failure, including fiber, matrix and interfacial failure mode, can be adapted in to multi-scale PFA analysis constituent failure strength. The kernel algorithm of MMF will become securing amplification factor which bridging micro and macro level stress as referred. However, because of the periodicity and symmetry of representative model, it will be impossible to consider uncertainty for micro level mechanical properties. Composite ply failure strength which is led by MMF with micromechanical material properties is compared with the actual strength of the ply as shown in Table. 3.1. The reason why MMF results give correspondingly exaggerated failure strength is that MMF theory does not consider about influence of fiber bundle with fiber flaw. In actual problems for laminates properties analysis, ply level material property tests is used instead of fiber/matrix properties because MMF is unable to predict exact properties of the ply.

In conventional MMF approaches, micro mechanics modification (MMM) is one of solution to overcome the problem. This method uses to obtain constituent failure strength which has compatibility with ply-level strength. Figure 3.7 describes whole procedure to obtain the properties. Therefore, MMF should have not only constituent properties but also ply properties. There are six failure strengths in constituent level, but transverse tensile and compressive strength is not dominating failure mode.

Table 3.1 Longitudinal tensile failure strength of comparison MMF using micromechanical properties with experimental results

Methods	Longitudinal tensile strength (MPa)	
	IM7/8552	AS4/8552
MMF	3376.94	2675.28
Experimental test	2500.65	1995.82

Therefore only four components, T_{f1}, C_{f1}, T_m, and C_m are assigned as modified properties. If local failure of fiber is propagated in an instance, then fiber strength can be chosen as follow.

$$T_f = X_t \max_{i \in fiber} \left(M_{11}^{(i)}, M_{21}^{(i)}, M_{31}^{(i)}, M_{41}^{(i)} \right) \tag{3.13}$$

$$C_f = X_c \max_{i \in fiber} \left(M_{11}^{(i)}, M_{21}^{(i)}, M_{31}^{(i)}, M_{41}^{(i)} \right)$$

Where $M_{jk}^{(i)}$ is component of i−th stress amplification factor. Above equation is obtained by equation (3.8). In the case of matrix failure strength, equivalent stress is defined then it is calculated using iterative procedure. If n_p of equation (3.10) is assumed as 2, then the equivalent stress can be calculated as follow.

$$\sigma_{eq} = \frac{(\alpha-1)I_1 + \sqrt{(\alpha-1)^2 I_1^2 + 4\alpha\sigma_{VM}^2}}{2\alpha} \tag{3.14}$$

Where α is ratio of compressive and tensile failure strength as

previous chapters. To find envelop curve of stress state, p is defined as follow.

$$p_n = \sigma_{eq} T_m \tag{3.15}$$

Iterative procedure to obtain the envelop curve's coefficient is described as Figure 3.8. Initial value of α is given by unit which means same magnitude of tensile and compressive failure strength.

Modified constituent-level failure strength is calculated in Table 3.2, and failure envelops curve using that strength is described in Figure 3.9. Failure strength which is predicted by the iteration is quietly smaller than the value of fiber bundle's tests. It is reason why fiber and matrix failure strength cannot be used directly. MMM is in good agreement with the experimental tests of lamina.

Therefore, it is required to suggest novel upscaling method for failure strength will be discussed. Developed MMM is only effective when it is used with lamina properties.

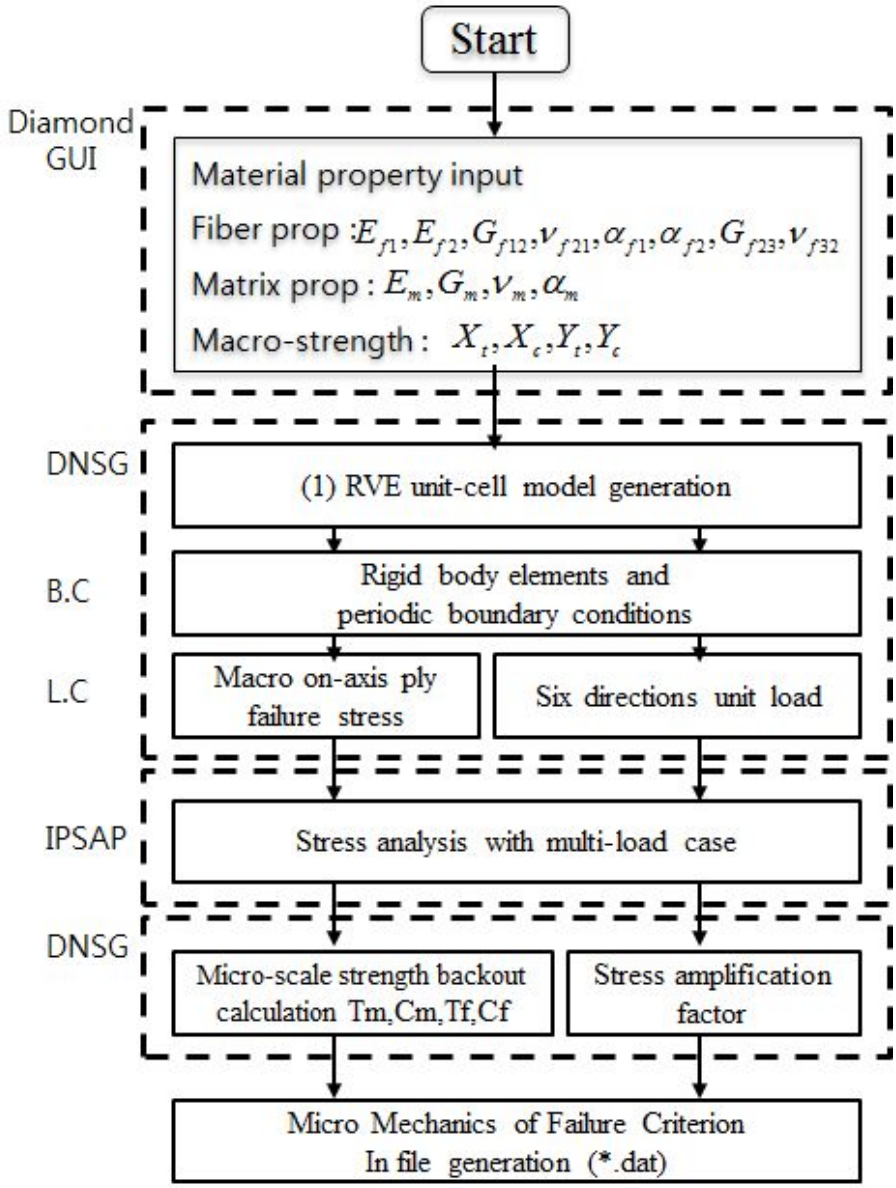

Figure 3.7 MMM procedure to obtain stress amplification factors and micro-scale failure strength using ply-level properties.

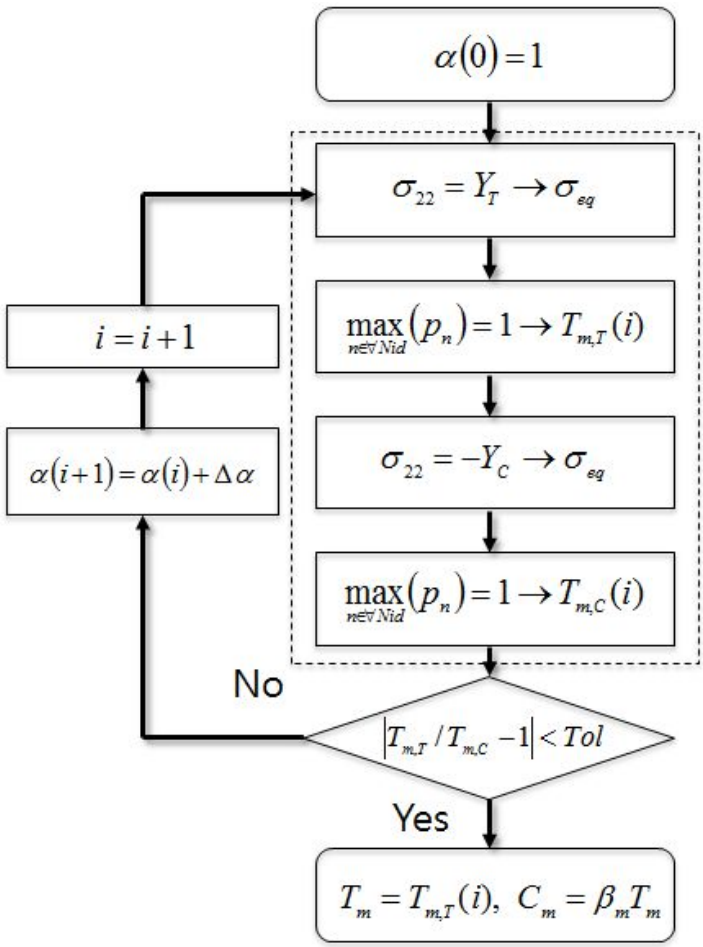

Figure 3.8 Numerical procedure to obtain matrix failure strength using lamina strength

Table 3.2 Constituent strength

Material	Strength Parameter	Original Properties from tests	Modified Constituent Properties
Matrix	T_m[MPa]	120.66	31.384
	C_m[MPa]	-	100.775
Fiber	T_f[MPa]	5480	4934.6
	C_f[MPa]	-	2596.7

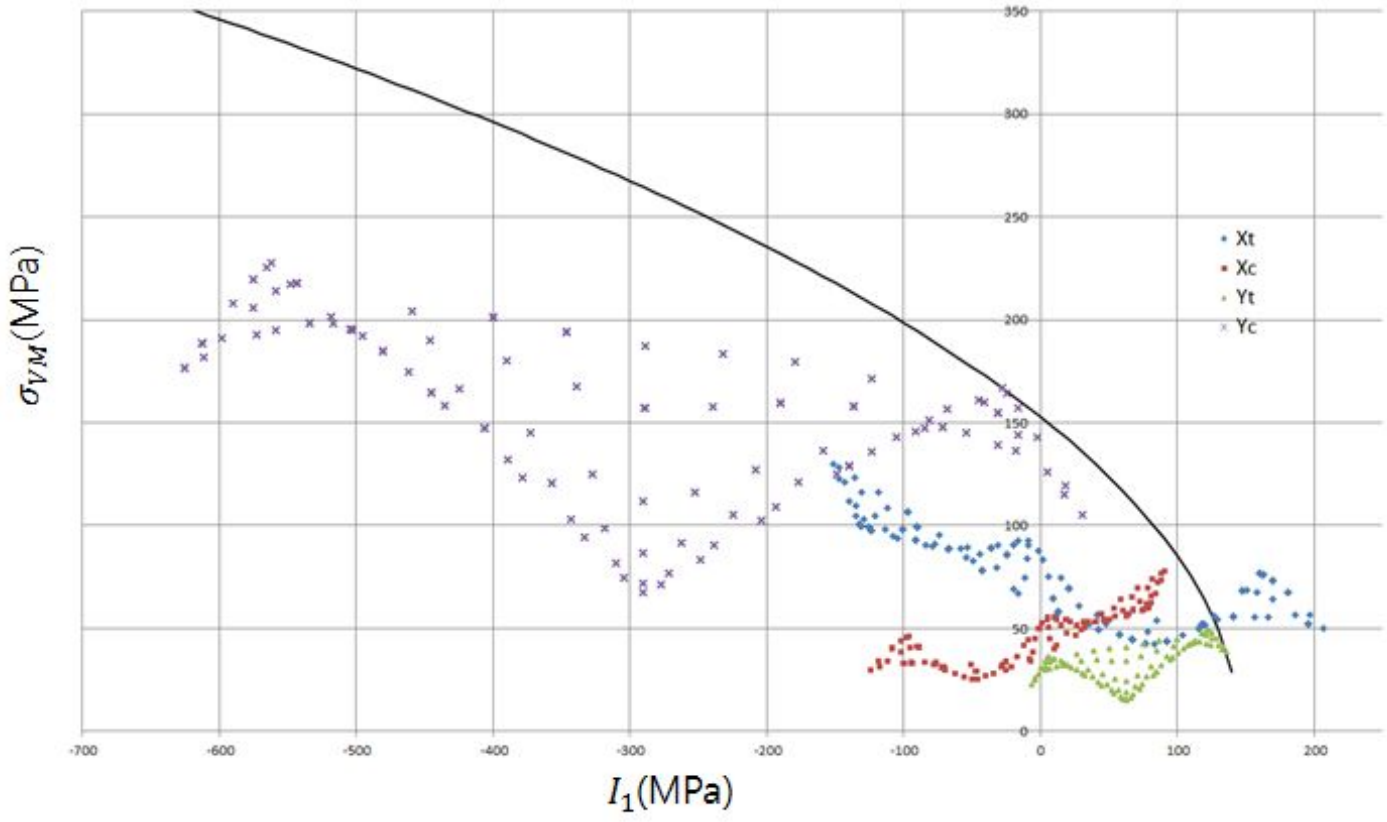

Figure 3.9 Distribution of micro stress invariants in matrix under macro on-axis ply failure stresses (Material : Hexcel 8552/IM7, RTD)

3.2 Micro Mechanics of Continuum Damage

Stress amplification factor in the MMF cannot be used for general PFA solver because degraded properties have no guarantee using stress amplification factor. There are several trials about implementation of stress amplification into PFA. In this chapter, three methods to adapt degradation are introduced.

3.2.1 Micro-scale Degradaton Factor

The degradation methods which are mentioned in Chapter 2 are methods changing material characteristics after initial failure. However, the degradation procedure is a hindrance using stress amplification factor.

In the macro-scale structural analysis using finite element, stress vector is defined as element-averaged value. Equation (3.1) is changed to inequality as follow if degradation is occurred.

$$\boldsymbol{\sigma}^{(i)} > M_{\boldsymbol{\sigma}^{(i)}}(\boldsymbol{\sigma}) + A_{\boldsymbol{\sigma}^{(i)}}\Delta\mathbf{T} \tag{3.16}$$

Where macro-scale stress vector $\boldsymbol{\sigma}$ is expressed as follow

$$\boldsymbol{\sigma} = \mathbf{diag}(\boldsymbol{d}) \cdot \hat{\boldsymbol{\sigma}} \tag{3.17}$$

Where $\mathbf{diag}(\boldsymbol{d})$ is diagonal matrix with diagonal entry of degradation factor $\boldsymbol{d}$. It is required to add damage variables in

Equation (3.16). Micro-scale degradation factor can be considered as one of solution. The degradation of stress amplification factor can be expressed as follow.

$$M_{deg,\boldsymbol{\sigma}_{\boldsymbol{m}}^{(i)}} = \begin{bmatrix} d_m^{mic}M_{11} & M_{12} & M_{13} & M_{14} & 0 & 0 \\ M_{21} & d_m^{mic}M_{22} & M_{23} & M_{24} & 0 & 0 \\ M_{31} & M_{32} & d_m^{mic}M_{33} & M_{34} & 0 & 0 \\ M_{41} & M_{42} & M_{43} & M_{44} & 0 & 0 \\ 0 & 0 & 0 & 0 & M_{55} & M_{56} \\ 0 & 0 & 0 & 0 & M_{65} & M_{66} \end{bmatrix} \quad (3.18)$$

$$M_{deg,\boldsymbol{\sigma}_{\boldsymbol{f}}^{(i)}} = \begin{bmatrix} d_f^{mic}M_{11} & M_{12} & M_{13} & M_{14} & 0 & 0 \\ M_{21} & d_f^{mic}M_{22} & M_{23} & M_{24} & 0 & 0 \\ M_{31} & M_{32} & d_f^{mic}M_{33} & M_{34} & 0 & 0 \\ M_{41} & M_{42} & M_{43} & M_{44} & 0 & 0 \\ 0 & 0 & 0 & 0 & M_{55} & M_{56} \\ 0 & 0 & 0 & 0 & M_{65} & M_{66} \end{bmatrix} \quad (3.18)$$

Then equation is written over again as follow.

$$\boldsymbol{\sigma}^{(i)} = M_{deg,\boldsymbol{\sigma}^{(i)}}(\boldsymbol{\sigma}) + A_{\boldsymbol{\sigma}^{(i)}}\Delta\mathbf{T} \quad (3.19)$$

Above equation includes degraded amplification factor and degraded macro-scale stress. Since it is hard to find continuous micro-scale degradation factor $\boldsymbol{d}^{mic,(i)}$ and macro-scale degradation factor $\boldsymbol{d}$ to satisfy equation (3.19), sudden degradation is used. The micro damage vector $\boldsymbol{d}^{mic,(i)}$ can be defined as different thing according to their material. Therefore, it is required to obtain matrix and fiber damage variable but it cannot be obtained by experimental results, therefore it should be chosen by

engineering sense. Also, it is hard to integrate with PFA procedure including nonlinear iteration.

3.2.2 Degraded Stress Amplifcation Factor

The approach which was suggested in the previous chapter is considering micro-scale damage model. However, the micro-scale damage variable is unintuitive method. Also, it is not proper used with nonlinear iteration. Degraded stress amplification factor was suggested to overcome these shortcomings. It is a method using degraded RVE elements rather than degraded macro-scale elements. Then micro-scale damage of matrix and fiber can be defined. Constitutive equation including the degradation factors is described as follows.

$$\sigma_f = \left(D_f \circ C_f\right)\varepsilon_f,\ \sigma_m = (D_m \circ C_m)\varepsilon_m \tag{3.20}$$

Where D_f and D_m are degradation factors of fiber and matrix. The degradation factor is set as fixed variables if sudden degradation methods are used, otherwise, it should be surveyed by changing degradation. If each degradation is mixed each other, then it is hard to estimate degraded stiffness matrix according to given degradation state of macro-scale. Because fiber failure can be considered as brittle in many cases, D_m have only to survey estimating macro-scale degradation factor. After the matrix

degradation factor is extracted 0.1 to 1.0 uniformly, RVE linear static analysis can be applied. Then degradation factor of micro-scale can be inferred by macro-scale degradation factor as follow.

$$M_{deg,\sigma_m^{(i)}}(j) = \begin{bmatrix} jM_{11}/n & M_{12} & M_{13} & M_{14} & 0 & 0 \\ M_{21} & jM_{22}/n & M_{23} & M_{24} & 0 & 0 \\ M_{31} & M_{32} & jM_{33}/n & M_{34} & 0 & 0 \\ M_{41} & M_{42} & M_{43} & M_{44} & 0 & 0 \\ 0 & 0 & 0 & 0 & M_{55} & M_{56} \\ 0 & 0 & 0 & 0 & M_{65} & M_{66} \end{bmatrix} \quad (3.21)$$

Where $j = 0,1,2,\ldots n$. Then macro-scale degradation factor can be obtained by averaging the stress on the surface of RVE model.

$$\boldsymbol{d_j} = f(j) \quad (3.22)$$

Where $f(j)$ includes analysis of RVE model and post processing to obtain averaged stress of face. $\boldsymbol{d_j}$ is the degradation factor of macro-scale which was referred in the Chapter 2 which is obtained by j-th degradation model of micro-scale in equation (3.21). Then according to the results of PFA, macro-scale degradation factor is calculated by linear interpolation from $\boldsymbol{d_j}$

Degraded amplification factor is used to construct MMF-PFA code in this research after defining micro-scale degradation factor of RVE model.

3.2.3 Upscaling Method for Amplification Factor

Considering degradation of micro-scale model in terms of modifying the stress amplification factor is very inefficient way to reflect micro-mechanics in PFA, because of several reasons. First, in the PFA procedure, most calculation is based on macro-scale properties. Second, constituent properties are hard to obtain comparing with lamina-level of laminate level properties. Third, it consumes too much elapse time rather than macro-scale failure criterion because it should be calculated for nodal points chosen for micro-macro relationship. If non-linear iteration is implemented in PFA procedure, the calculation time of failure criterion has an effect to solver's performance. To overcome these problems, the way to extract stress amplification factor is changed. Using the concept of intact-fiber based stress vector and damaged fiber stress, stress amplification factor is separated from the PFA procedure as Figure 3.10. In this approach, stress based on micro-scale is used for calculating damage variables. However, if the damage variable based on intact fiber stress in contrast with conventional CDM method such as gradual selective stiffness degradation, it is required to obtain intact fiber stress to estimate the damage variables. And degraded stiffness matrix is used to solve structural analysis. Therefore, it is not necessary to obtain micro-scale degradation if noncumulative degradation function is used. In other word, the usage of noncumulative degradation function enables stress amplification factor to be obtained without degraded

amplification factor.

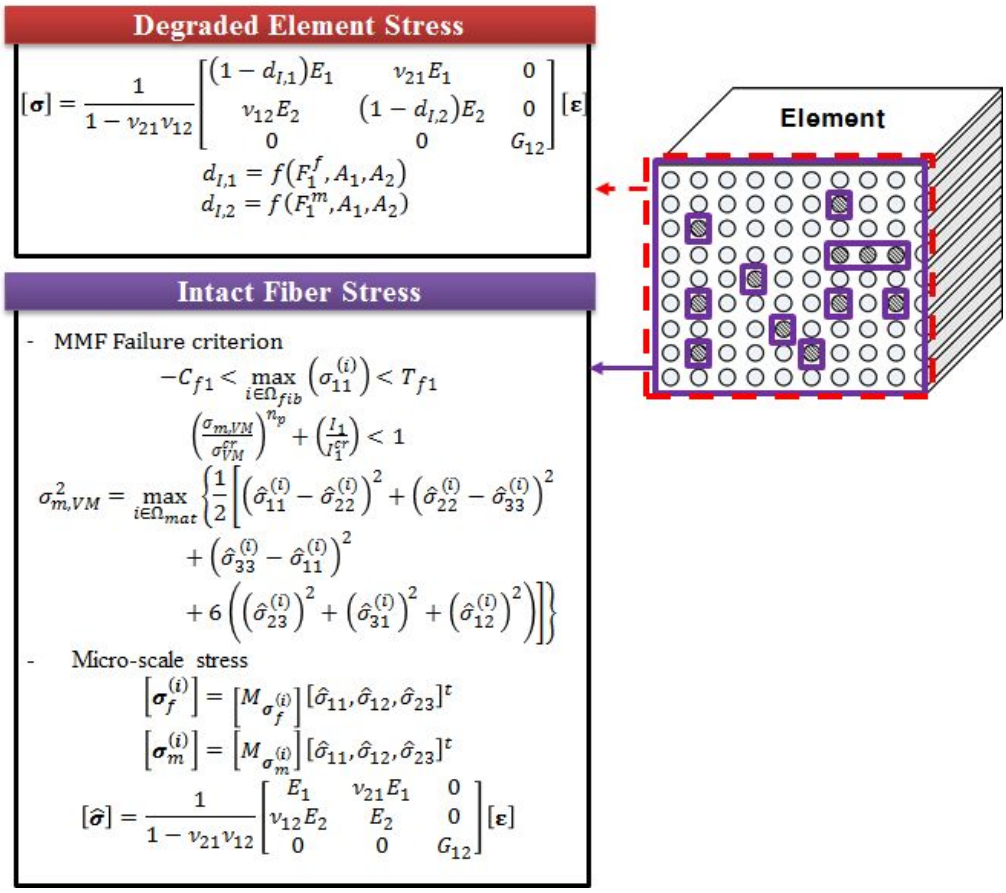

Figure 3.10 Stress amplification factor based on intact fiber stress

3.3 Fiber Bundle Method for Continuum Damage Model

The micro-scale approach to obtain micro-scale failure mode in the section 3.2.3 can be one of method reflect micro-scale mechanics in the PFA procedure. However, it has not guarantee to secure more accurate analysis results. Because fiber strength and distribution depend on fiber fracture behavior of nanostructure, it is necessary to know the relationships between fiber bundle and fiber strength distribution. In order to predict the damage and fiber reinforced composite failure under mechanical loads, several modelling approaches will be available to analyze the load transfer and sharing between fibers in composites. Recently, the reason why MMF results give correspondingly exaggerated failure strength is that MMF theory does not consider about influence of fiber bundle with fiber flaw. In actual problems for laminates properties analysis, ply level material property tests is used instead of fiber/matrix properties because MMF is unable to predict exact properties of the ply. It is the reason why backward calculation for the fiber and matrix strength will be required to set MMF procedure.

3.3.1 Fiber Bundle Damage Model

The development of fiber bundle models encountered two kinds of challenges : it works out realistic models of material failure which have a detailed representation of the microstructure of the material, the local stress fields and their complicated introduction. Such models make possible to clarify the effect of microscopic material parameters on the macroscopic response of solids. In this context, fiber bundle models served as a starting point to develop more realistic micromechanical models of the failure of fiber reinforced composites widely used by the modern aerospace and automobile industry. Analytical methods and numerical techniques have been developed making possible realistic treatment of even large scale fibrous structures.

On the other hand, the damage and fracture of disordered materials addresses several interesting problems also for statistical physics. Embedding the failure and breakdown of materials into the general framework of statistical physics and clarifying its analogy to phase transitions and critical phenomena, still keep scientists fascinated. Here fiber bundle models provide an excellent testing ground of ideas offering also the possibility of analytic solutions.

In this section, sudden-degradation based PFA solvers for fiber bundle model is formulated. After performing PFA analysis for multi-cell based RVE model, the damage evolution model will be generated. Damage evolution model is obtained by three-dimensional representative volume element models. Progressive

failure of the carbon fiber should have a relationship with the nature of brittle material. A sudden degradation property will be useful to predict the behavior of brittle material. According to the previous sentence, stiffness properties of a failed element may be set to zero values. However, sudden degradation method has problems which give underestimated strength and stiffness because it does not account for the residual load-carrying capability that a failed element has in reality. In some cases it may lead to the computational convergence problem that arises from the aero-stiffness in the tangent stiffness matrix. Degradation factors for residual stiffness set as 10% of the original material stiffness will overcome these drawbacks. Constitutive equation including the degradation factors is described as follows.

$$\boldsymbol{\sigma}_f = \mathbf{C}_f \boldsymbol{\varepsilon}_f, \ \boldsymbol{\sigma}_m = \mathbf{C}_m \boldsymbol{\varepsilon}_m \tag{3.23}$$

where $\boldsymbol{\sigma}_f$ is fiber stress, $\mathbf{C}_f$ is stiffness matrix and $\boldsymbol{\varepsilon}_f$ represents mechanical strain of element which has fiber material; $\boldsymbol{\sigma}_m$ is matrix stress, $\mathbf{C}_m$ is stiffness matrix and $\boldsymbol{\varepsilon}_m$ is mechanical strain of matrix element. Because fiber is considered as orthotropic material while matrix to be as isotropic material, it can be written as follows.

$$\mathbf{C}_f = \begin{bmatrix} d_{f1}\mathrm{C}_{f11} & \mathrm{C}_{f21} & \mathrm{C}_{f31} & 0 & 0 & 0 \\ \mathrm{C}_{f12} & d_{f2}\mathrm{C}_{f22} & \mathrm{C}_{f32} & 0 & 0 & 0 \\ \mathrm{C}_{f13} & \mathrm{C}_{f23} & d_{f3}\mathrm{C}_{f33} & 0 & 0 & 0 \\ 0 & 0 & 0 & \mathrm{C}_{f44} & 0 & 0 \\ 0 & 0 & 0 & 0 & \mathrm{C}_{f55} & 0 \\ 0 & 0 & 0 & 0 & 0 & \mathrm{C}_{f66} \end{bmatrix} \tag{3.24}$$

$$\mathbf{C_m} = \begin{bmatrix} d_{m1}C_{m11} & C_{m21} & C_{m31} & 0 & 0 & 0 \\ C_{m12} & d_{m2}C_{m22} & C_{m32} & 0 & 0 & 0 \\ C_{m13} & C_{m23} & d_{m3}C_{m33} & 0 & 0 & 0 \\ 0 & 0 & 0 & C_{m44} & 0 & 0 \\ 0 & 0 & 0 & 0 & C_{m55} & 0 \\ 0 & 0 & 0 & 0 & 0 & C_{m,66} \end{bmatrix}$$

where degradation factor d_{fi} and d_{mi} is further defined as follows:

$$d_{fi} = \begin{cases} 1 & -C_f < \sigma_I < T_f \\ 0.01 & \sigma_I < -C_f \; or \; \sigma_I \geq T_f \end{cases} \tag{3.25}$$

$$d_{mi} = \begin{cases} 1 & \left(\frac{\sigma_{VM}}{\sigma_{VM}^{cr}}\right)^{n_p} + \left(\frac{I_1}{I_1^{cr}}\right) < 1 \\ 0.01 & \left(\frac{\sigma_{VM}}{\sigma_{VM}^{cr}}\right)^{n_p} + \left(\frac{I_1}{I_1^{cr}}\right) \geq 1 \end{cases}$$

If there are no degradation, macro stiffness component can be defined as an inverse of the compliance matrix. Thus, stiffness components can be expressed in terms of effective matrix properties or engineering constants as follows.

$$E_{f11} = \frac{1}{S_{f11}}, \; \nu_{f12} = -\frac{S_{f21}}{S_{f11}}, \; G_{f12} = \frac{1}{S_{f66}}$$
$$E_{f22} = \frac{1}{S_{f22}}, \; \nu_{f13} = -\frac{S_{f31}}{S_{f11}}, \; G_{f13} = \frac{1}{S_{f55}} \tag{3.26}$$
$$E_{f33} = \frac{1}{S_{f33}}, \; \nu_{f23} = -\frac{S_{f32}}{S_{f22}}, \; G_{f23} = \frac{1}{S_{f44}}$$

$$E_m = \frac{1}{S_{m11}}, \nu_m = -\frac{S_{m21}}{S_{m11}}, \; G_m = \frac{1}{S_{m66}} S_{m11} = S_{m22} = S_{m33} \tag{3.27}$$
$$S_{m21} = S_{m31} = S_{m32}$$
$$S_{m66} = S_{m55} = S_{m44}$$

RVE model represents fiber and matrix as material properties while fiber volume fraction is considered as geometrical condition in the analysis. Overall properties for a unidirectional ply can be derived from the constituent properties.

Single fiber strength distribution is used in order to assign random strength value of the multi cell model. Composites strength is dominated by the fiber even if non-linearity can arise from matrix constituent. Therefore, it is important to give accurately single fiber strength as distribution. Single fiber tensile (SFT)tests are widely used for the determination of fiber strength although it presents a problem that the average strength is underestimated. Tanaka [40] suggested the Weibull parameters for the single fiber strength distribution for carbon fiber strand. It can be parameterized as the following well-known Weibull expression.

$$\mathrm{F} = 1 - \exp\left(-\frac{L}{L_0}\left(\frac{\sigma}{\sigma_0}\right)^m\right) \tag{3.28}$$

where two-parameter Weibull cumulative distribution is used. L_0 is a representative length, L is a fiber length, σ_0 is the Weibull scale parameter, and m is the shape parameter, which is obtained by using results by Tanaka [60]. Shape parameter m is controlled for set average of the distribution as experimental mean of single fiber strength.

3.3.2 Multi-cell based RVE Model

Multi fibers unit cell model is shown in Figure 3.11. Its dimension is $10 \times 10 \times 10$ and consists of 20,000 hexahedral elements. Each multi-fiber model is assembled by 10,000 single unit cells which have a different strength value obtained from the single fiber strength distribution. Also it has square array structure. Load conditions for longitudinal tension tests are prescribed by the tensile displacement along the x-axis which is the fiber direction. The degree of freedom in the z-direction of nodes on the top and on bottom is fixed. The nodes, which are located at the boundary surface whose normal vector is along the y-direction, are fixed in the y-direction. This symmetric boundary conditions give similar result to the periodic boundary conditions, for unit cell model. Even if this model does not satisfy the symmetric condition because of considerations for fiber defects, it is reasonable to assume the periodic boundary conditions to make local load sharing from outside cells of the model.

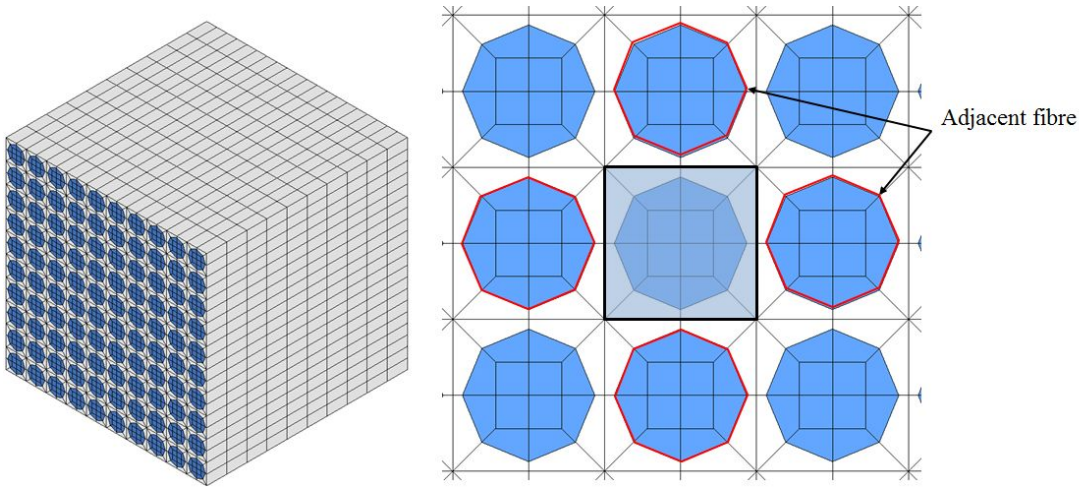

(a) (b)

Figure 3.11 Multi fiber bundle in square fiber arrangement (a) 10x10x10 multi cell FEM model (b) Fiber arrangement and adjacent fiber for local load sharing

3.4 Micro-scale Progressive Failure Analysis

3.4.1 Micro-Mechanics of Degradation

For simulating the multi cell PFA tests under longitudinal tension load, ply-discounting approach which assumes the internal load after failure set as zero is used. 10%, 15%, 20% of coefficients of variation for single fiber strength distribution are used. The distribution is assumed to be the normal distribution.

Figure 3.12 describes a front view of failure index contour under longitudinal tension load of multi cell model after initial failure occurs. Complex damage process initiates with the breakage of the weak fibers. After each fiber exceeds critical load, the loads will be redistributed over the surviving intact ones. These loads are shared by adjacent fibers according to PFA results. It means that the local load sharing occurs rather than global load sharing does. In this analysis, even if no damage evolution method is used, damage evolution will occur after failure initiated. This mechanism is described in Figure 3.13. Each fiber has four adjacent fibers which carry the load after weak fiber is broken. In the description, the green area has lower strength, than the purple one has. The fiber which is marked with red is located in the same position with the green one. And all of them have lower strength than the overall strength of fiber. After first fiber occurs through ply stress, σ_{∞} will reach $\delta_2 X_{f,avg}$. By definition of the solid elements degradation in

Equation (3.24), the stress of the broken position should be close to zero. Then adjacent fibers will receive the load instead of the broken one (green curve). If the distance between two weak fibers is larger than critical distance between fiber breaks, the bundle will not break unless the summation of distributed stress from broken and adjacent fiber itself reaches failure strength (blue curve). However, when some fibers are broken near the weaker fibers, intact fiber may receive the load greater than their

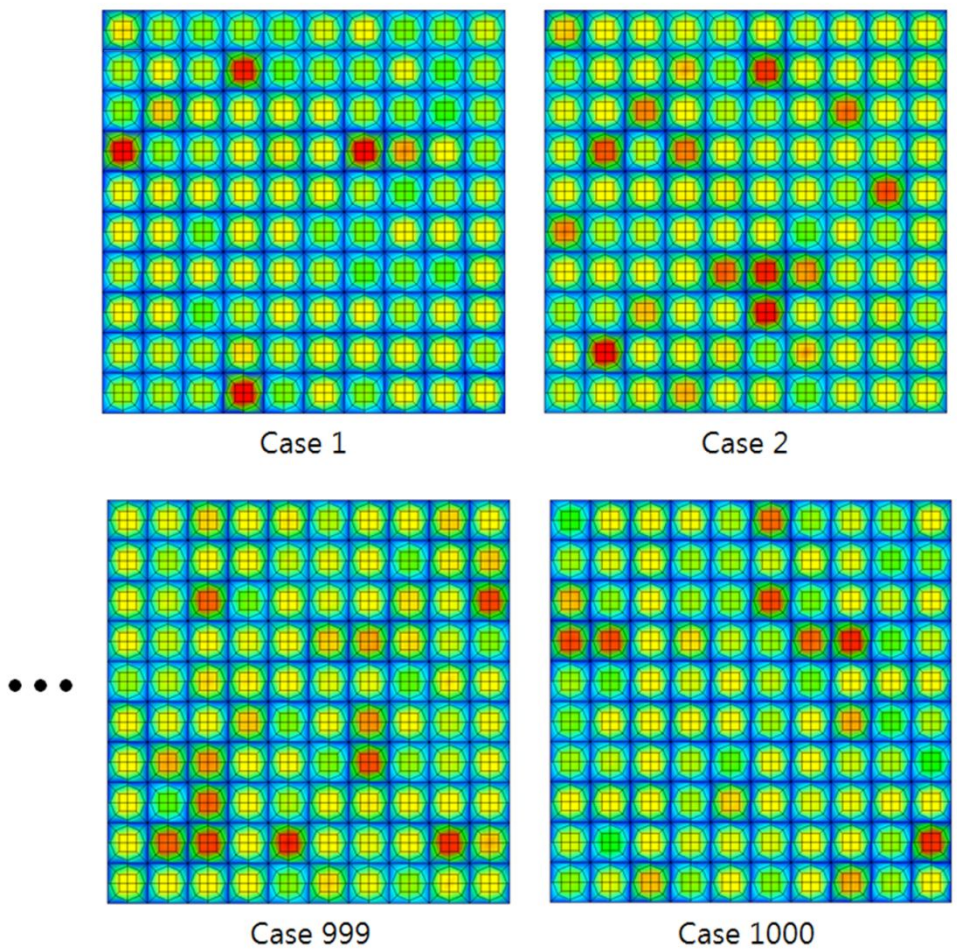

Figure 3.12 Failure index contour of multi-cell PFA analysis under longitudinal tension loads with random fiber strength

endurance. If the stress exceeds$X_{f,avg}$, it cannot withstand the load anymore. Then it leads to bundle failure. Figure 3.14 is one of the examples for such analysis. The load sharing occurs locally, and then it seems to little affect stress of fiber which is apart from the broken fiber.

Damage evolution model can be captured when macro scale analysis is performed. Moreover, a degradation curve of multi-cell depends on the distribution of fiber strength and their arrangements. Therefore, it is required to process the statistical results of multi-cell analysis. As a result of the evolution of the fracture process, residual stiffness of the cluster is decreased. Figure 3.15 describes the stress-strain curves of longitudinal tension tests of multi-cells. The cluster has lower failure stress when weak fibers are concentrated locally, while it has upper critical stress when weak fibers are evenly distributed. Dependence on the coefficient of variation of single fiber strength distribution is ascertained.

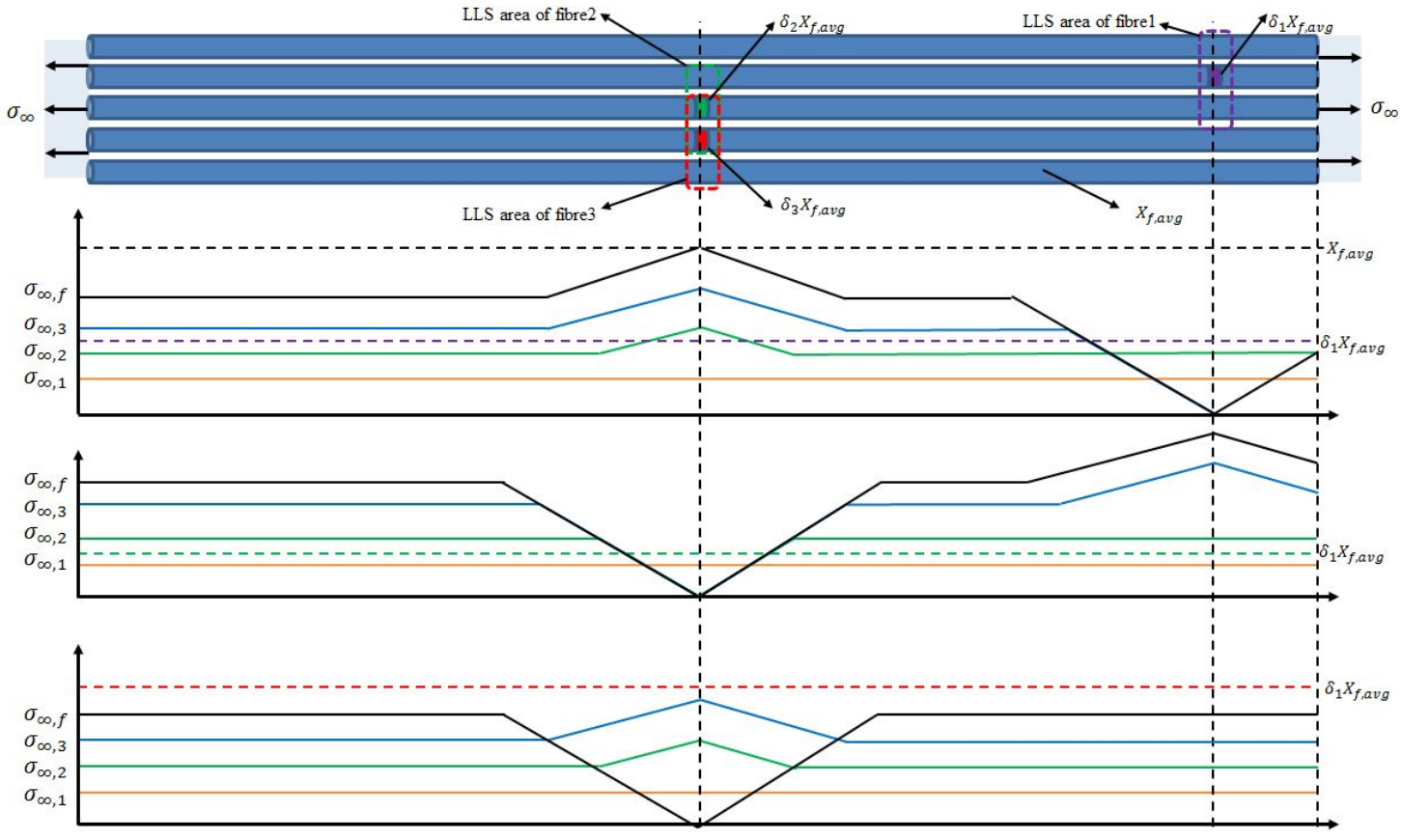

Figure 3.13 Stress field under an increasing load of fiber bundles.

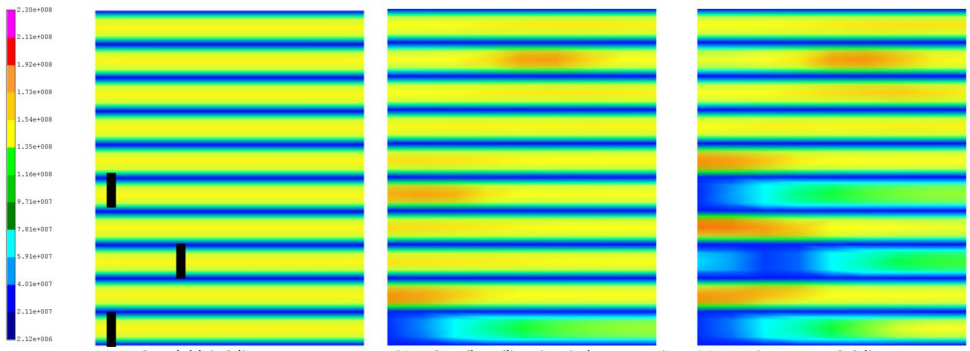

Figure 3.14 Load sharing after local failure initiation

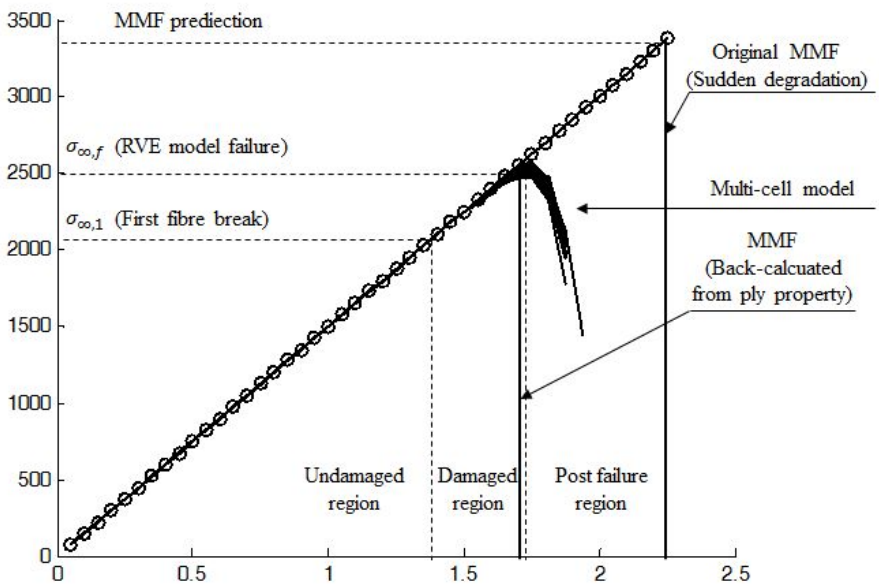

Figure 3.15 Stress vs. strain curve of RVE model analysis results and MMF prediction under longitudinal tension condition (20 samples)

3.3.2 Computational Procedure for Micro-scale PFA

Micro-scale PFA is solved by IPSAP, because it is supposed to solve both solid and shell problems for nonlinear PFA. Figure 3.16 shows the specific procedure to obtain those degradation factors.

First of all, the statistical distribution of single fiber strength should be defined. Generally, the distribution can be described as Weibull or normal (standard) distribution. Both cases have two or three parameters, including the location parameter. Discrete data of failure strength for single fiber can be expressed by using two-parameter Kolmogorov-Smirnov (K-S) test. Until p-value of assumed distribution exceeds 0.05, K-S test should be repeated while changing Weibull parameters a_1 and a_2. The Weibull parameters are used to generate strength distribution of multi-fiber representative volume element model. Using the random variable α which has values from zero to unity, random distribution of strength will be obtained, then, the unit cells are generated. And, then the cells are clustered as multi-fiber unit cell. After solving the PFA of multi-fiber model, degradation curves are obtained by stress-strain curves. Micro-mechanical properties should be assigned to describe the material properties of the multi-fiber model. The cumulative density function for macro scale PFA will be obtained by thousands of the failure strengths which were obtained from micro mechanical model analysis. In this paper, K-S test will be repeated until macro scale parameters A_1, A_2 and h becomes settled.

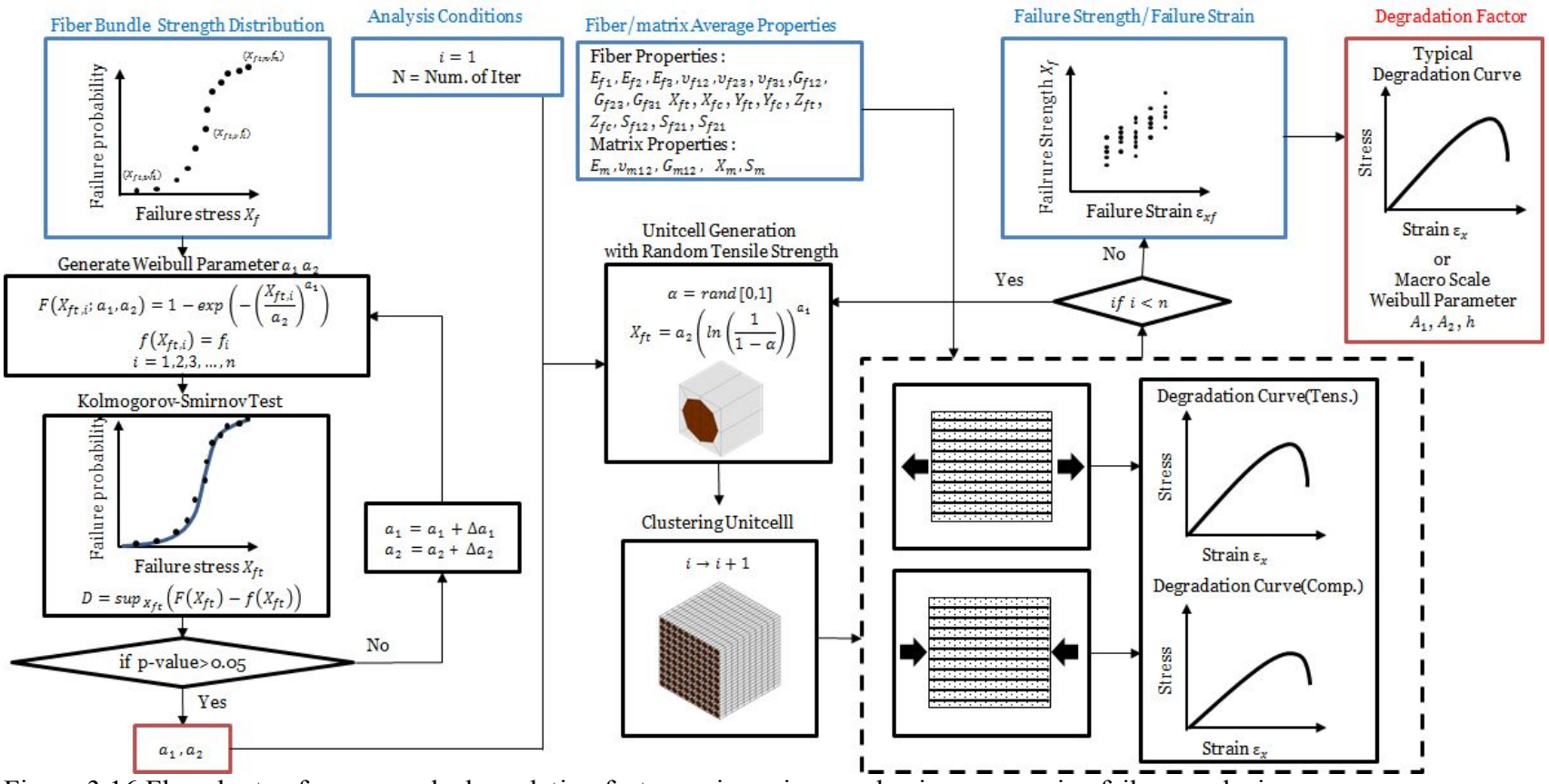

Figure 3.16 Flowcharts of macro scale degradation factors using micromechanics progressive failure analysis

3.4.3 Determination of Weibull shape and scale parameter by statistical approaches of micro-scale analysis

Further, the micro level PFA results from the previous sections can be used to set degradation factor of the macro-scale model. In conventional multi-scale approaches such as MMF and SIFT, micro mechanics are reflected in failure mode only. It has an advantage over macro scale failure criteria like Hashin, Tsai-Wu and Tsai-Hill, in terms of predicting exact initial failure of laminates. However, critical value of strength is strongly influenced by weak fiber instead of average strength of fiber in practice. It is obvious that MMF methods predict relatively larger failure strength rather than experimental results when weak fiber exists. Also, in order to solve the problems, macro-scale stress and strain should be used because all the mathematical formulations of PFA require it. Therefore, even if all the micromechanical properties are identified, laminates properties should be derived to enforce static equilibrium. It presents an obstacle to predict post failure behavior using the degradation factor. If fiber or matrix failure is detected, material degradation should be applied for the constitutive equation. After degradation occurs, elemental failure index becomes smaller than unity because their elastic modulus is decreased while strain is not changed. Thus it is impossible to divide macro-scale stress into micro-scale stress after failure is initiated. For this reason, it is difficult to combine micro-scale stress with material degradation. It is the reason why macro-scale failure mode is preferred than that

for the micro-scale.

Consequently, macro-scale failure mode is used to set initial failure of the shell elements. Also, PFA results of fiber bundle model can be used as degradation parameter for macroscopic model because post failure behavior depends on the number and arrangement of weak fiber. In order words, micro mechanical approaches can be used to take degradation factor instead of searching initial failure. For that, it is necessary to set element size to be the same as RVE model size for multi-fiber unit cell in order to remove size effect of degradation process.

Degradation factor is obtained by typical curves of stress vs. strain obtained from the RVE analysis. Three Weibull parameters are used to obtain approximate curves from the result. Shape and scale parameters are influenced by weak fiber distribution while location parameter is defined as ratio of weakest and average fiber strength. Degradation curves using the three parameters are approximated from a thousand RVE analysis results are shown in Figure 3.17. It is representative cumulative density function of degradation factor according to intact failure index.

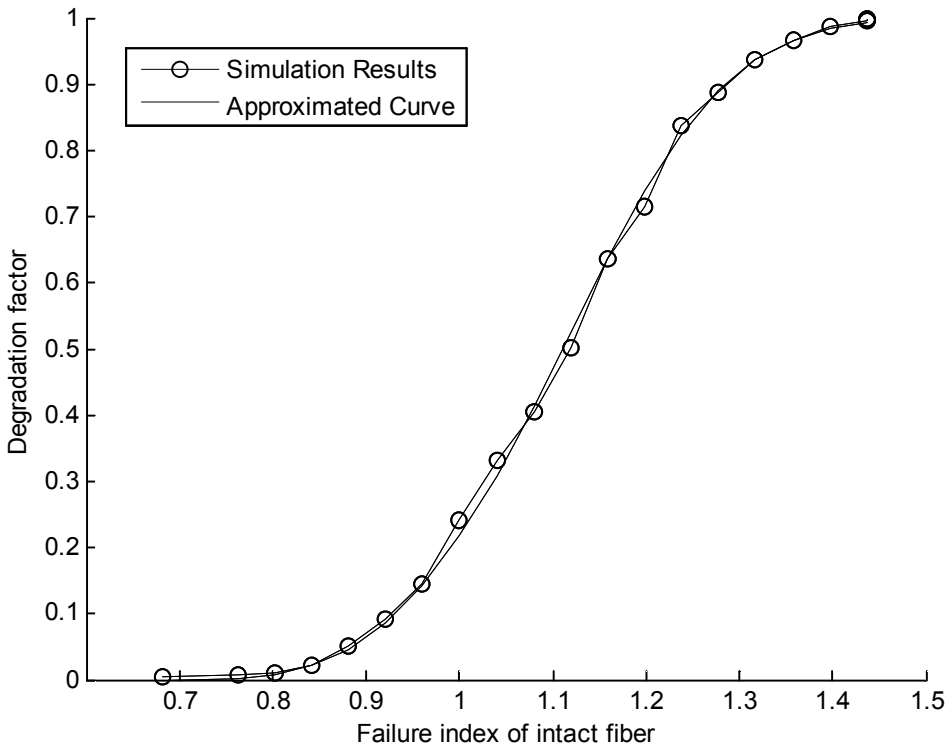

Figure 3.17 Representative cumulative density function of degradation factor of IM7/8552 material

3.5 Multi-Scale PFA Procedure using Micro Mechanics of Damage

PFA procedure is reconstructed for adopting multi-scale approaches as shown in Figure 3.18. The procedure is divided into the following two steps. The first step is to obtain degradation factors in order to set CDM model. It is required to use the statistical method to analyze micro mechanics of fiber failure. Pre/post-processor program, i.e., Diamond/IPSAP, produces a 3-D unit and multi cell model of composite including pre-defined random parameters for a fiber bundle. Each case has different stress-strain curve induced from difference in the strength. After gathering the strength data from PFA, cumulated distribution function (CDF) will be obtained by strength results.

Laminate analysis should be done by using the shell elements. Otherwise, it will be required to use multiple elements through the thickness for solid elements. Because composite laminates typically behave in a linear elastic region unless initial failure occurs. Therefore, if degradation does not occur ($d_i = 1$), tangential stiffness matrix will not be changed. Accordingly it follows the linear analysis procedure, in which the applied load is increased, and the analysis continues. If failures occur by stress criterion based on the failure, failure index will be obtained by degradation factor from statistical results of micromechanics PFA analysis. Using material degradation, a change in the stiffness matrix will be estimated. This adjustment accounts for the material nonlinearity

associated with PFA embedded within a nonlinear finite element analysis. It is required to re-establish static equilibrium by repeating the nonlinear analysis at the current load step using the updated material properties from tangent stiffness matrix. The number of the degraded elements can be increased as well as failed element degradation factor can be selected. Such iterative procedure will be repeated until additional displacement is reached within the tolerance. Displacement increment is preferred rather than load increment because it is more suitable to Newton-Raphson method. If initial load is given by force, linear static analysis will be performed to obtain displacement boundary conditions.

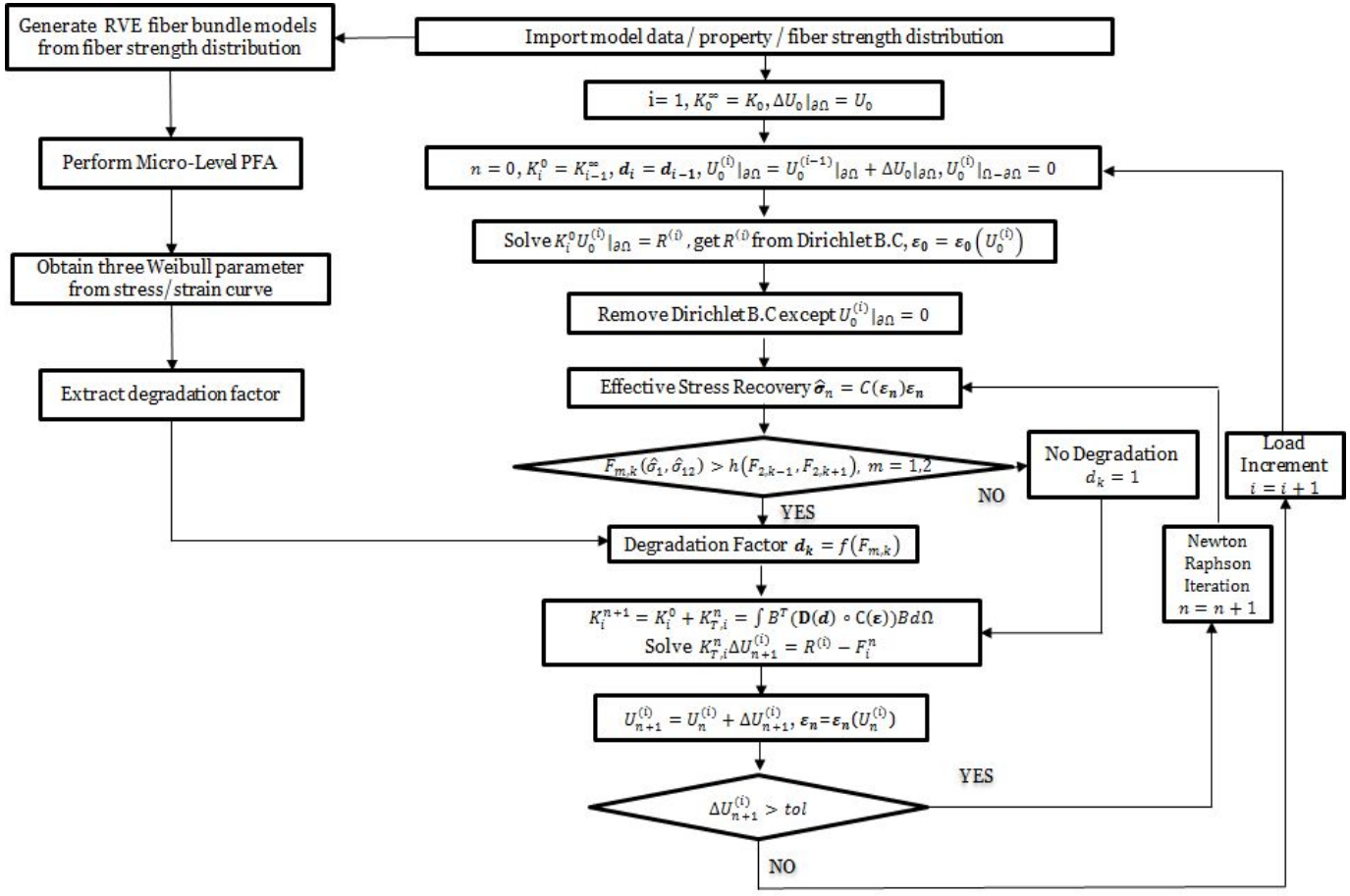

Figure 3.18 Multi-scale progressive failure analysis procedures

3.6 Open-Hole Tension Results for Quasi-Isotropic Laminates

3.6.1 Laminates Problems Description and Comparable Model

Figure 2.25 summarizes a model for laminates tension tests. Four groups of different laminates problems are considered in this section. Open-hole tension cases with IM7/8552, AS4/8552 are solved by developed PFA code. The composite material properties and uniaxial strength used in the demonstration are listed in Tables 3.3 and Table 3.4. CDM parameters which are obtained by RVE analysis are applied to solve these examples. The present models are based on ASTM D5766, which is a standard test method for open-hole tensile strength of polymer matrix composite laminates. Each coupon test type is described in Table 3.5. Three kinds of stacking sequences are considered to validate the present PFA analysis. OHT1, which is composed of 50/40/10 lay-up, has fifty percent of 0° plies. In this case, 45° and -45° plies will have small proportion for sustaining tensile load. Even if those plies have high non-linearity in the shear direction, it will seldom affect laminate's failure strength. In fact, its contribution is one-tenth of the strength or stiffness of a 0° ply to the overall performance of the laminate. Stiffness will not be changed much because the change mainly originates from the angle plies. OHT2 which is set as 25/50/25 lay-up is called as quasi-isotropic lay-up because it

exhibits isotropic in-plane response. And OHT3 consists of eighty percent of $45^\circ/-45^\circ$ plies and only ten percent of 0° plies. Thus the angle plies contribute half of the strength in OHT3 case.

Table 3.3 Material properties of the carbon/epoxy unidirectional laminate (IM7/8552 and AS4/8552)

Material Properties	Ply (IM7/8552)	Ply (AS4/8552)	Fiber (IM7)	Fiber (AS4)	Matrix (8552)
Fiber volume fraction V_f (GPa)	0.6	0.6	1	1	0
Longitudinal modulus E_1 (GPa)	159	127	276	225	4.60
Transverse modulus E_2 (GPa)	8.96	9.24	19	15	4.60
Shear modulus $G_{12} = G_{13}$ (GPa)	4.69	4.83	27	15	1.70
Shear modulus G_{23} (GPa)	-	-	7	7	1.70
Poisson's ratios $\upsilon_{12} = \upsilon_{13}$	0.316	0.302	0.2	0.2	0.35
Poisson's ratio υ_{23}	-	-	0.351	0.071	

Table 3.4 Uniaxial strength of materials

Material Properties	IM7/8552	AS4/8552
Longitudinal tensile strength X_t (MPa)	2500.65	1995.82
Longitudinal compressive strength X_c (MPa)	1716.37	1397.56
Transverse tensile strength Y_t (MPa)	64.05	63.91
Transverse compressive strength Y_c (MPa)	285.72	267.86
Shear strength (5% strain)	91.15	91.56
Fiber tensile strength (MPa)	5450	4600
Matrix tensile strength (MPa)	120.66	120.66

Table 3.5 Lay-ups for OHT coupon tests

Case	Lay-up (%0°/%45°/%90°)	Stacking sequence
OHT1 (hard)	50/40/10	[0/45/0/90/0/-45/0/45/0/-45]s
OHT2 (quasi-isotropic)	25/50/25	$[45/0/-45/90]_{2s}$
OHT3 (soft)	10/80/10	[45/-45/90/45/-45/45/-45/0/45/-45]s

Prediction of failure initiation and propagation can be affected by PFA algorithms. And their accuracy can be improved by failure criteria to find failure initiation and degradation method to cause accurate estimate propagation. In this paper, thus, the following two methods will be used for comparing accuracy of PFA results. Gradual Selective Stiffness Degradation (GSSD) is a method taking degradation by accumulated damage using failure index with macro-scale failure criteria. It is a method using macro scale degradation method. The damage is calculated by macro-level stress, and the degradation factor should be given as input variables. It can also be affected by load increment. Damage variables are obtained from quadric failure criterion like Hashin failure criteria or Tsai-Wu failure criteria, while element averaged stress is used to get failure index. It is great difference from the present attempt. In GSSD method, failure index of elements is smaller than unit after initial failure occurs. Thus there are no additional load sharing before additional external load is applied. Therefore failure index will remain to be approximately unity. In this model, material nonlinearity is involved in degradation factor, and thus it cannot

satisfy nonlinear material property from longitudinal tension and shear experiment of ply precisely. Also, it adopts forward integral for load increment because it is impossible to satisfy force equilibrium for GSSD. Alternatively, the PFA procedure in NASTRAN solves repeatedly linear problem which uses re-assembled stiffness matrix with integrated damage variables.

On the other hand, MMF analysis can obtain improved results in an advanced way to determine failure initiation by multi-scale approaches. However, a predicted laminate strength from MMF-PFA has lower accuracy because it has no guarantee about ply and constituent properties. In this paper, to improve the results from MMF, fiber and matrix strength is estimated backwards from the ply properties. After fiber failure occurs, their residual stiffness is set as 1% of intact element because the stiffness matrix must be a non-singular matrix. Such setting prevents the problem from numerical error. Also, the PFA procedure cannot be used nonlinear properties since it has difficulty to apply nonlinear procedure for a stress amplification factor. The factor is defined as relation between macro and micro level stress, and thus it is impossible to use the factor when gradual stiffness degradation occurs.

The third suggestion is using the present PFA procedure. It contains elasto-plasticity properties about shear modulus and nonlinear elasticity in a fiber direction. The two nonlinearities are separated from degradation factor which is defined by strength distribution of fiber bundle model. Material nonlinearities are obtained by the ply test results meanwhile MMF used tuned factor

for MMF criteria. NASTRAN uses tuned degradation factor and load increment step by in-plane shear test.

3.6.2 Open-Hole Tension Results

The PFA results of laminates using three different stacking sequences are described in Figures 3.20 and Figure 3.21. Comparison experimental results are obtained from NCAMP database. Minimum, maximum, and averaged value of strength is used. Final strength of OHT is calculated when summation of internal force of the right hand side node has peak value. External forces may be different from the summation before force equilibrium is satisfied. As shown in the procedure in Figure 3.18, even if displacement step is given to describe force increment, it should be converted to external force to conduct Newton-Raphson iterative procedure. Initial force increment is determined by displacement increment but it is not equal to peak internal force. Therefore there is no equilibrium, and the analysis is finished. Therefore, the load-displacement graph can be broken up to failure strain. It is a difference of the PFA of this paper and GSSD which is used in NASTRAN. In the case of NASTRAN, peak value predicts strength but post behaviour of failure can appear. In general, PFA results from NASTRAN give convex curves. Because MMF uses sudden degradation method, it is terminated after it has peak value of internal load.

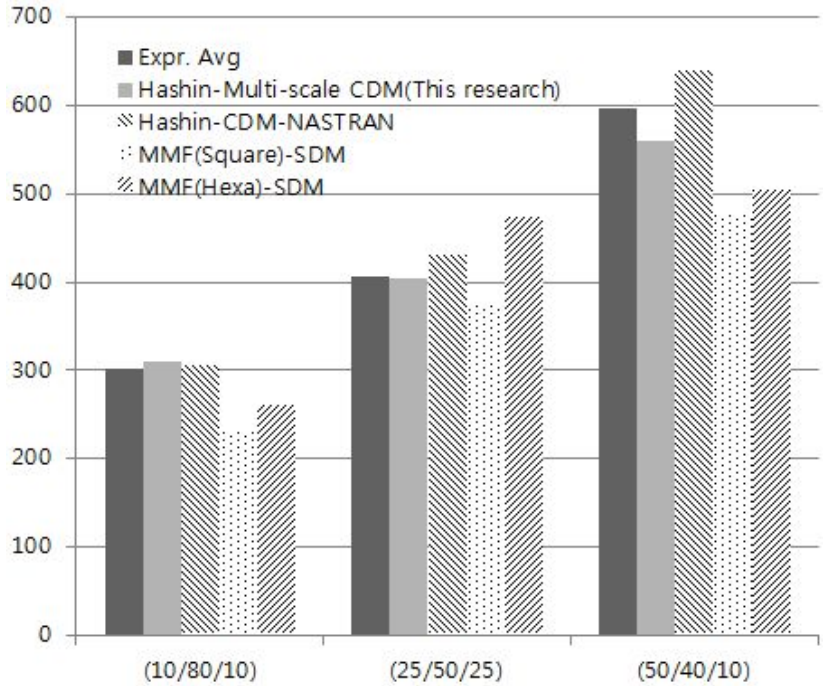

Figure 3.20 Comparison of result predicted by different methods for ultimate strength of IM7/8552

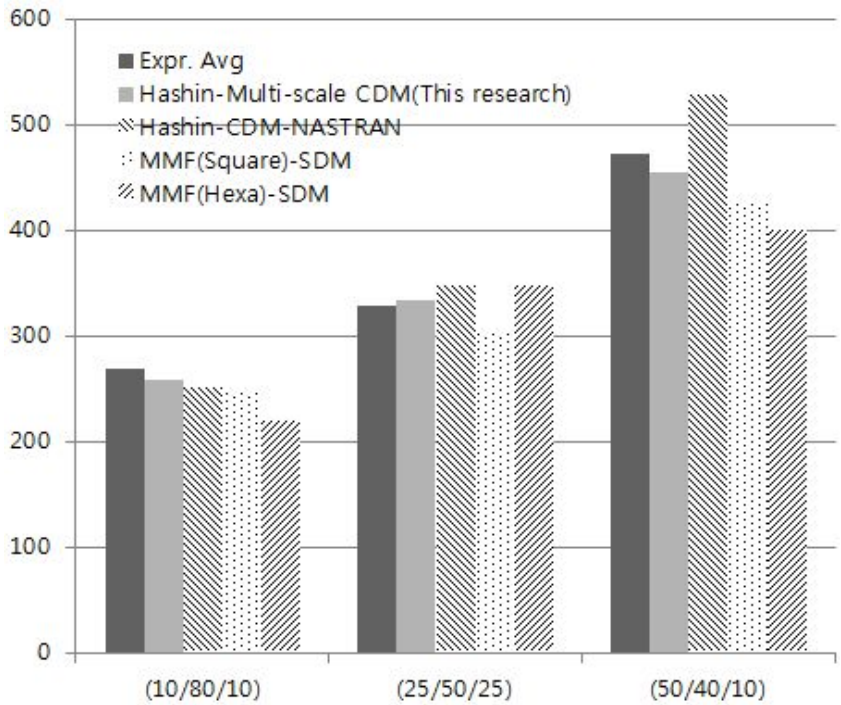

Figure 3.21 Comparison of result predicted by different methods for ultimate strength of AS4/8552

Failure index and damage variables just before rupture are described in Figures 3.22 for each case. Nonlinear procedure for PFA enables failed elements to redistribute internal load to adjacent elements.

The multi-scale approach which is used in this paper gives more accurate results comparing with the other analysis results for most of stacking sequence and material. At first, OHT1 has fifty percent of 0° plies, thus there are few contribution of internal force from 45°, -45° and 90°. Actually, 0° plies contribute to the internal force about 90% or more. Therefore, this sequence is influenced by failure initiation of 0° plies. If the other plies are broken in advance, shared load from the plies is negligible value comparing with load increment of the fiber direction plies. Therefore, degradation method of fiber direction is a major influence to obtain the failure strength. In the case of NASTRAN results, the strength prediction is accurate about IM7/8552 while the strength of AS4/8552 has relatively large strength value from NASTRAN. MMF gives relatively small strength because it was hard to transfer the load after failure is initiated. Because this approach does not have residual stiffness after failure, the averaged stress of the right side immediately after initial failure becomes the final strength. Therefore, it is smaller than the other predictions. PFA results suggested from this paper gives best results among the three ways. This suggests the attempt to describe load sharing after failure initiation occurs in fiber direction was applied with success.

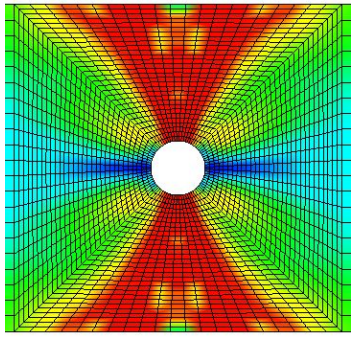

(a) $\boldsymbol{f_1}$ distribution with (50/40/10) lay-up

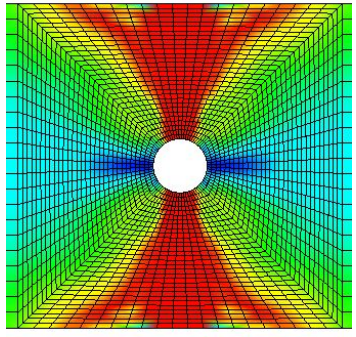

(b) $\boldsymbol{f_1}$ distribution with (25/50/25) lay-up

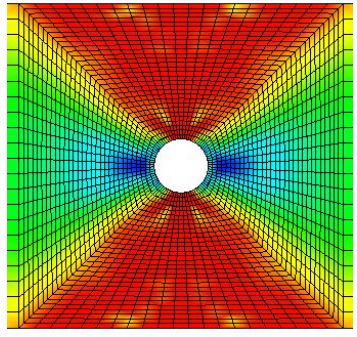

(c) $\boldsymbol{f_1}$ distribution with (10/80/10) lay-up

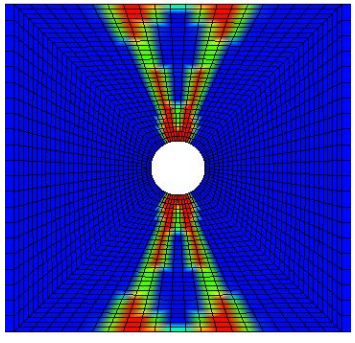

(d) $\boldsymbol{d_1}$ distribution with (50/40/10) lay-up

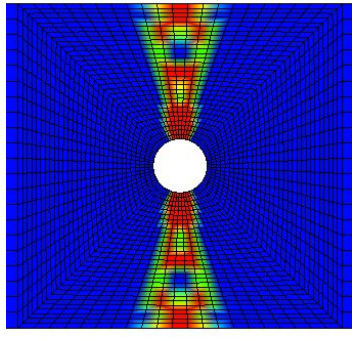

(e) $\mathbf{d_1}$ distribution with (25/50/25) lay-up

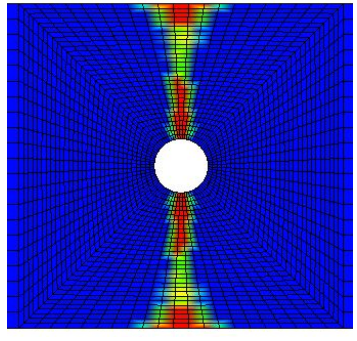

(f) $\mathbf{d_1}$ distribution with (10/80/10) lay-up

Figure 3.22. $\mathbf{0}°$ layer's failure index $\boldsymbol{f_1}$ and damage variable $\boldsymbol{w_1}$ distribution of fiber direction about each lay-up just before rupture

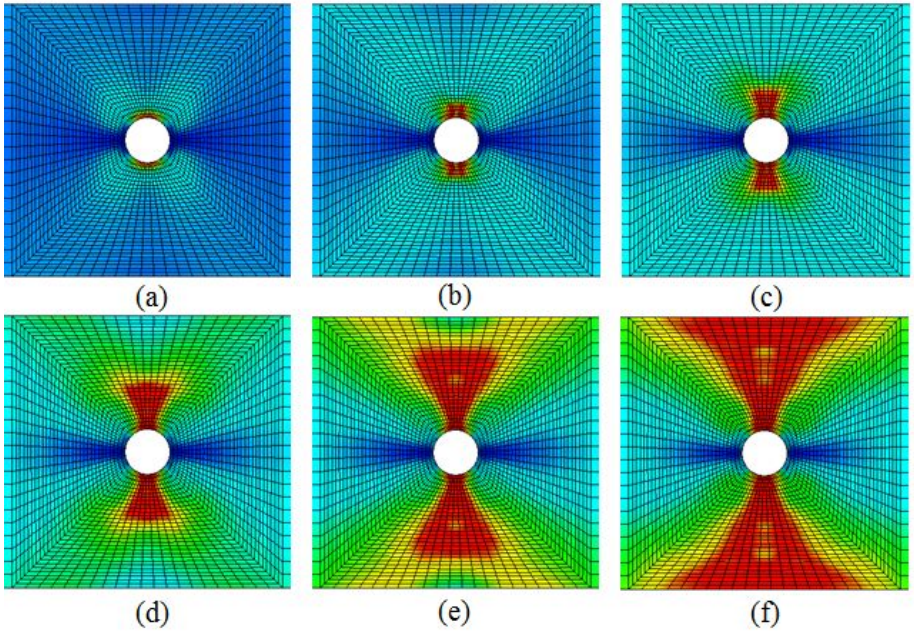

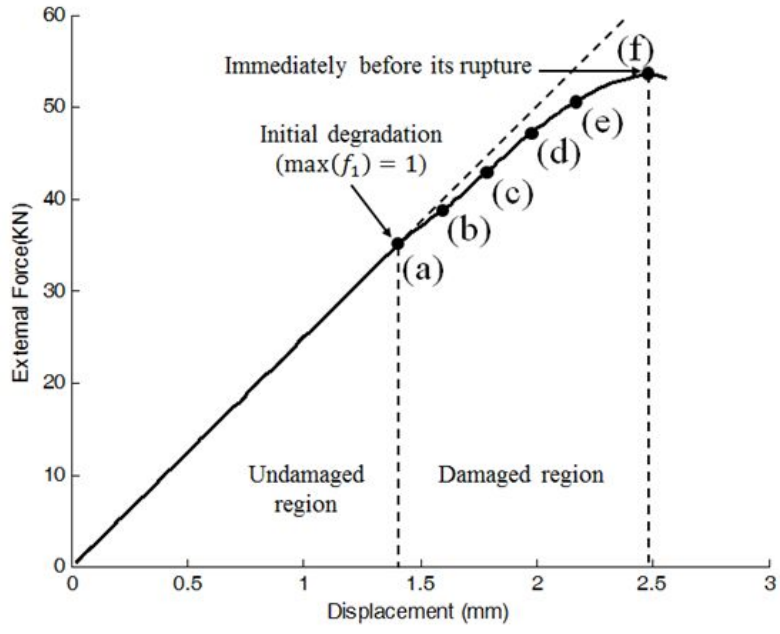

Figure 3.23 Force vs displacement curve with quasi-isotropic lay-up of IM7/8552

Inasmuch as OHT1 does not appear shear non-linearity, it indicates the results are improved by assumed degradation from the present fiber bundle model.

As a second, even if OHT2 has one fourth of 0° plies, which is half of 45°, -45° plies, it still predominates the other plies in terms of fraction of internal load. After initial failure locally occurs in 0° plies, it can be sustained by the other plies and adjacent elements. Therefore, there are difference between initial failure and final failure. It can be confirmed in Figure 3.23. MMF predicts too large strength since failure initiation occurs too late. NASTRAN and the present results give improved results comparing with MMF, because load can be shared after failure occurs as OHT1 case.

Third case using 10/80/10 composition has highly nonlinearity in shear direction. Only ten percent of plies have 0° of fiber direction while most of them are angle plies which have shear non-linearity. Their composition of internal load is almost the same. In this case, assumed nonlinear model affects the results. NASTRAN and the present results have an approximate value of strength. In here, initial failure is comparatively negligible because the load after initial failure of 0° plies can be sustained by neighbouring elements and plies. Because Hashin failure criterion improves the results of shear nonlinearity by coupling longitudinal tension and shear stresses, NASTRAN results also gives accurate strength value if displacement increment is set properly. MMF case gives bit un-reasonable results because it uses sudden degradation method.

3.7 Chapter Summary

The results can be summarized as follows. First, existing multi-scale approaches like MMF have no effect for stress concentrated situations because it requires sudden degradation method to describe stiffness degradation. On the other hands, GSSD method ensures accuracy of strength, although it requires additional input variables. Also, GSSD used in NASTRAN requires suitable load increment step to obtain guarantee of strength. But it does not have any physical meaning but numerical treatment. Therefore, the settings do not guarantee for the other stacking sequence and materials. In contrast, the present PFA method maintains physical sense in an appropriate manner.

3.7.1 Physically meaningful degradation model features from micro mechanic model.

Material nonlinearity and damage variables are used to derive damage variables to set CDM model. The CDM model was adapted into the present solver. Conventional CDM method decides damage variable empirically and then it requires appropriate load increment and degradation factors. It is restricted to specific stacking sequence, and thus it has no guarantee about the other laminates. In this paper, RVE model using multi-cell is modelled with two constituent material, fiber and matrix. Newton-Raphson method enables force equilibrium to balance but it is unable to use in the

conventional PFA procedure since nonlinear iterative method is not compatible with accumulated damage. This restriction was overcome by separating intact element stress which has a role to determine failure index from element-averaged stress for the PFA procedure. Moreover, CDM coefficients can be obtained from experimental results of single fiber strength distribution. There is a little effort needed to obtain additional properties.

3.7.2 Significance of fiber bundle for micro mechanics of failure

Micro-mechanics based RVE model from fiber bundles is used to reflect three-dimensional characteristic of fiber-reinforced composite material in micro-level. MMF methods do not have any components to describe fiber direction in calculation of stress amplification factors. MMF approaches are outstanding methods to configure failure mode of fiber, matrix and interface, but it will provide unreasonable prediction for the stress concentrated examples like an open-hole specimen. It is an effective method when un-notched cases with various force combination. Also, it does not give any guarantee of compatibility of micro level constituent properties and ply properties. It is limitation of representative model of multi-scale approaches.

In contrast to the above, RVE model is extended to multi-cell model with defect fibers which have lower strength comparing with their adjacent fibers. It induce post behavior after initial failure of fiber, thus degradation can be measured using the multi-cell model.

As mentioned previously, local load sharing after weak fiber failure occurs, thus stiffness is degraded continuously. After receiving load pass peak points, it is able to withstand somewhat of the external load. It generates large difference when initial failure occurs locally. Using the degradation model from fiber bundle, it is able to postpone rupture of the coupon. It is maintained until the coupon is applied over several load steps. If the coupon is split up to two pieces, the analysis will be terminated because it cannot find force equilibrium. This method will be applicable identically even if it has different lay-up and material. So it has the advantage of properties prediction, especially, when failure occurs locally. Also, in the proposed method, damage variables are directly obtained by intact element's failure index rather than cumulating damage variables. Therefore it is not influenced by the load increment amount.

Chapter 4. Applications to Laminate PFA Test

In this chapter, several applications of laminates are solved using proposed PFA solver. In this chapter, laminates properties of carbon epoxy CP150NS/K.015, IM7/8552 and AS4/8552 are discussed from the lamina properties. After the material's property of lamina is tested using MTS machine, then it is used as input variables of PFA simulation test of laminates. First, experimental environment and target problem will be discussed. Second, numerical model of nonlinear materiality is acquired as the parameter which is defined in the previous chapter. Last, laminate failure strength for each lay-up is predicted using present PFA solver.

4.1 Methodology

4.1.1 Specimen Dimensions & Testing Details

Specimen dimensions and detail conditions are described in this section. Every test dimensions is based on American Standard Test Method (ASTM). Open-Hole Tension (OHT) and Open-Hole Compression (OHC) are the test methods to evaluate failure strength of composite material. All tests are in accordance with ASTM. Specific mechanical property test methods applicable to the test in this chapter include:

- ASTM D3039/D3039M-08 – Standard Test Method for Tensile Properties of Polymer Matrix Composite Materials
- ASTM D3518/D3518M-94(2007) – Standard Test Method for In-Plane Shear Response of Polymer Matrix Composite Materials by Tensile Test of a ± 45° Laminate In-Plane Shear Strength and Modulus
- ASTM D5766/D5766M-02a – Standard Test Method for Open Hole Tensile Strength of Polymer Matrix Composite Laminates
- ASTM D6484/D6484M-04 – Standard Test Method for Open-Hole Compressive Strength of Polymer Matrix Composite Laminates

Test results of NCAMP for IM7/8552 and AS4/8552 are referred and KARI's results are referred to validate material properties of CP150NS/K.015. Test matrix of lamina is described in following Table 4.1. In here, RTD means room temperature dry condition which has $21 \pm 5℃$. CTD means cold temperature dry with $-54 \pm 3℃$ and ETW is an environment of elevated temperature wet with $82 \pm 3℃$. The setting of ETW is based on ASTM D5229, which is standard test method for moisture absorption properties and equilibritum conditioning of polymer matrix composite materials.

Most of the test results data is used to construct input model of laminates test. For longitudinal tensile and in-plane shear, it is required to set additional procedure to obtain nonlinear factors and degradation factors. In the section 4.2, how to extract nonlinear

Table 4.1 Test matrix of lamina and laminate

Layup	Test Type and Direction	Property	Environment	Number of specimen		
				IM7/8552	AS4/8552	CP150NS/K.015
$[0]_n$	ASTM D3039 0° Tension ASTM D6641 0° Compression	Strength/Modulus/Degradation and Nonlinear factor	RTD	$3 \times 2 \times 3$	$3 \times 2 \times 3$	$5 \times 2 \times 3$
			ETW	$3 \times 2 \times 3$	$3 \times 2 \times 3$	$5 \times 2 \times 3$
			CTD	$3 \times 2 \times 3$	$3 \times 2 \times 3$	$5 \times 2 \times 3$
$[90]_n$	ASTM D3039 90° Tension ASTM D6641 90° Compression	Strength/Modulus	RTD	$3 \times 2 \times 3$	$3 \times 2 \times 3$	$5 \times 2 \times 3$
			ETW	$3 \times 2 \times 3$	$3 \times 2 \times 3$	$5 \times 2 \times 3$
			CTD	$3 \times 2 \times 3$	$3 \times 2 \times 3$	$5 \times 2 \times 3$
$[0/90]_{ns}$, $[90/0/90]_{ns}$	ASTM D3039 0° Tension ASTM D6641 0° Compression	Degradation Factor	RTD	$3 \times 2 \times 3$	$3 \times 2 \times 3$	
			ETW	$3 \times 2 \times 3$	$3 \times 2 \times 3$	
			CTD	$3 \times 2 \times 3$	$3 \times 2 \times 3$	
$[45/-45]_{ns}$	ASTM D3518 In-Plane Shear	Strength/Modulus/ Nonlinear factor	RTD	$3 \times 2 \times 3$	$3 \times 2 \times 3$	$5 \times 2 \times 3$
			ETW	$3 \times 2 \times 3$	$3 \times 2 \times 3$	$5 \times 2 \times 3$
			CTD	$3 \times 2 \times 3$	$3 \times 2 \times 3$	$5 \times 2 \times 3$

factor is discussed.

On the other hand, laminate level test matrix for each material is described in Table 4.2. it include OHT and OHC as referred. Simulation results of strength are compared for OHT/OHC. Each test-layup has 18 results for test, then average, minimum and maximum value of strength is compared with the simulation results.

Table 4.2 Laminate Level Test Matrix

(%0°/% ± 45°/%90°) Test Type	Test Type and Layup	Property	Environment	Number of specimen		
				IM7 /8552	AS4 /8552	CP150NS /K.015
(25/50/25 - QI) OHT1	ASTM D5766 Open Hole Tension (1) [45/0/-45/90]2S	Strength	RTD/ETW/CTD	3 × 2 × 3	3 × 2 × 3	3 × 2 × 3
(10/80/10) OHT2	ASTM D5766 Open Hole Tension (1) [45/-45/0/45/-45/90/45/-45/45/-45]S	Strength	RTD/ETW/CTD	3 × 2 × 3	3 × 2 × 3	3 × 2 × 3
(50/40/10) OHT3	ASTM D5766 Open Hole Tension (1) [0/45/0/90/0/-45/0/45/0/-45]S	Strength	RTD/ETW/CTD	3 × 2 × 3	3 × 2 × 3	3 × 2 × 3
(25/50/25 - QI) OHC1	ASTM D6484 Open Hole Compression (1)(4) [45/0/-45/90]3S	Strength	RTD/ETW	3 × 2 × 3	3 × 2 × 3	3 × 2 × 3
(10/80/10) OHC2	ASTM D6484 Open Hole Compression (1)(4) [45/-45/0/45/-45/90/45/-45/45/-45]S	Strength	RTD/ETW	3 × 2 × 3	3 × 2 × 3	3 × 2 × 3
(50/40/10) OHC3	ASTM D6484 Open Hole Compression (1)(4) [0/45/0/90/0/-45/0/45/0/-45]S	Strength	RTD/ETW	3 × 2 × 3	3 × 2 × 3	3 × 2 × 3

4.1.2 Solver Type

PFA analysis is performed using three kinds of solver as Table 4.3. In this paper, there are three kinds or trial to improve PFA. First, PFA procedure is revised to solve material nonlinearity from nonlinear elasticity and plasticity, viscosity to shear direction and degradation separately. Solver type A and B, or C and D are pairs to compare the effect of the process revolution which uses intact fiber stress when failure criterion is calculated. The revised procedure has non-cumulative damage even if stress components are used. Second, revision of damage evolution mechanism can be evaluated by comparing Type A and C, or B and D. We can observe the quality of developed CDM method. Third, from Type D and E, the methods are compared in terms of how to determine degradation factors.
Finally, Type E and F are pairs to compare quality of advanced failure criterion. Each solver's procedure is described in the Appendix B,

Table 4.3 Solver Type for Laminate Level Test Matrix

Solver Type	Property Scale	Nonlinear elasticity	Shear Nonlinearity	Failure Criteria	Degradation Algorithm and Factor
SOL-A1	Macro	X	X	Hashin	Ply-discount
SOL-A2	Macro	O	X	Hashin	MLT method (MAT58)
SOL-B1	Macro	X	O	Hashin	Novel method, from lamina-test
SOL-B2	Macro	O	O	Hashin	Novel method, from lamina-test
SOL-B3	Macro, Micro	O	O	Hashin	Novel method, from fiber bundle
SOL-C1	Micro	O	O	MMF	Novel method, from lamina-test
SOL-C2	Micro	O	O	MMF	Novel method, from fiber bundle

4.2 Nonlinear Property Extraction

4.2.1 Nonlinear Elasticity Coefficients

As referred, nonlinear elasticity factors and shear nonlinearity should be obtained by experiments. For CP150NS/K.015, experimental test results are composed of extension displacement, load and normal strain estimated by strain gage. Using the stress/strain curve, nonlinear factor can be approximated using least-square method. Reminding the Equation (2.35) for longitudinal tension test of $[0]_n$, Representative longitudinal modulus $E_{1,avg}$ usually referred as E_1 and failure strength X_t can be function of each nonlinear coefficients. It is required to optimized variables: amplifying factor of elasticity a_1, power of curve a_2 and initial modulus $E_{1,0}$. The optimal problem is described as follow

$$\text{Minimize } \int_0^{\varepsilon_{11,f}} \left(\sigma_{11,expr}(\varepsilon_1) - \sigma_{11,approximate}(\varepsilon_1)\right)^2 \mathrm{d}\varepsilon_{11} \tag{4.1}$$

Subject to:

$$-0.5 < a_1 < 0.5$$

$$0.5 < a_2 < 5.0$$

$$0.5E_1 < E_{1,0} < 2.0E_1$$

Where constraints are chosen empirically. $\sigma_{11,expr}(\varepsilon_1)$ is test result. Longitudinal stress component of the numerical model under tensile load can be obtained by following equation

$$\sigma_{11,approximate}(\varepsilon_{11}) = \int_0^{\varepsilon_{11}} E_{1,0}\left\{1 + a_1\left(\frac{\varepsilon}{\varepsilon_f}\right)^{a_2}\right\}\mathrm{d}\varepsilon \quad (4.2)$$

Where ε_f is longitudinal failure strain. Coupling component of transverse direction is negligible. From the Equation (4.2), longitudinal ultimate strength X_t can be obtained by giving ε_{11} as ε_f. Then the relationship between X_t and ε_f can be derived as follow.

$$X_t = \int_0^{\varepsilon_f} E_{1,0}\left\{1 + a_1\left(\frac{\varepsilon}{\varepsilon_f}\right)^{a_2}\right\}\mathrm{d}\varepsilon \quad (4.3)$$

By integrating Equation (4.3),

$$X_t = E_{1,0}\left\{\varepsilon_f + \frac{a_1\varepsilon_f}{1+a_2}\right\} \quad (4.4)$$

Then corrected failure strain is given as follow.

$$\varepsilon_f = \frac{(1+a_2)X_t}{(1+a_1+a_2)E_{1,0}} \quad (4.5)$$

If ratio of average modulus E_1 and initial modulus $E_{1,0}$ set as a_3,

$$\varepsilon_f = \frac{(1+a_2)a_3X_t}{(1+a_1+a_2)E_1} \quad (4.6)$$

For linear material, $a_1 = 0, a_2 = 0, a_3 = 1$. Then Equation (4.6) can be summarized as follow.

$$\varepsilon_f = \frac{X_t}{E_1} \tag{4.7}$$

For the CP150NS/K.015 material, stress strain curve for 0° Tension test are described in Figure 4.1 (a)~(d). The curves are under the room temperature conditions. Dash line indicate linear elastic model using average elastic modulus of longitudinal tension model. Nonlinear parameters obtained by the optimal process are described in Table 4.4~Table 4.6. Initial modulus of longitudinal tension of **0°** is almost 99% of estimated linear elastic modulus. However, most of the elastic modulus is amplified during tensile load with 13.18% average of increasing rate. Therefore, the tested failure strain is different to linear elastic model result. It induces different of stress state when ultimate strength is predicted for laminates. Also, in the case of Figure 4.1-(c), it looks damage is occurred locally. In this case, it is hard to use their failure strength as input variable, while degradation factor is applied, because the damage is duplicated. Therefore, it is required to remove under-estimated failure strength if localized damage exists. For the RTD model, average strength is 2517MPa, but it can be corrected by 2621MPa by removing case of localized damage.

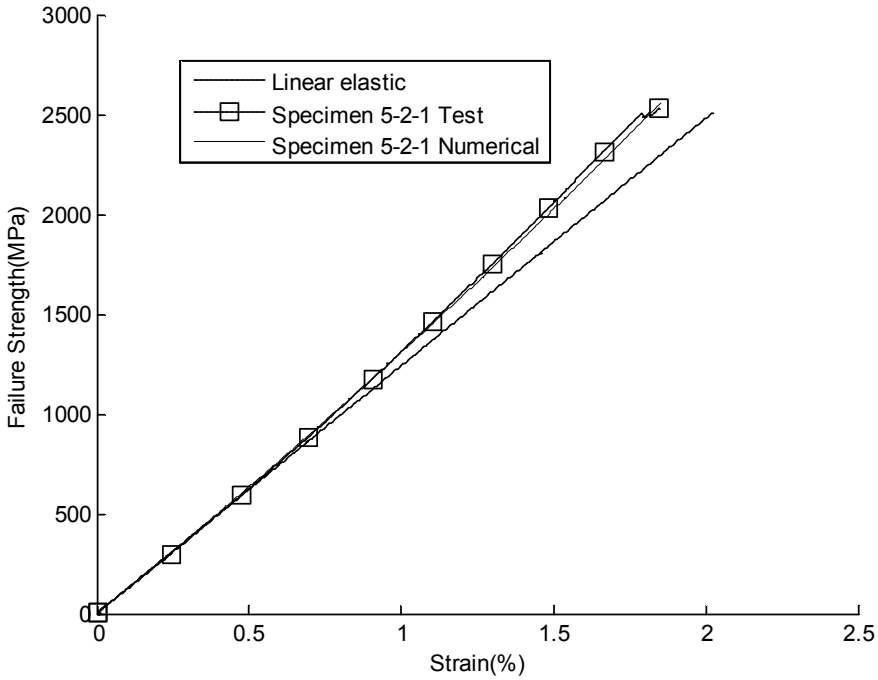

(a) Specimen 1-3-1

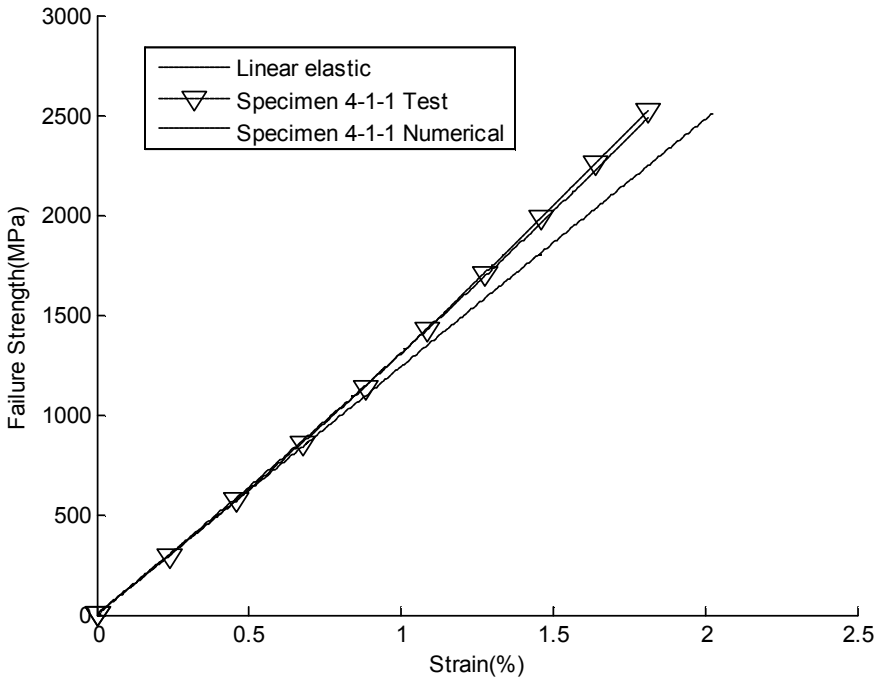

(a) Specimen 4-1-1

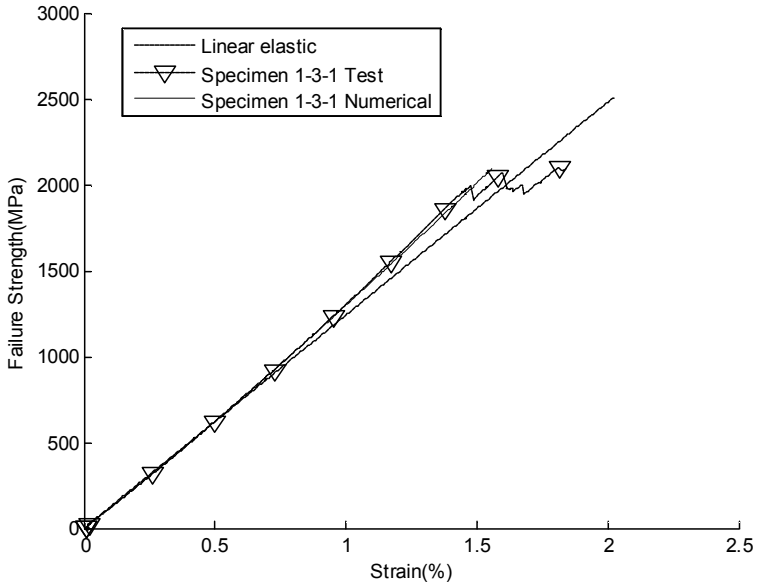

(c) Specimen 1-3-1

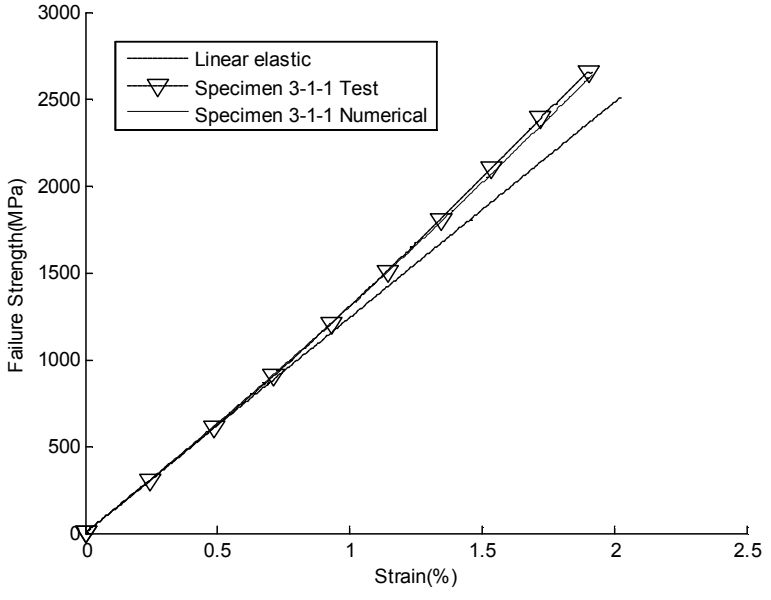

(d) Specimen 3-1-1

Figure 4.1 Stress/strain curve examples under longitudinal tension load of 0 degree lamina about linear material model, test results and numerical assumed model of nonlinear elasticity for CP150NS/K.015, RTD condition

Table 4.4 Nonlinear fiber-direction parameters at RTD condition

Specimen number	E_1(GPa)	X_t(MPa)	a_1	a_2	a_3
2	126.04	2210.18	0.200220	0.562	1.094718
3	123.10	2078.68	0.245137	0.489	1.134413
4	121.83	2104.14	0.199528	0.552	1.078922
5	122.93	2240.24	0.105218	1.074	1.006578
6	122.10	2287.17	0.069951	1.960	0.965597
7	123.99	2504.86	0.108576	1.233	0.991146
8	125.62	2412.06	0.134437	1.073	1.011582
9	124.15	2602.08	0.169815	0.837	1.036011
10	124.06	2684.25	0.156179	0.953	1.020771
12	124.75	2488.30	0.132252	1.117	1.002656
13	126.31	2562.72	0.108081	1.399	0.987039
14	123.65	2654.09	0.136782	1.067	1.006711
15	122.12	2661.27	0.124962	1.116	0.998769
16	121.86	2631.80	0.059699	2.209	0.946855
20	123.67	2524.31	0.111981	1.332	0.988268
21	122.91	2651.82	0.092601	2.000	0.969769
22	123.96	2794.99	0.089362	2.000	0.963303
23	124.07	2628.37	0.108407	1.348	0.989718
24	124.18	2620.21	0.083707	1.488	0.971667
25	124.68	2607.57	0.165588	0.824	1.036633
26	123.26	2532.74	0.137912	1.116	1.002535
27	123.42	2534.45	0.144163	0.920	1.020726
28	125.23	2439.35	0.151964	0.899	1.036556
29	122.40	2632.06	0.140607	1.128	1.004055
30	124.32	2604.59	0.110608	1.179	0.997203
31	126.81	2758.23	0.139898	1.057	1.005304
Average	123.90	2517.33	0.131832	1.190	1.010289

Table 4.5 Nonlinear fiber-direction parameters at CTD condition

Specimen number	E_1(GPa)	X_t(MPa)	a_1	a_2	a_3
1	130.42	2112.56	0.108445	2.015	0.929062
2	131.89	2278.86	0.16556	1.174	1.0058
3	133.65	2411.58	0.13	1.247	0.9829
4	132.32	2488.04	0.103176	1.366	1.015602
5	132.27	2523.52	0.166484	1.109	0.991325
6	128.52	2565.89	0.216832	0.914	0.993374
7	132.74	2574.23	0.138241	1.415	0.964087
8	130.67	2575.58	0.212565	1	1.006996
9	133.09	2584.69	0.183788	1.123	0.9997
10	136.15	2589.75	0.242643	0.851	1.054417
11	129.57	2604.48	0.242906	0.914	1.028978
12	133.76	2620.49	0.266477	0.786	1.065243
13	133.35	2646.61	0.234878	1.212	0.994564
14	137.3	2648.32	0.201077	1.091	1.008842
15	131.8	2675.56	0.119418	1.218	0.951172
16	133.48	2687.1	0.150434	1.439	0.962855
17	135.01	2724.81	0.261393	0.868	1.05772
18	132.71	2726.42	0.211152	1.011	0.997481
19	135	2728.4	0.267643	0.846	1.059554
20	135.24	2753.54	0.195788	1.115	0.990944
21	134.79	2766.65	0.221137	1.028	1.017921
22	131.32	2786.04	0.217018	1.027	0.996931
23	133.05	2803.34	0.270869	0.84	1.052467
24	132.74	2812.61	0.205357	1.082	0.992301
25	133.6	2834.87	0.2778	0.768	1.069792
26	133.09	2835.53	0.195425	1.117	0.984602

27	133.83	2885.47	0.21735	0.98	1.00118
Average	133.01	2638.70	0.200883	1.095	1.006512

Table 4.6 Nonlinear fiber-direction parameters at ETW condition

Specimen number	E_1(GPa)	X_t(MPa)	a_1	a_2	a_3
1	127	2195.1	0.134162	0.94	1.029016
2	127.11	2373.07	0.087434	1.067	0.981782
3	122.58	2392.09	0.120805	1.076	1.004216
4	123.64	2421.64	0.129234	0.823	1.022465
5	124.17	2459.84	0.104623	0.957	0.999891
6	125.69	2502.71	0.129477	1.074	1.002751
7	126.76	2505.34	0.261506	0.756	0.995305
8	124.7	2512.13	0.097491	1.044	0.991672
9	125.7	2528.42	0.140999	0.86	1.016436
10	125.67	2534.88	0.172232	0.735	1.051413
11	127.01	2536.47	0.119055	0.915	1.005669
12	128.68	2554.08	0.26136	0.698	1.060941
13	124.48	2595.87	0.122686	0.826	1.016397
14	127.21	2619.69	0.452086	3.473	1.006453
15	130.45	2639.11	0.198756	0.617	1.096684
16	125.32	2671.56	0.135381	0.818	1.009041
17	125.94	2683.73	0.111938	1.106	0.986794
18	123.15	2687.23	0.090327	0.793	0.994602
19	125.71	2687.71	0.120274	0.998	0.993566
20	127.12	2697.25	0.13322	1.098	1.01882
Average	125.91	2539.9	0.156152	1.034	1.014196

4.2.2 Shear Nonlinear Coefficients

Nonlinearity of laminate composite mainly comes from shear nonlinearity as referred in the Chapter 2. However, it is impossible to decouple degradation factors, plasticity and viscosity. Therefore, all of the nonlinearity of in-plane shear will be integrated as regression model using the model suggested in the Chapter 2. The coefficient of shear nonlinearity is based on stress and modulus at the yield and ultimate failure. Figure 4.2 is the representative pattern of shear stress under in-plane shear test. Initial shear modulus, and shear modulus immediately before failure, yield strength, ultimate failure strength failure strain are used to set the model. Because stress can be decreased by increasing strain after shear strain passes through maximum point, failure strain is set as the strain which has maximum stress. It is a reasonable assumption because the value of shear strain is relatively larger than normal strain when tensile/compressive force is applied in the laminate. Obtained additional properties are described in the Table 4.7~ 4.9.

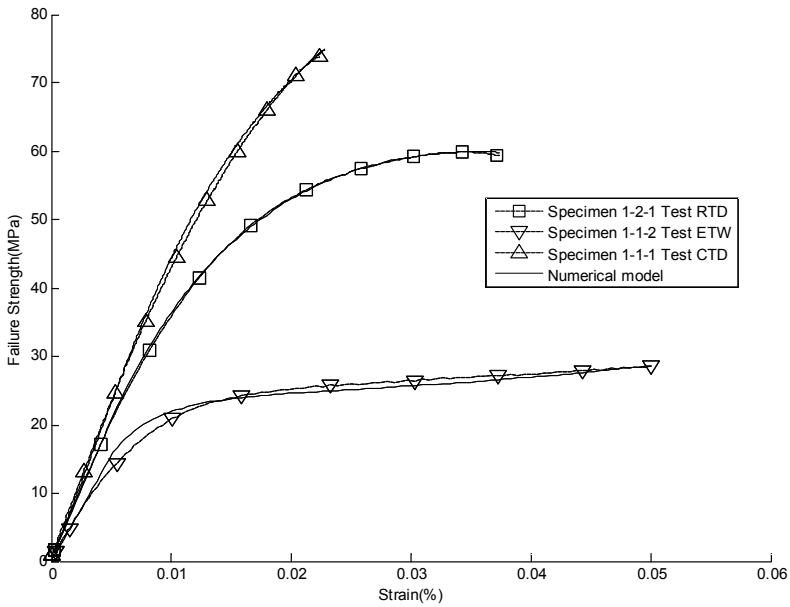

Figure 4.2 Stress/strain curve examples under in-plane shear load of 0 degree lamina about test results and numerical assumed model of shear nonlinearity for CP150NS/K.015 with RTD/CTD/ETW condition

Table 4.7 Nonlinear shear-direction parameters at RTD condition

Specimen Number	G_{12}(GPa)	G_{12f}(GPa)	S_y(MPa)	S_f(MPa)	ε_{11f}	Specimen Number	G_{12}(GPa)	G_{12f}(GPa)	S_y(MPa)	S_f(MPa)	ε_{11f}
1	4.188	0.057	14.83	59.84	0.034	16	4.326	0.158	14.75	59.59	0.031
2	4.205	0.099	16.02	60.02	0.032	17	4.276	0.223	14.28	59.58	0.031
3	3.895	0.095	18.00	57.43	0.029	18	4.767	0.128	11.96	59.78	0.033
4	4.400	0.066	13.12	59.42	0.034	19	4.818	0.143	12.85	59.55	0.031
5	4.543	0.045	13.36	59.42	0.033	20	4.208	0.244	13.69	59.53	0.031
6	3.961	0.072	20.94	58.67	0.036	21	4.242	0.056	15.59	58.80	0.031
7	4.170	0.173	14.00	59.89	0.032	22	3.801	0.067	17.56	58.09	0.035
8	4.277	0.267	16.73	56.29	0.025	23	3.809	0.303	23.85	57.45	0.029
9	4.197	0.065	14.52	59.45	0.034	24	4.185	0.169	13.46	59.70	0.033
10	4.284	0.074	14.58	59.57	0.033	25	4.341	0.181	13.76	59.95	0.033
11	4.604	0.168	12.87	58.95	0.032	26	4.080	0.495	13.43	55.10	0.026
12	4.250	0.201	13.62	59.52	0.031	27	4.240	0.057	13.45	59.22	0.034
13	4.328	0.177	15.00	59.40	0.029	28	4.228	0.063	15.70	59.06	0.031
14	4.382	0.804	15.72	54.72	0.021	29	4.290	0.131	12.95	58.23	0.033
15	4.948	0.068	11.57	59.41	0.033	Average	4.280	0.170	14.90	58.82	0.03

Table 4.8 Nonlinear shear-direction parameters at CTD condition

Specimen Number	G_{12}(GPa)	G_{12f}(GPa)	S_y(MPa)	S_f(MPa)	ε_{11f}	Specimen Number	G_{12}(GPa)	G_{12f}(GPa)	S_y(MPa)	S_f(MPa)	ε_{11f}
1	4.640	1.570	24.38	72.87	0.021	16	4.940	3.870	28.74	60.31	0.015
2	5.170	3.200	21.04	64.82	0.016	17	4.660	1.680	26.91	69.81	0.019
3	4.780	2.520	9.6	67.17	0.019	18	4.840	1.590	19.87	77.93	0.024
4	4.820	1.130	26.16	79.83	0.025	19	5.050	3.150	11.29	58.26	0.014
5	4.940	1.940	20.21	74.11	0.021	20	4.830	2.260	20.52	66.77	0.018
6	4.850	2.410	20.57	66.02	0.017	21	4.650	1.290	25.87	75.49	0.023
7	4.850	1.180	26	76.62	0.023	22	4.740	1.540	21.61	75.48	0.023
8	4.610	0.800	25.67	74.95	0.025	23	4.750	2.140	23.25	64.67	0.017
9	4.650	1.830	19.07	73.42	0.022	24	4.750	1.770	15.85	76.3	0.024
10	4.680	1.190	28.39	76.22	0.023	25	4.860	2.170	16.22	71.71	0.02
11	4.920	1.920	15.44	75.78	0.023	26	4.430	0.730	32.78	75.4	0.024
12	4.910	3.110	26.57	65.51	0.017	27	4.630	1.160	26.26	75.69	0.024
13	4.910	1.940	16.87	76.11	0.022	28	4.800	1.240	29.08	72.41	0.021
14	4.600	1.250	25.85	75.65	0.023	29	4.530	0.520	40.25	72.99	0.021
15	4.600	1.550	23.44	73.4	0.022	Avg.	4.760	1.780	23.27	72.02	0.02

Table 4.9 Nonlinear shear-direction parameters at ETW condition

Specimen Number	G_{12}(GPa)	G_{12f}(GPa)	S_y(MPa)	S_f(MPa)	ε_{11f}	Specimen Number	G_{12}(GPa)	G_{12f}(GPa)	S_y(MPa)	S_f(MPa)	ε_{11f}
1	3.100	0.190	14.41	28.65	0.05	15	7.320	0.360	12.31	37.68	0.05
2	8.610	0.420	13.28	41.28	0.05	16	7.260	0.490	12.53	39.19	0.05
3	6.780	0.580	17.13	38.56	0.05	17	7.650	0.330	11.16	38.19	0.05
4	7.490	0.490	13.48	38.61	0.05	18	8.110	0.380	12.81	39.12	0.05
5	7.210	0.400	12.23	38.17	0.05	19	3.060	0.150	13.61	27.37	0.05
6	7.130	0.380	12.18	37.11	0.05	20	7.130	0.330	12.29	37.17	0.05
7	3.080	0.060	13.52	28.86	0.05	21	6.460	0.480	14.69	38.05	0.05
8	7.050	0.420	14.12	40.45	0.05	22	7.480	0.450	13.88	37.67	0.05
9	7.020	0.420	14.08	38.88	0.05	25	8.030	0.320	11.47	38.72	0.063
10	7.460	0.390	12.31	37.85	0.05	26	3.120	0.070	10.86	27.77	0.05
11	7.590	0.300	12.56	37.38	0.05	27	7.220	0.370	12.23	37.24	0.05
12	7.590	0.410	13.75	39.57	0.05	28	7.210	0.350	12.24	37.02	0.05
13	3.010	0.100	12.67	28.5	0.051	29	6.460	0.420	15.02	37.36	0.05
14	7.690	0.330	11.26	39.12	0.05	Avg	6.570	0.350	13.04	36.5	0.051

4.3 Open-Hole Tension(OHT) Test Results

Open-hole tension tests are examples to evaluate accuracy of damage model, failure criterion and material nonlinear model. Because of local load sharing, damage propagation will be delayed until failure reaches bottom and top side of the coupon.

4.3.1 Room Temperature Dry(RTD) Condition

Figure 4.3-(a) is the analysis results of CP150NS/K.015 under the room temperature and tensile test. SOL-A group which uses conventional CDM methods, predicted lowest strength comparing with the other solvers. In the case of quasi-isotropic, it gives best quality regardless of solver type. Macro-scale failure criteria and meso-scale degradation model with nonlinear elasticity of fiber(SOL-B2) and micro-scale failure criteria and degradation model with nonlinear elasticity of fiber(SOL-C2) give better results relatively for every combinations of lay-up.

For IM7/8552 material, the lamina-level properties are given without raw data. Therefore, nonlinear parameters are obtained by referring CP150NS/K.015 material. Failure strength for each lay-up is described in Figure 4.3-(b). When only constituent properties are used such as SOL-C2, it gives worse results comparing with the other solvers. In the case of SOL-B2, for the ultimate strength of all lay-up, it was in good agreement with the experimental results.

AS4 is a carbon fiber material with lower strength comparing with IM7. In Figure 4.3-(c), the failure strengths for each lay-up are described. It also has good accuracy as IM7 case. Each solution including experimental results has lower failure strength than IM7/8552. Open-hole tension analysis results are good agreement with experimental results for all lay-up, for most of solvers. For OHT1 cases, degradation of 45 and -45 degree layers for each step has similar amount with longitudinal tensile modulus increment rate. It means nonlinear model seldom affect to the result of strength. Degradation method also is not effective in terms of stiffness, but it critically influence on peak because it decides post behavior after failure. OHT2 case, MMF with fiber bundle model has too high failure strength. The internal loads of 45 and -45 degree layer are over-estimated.

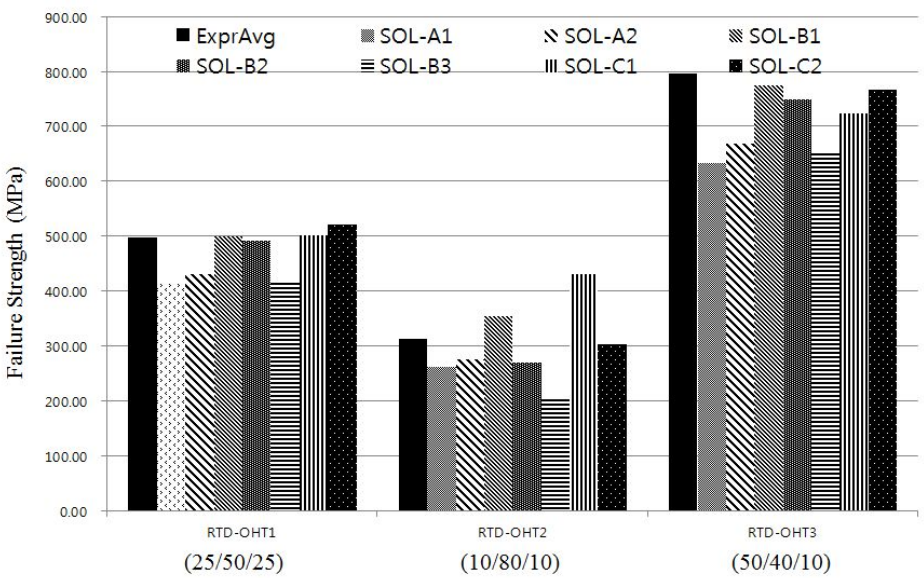

(a) CP150NS/K.015

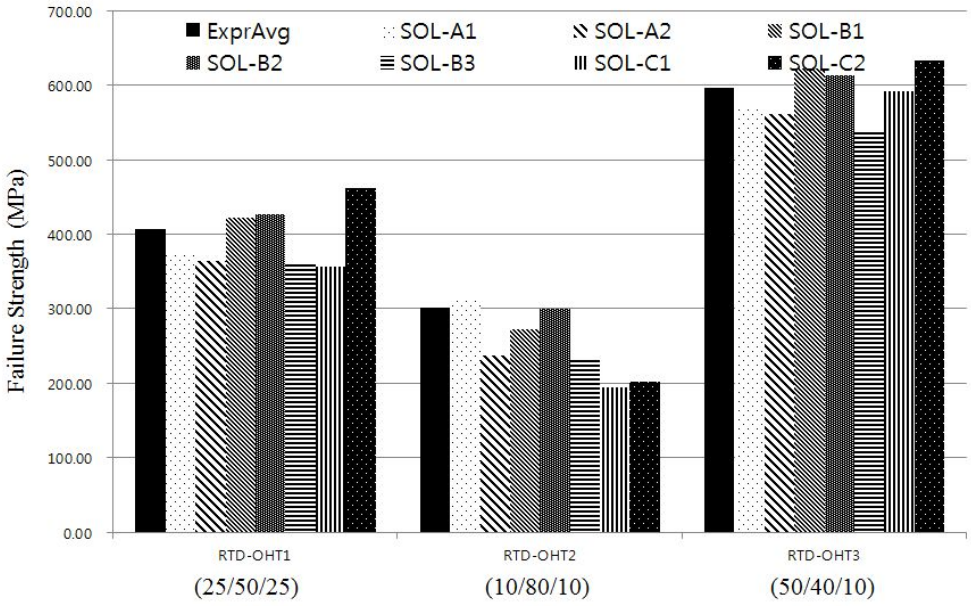

(b) IM7/8552

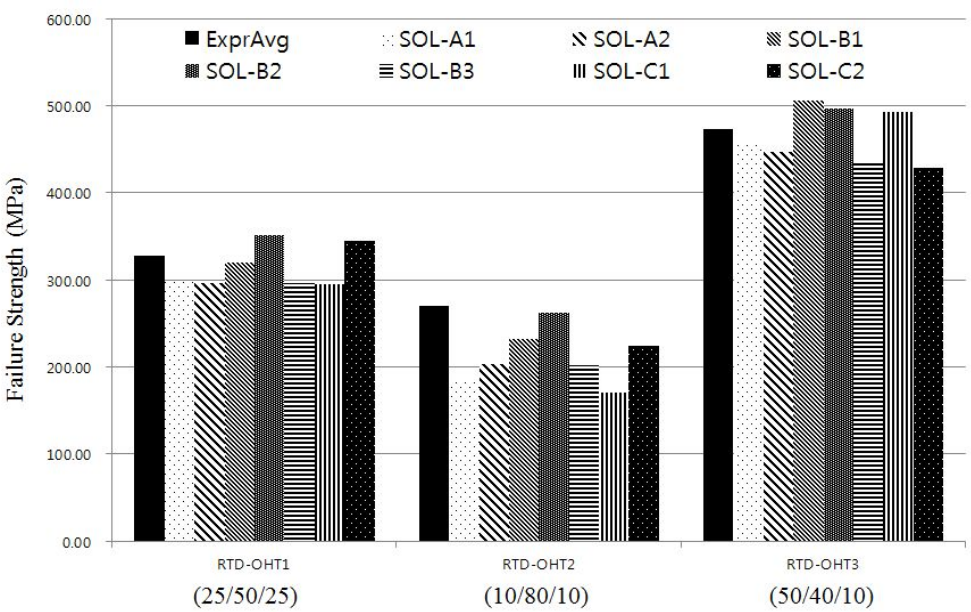

(c) AS4/8552

Figure 4.3 Failure strengths under tensile load on room temperature dry condition.

4.3.2 Elevated Temperature Wet(ETW) Condition

Figure 4.4-(a) is the open-hole tension results with CP150NS/K.015 material under elevated temperature wet condition. Most of solvers give acceptable prediction results except OHT 3. It is very exceptional case, because their average failure strength is almost 1.4 times RTD case's strength. Because the longitudinal tensile strength is almost same in the 0 degree lamina tests, it is expected to come from different failure mode.

In the Figure 4.4-(b), IM7/8552 and ETW-OHT1 strength are described. For the conditions, most of solvers give better results than CP150NS/K.015. Every solver's results have small difference to tests. Especially, OHT3 which have 50% of 0 degree plies are predicted well.

Figure 4.4-(c) is AS4/8552 material with ETW condition. It also have similar pattern to IM7/8552, but it has smaller failure strength than IM7/8552.

Even if the failure strength of 0 degree for elevated temperature and wet condition is similar or smaller than RTD results, its laminates gives higher strength. Also, the increasing rate is higher in the OHT3 case, when the number of 0 degree layer is larger. Exceptionally, OHT2 strength which has 80% of 45/-45 degree layers is smaller than RTD case. Numerical results of the each solver also have the tendency.

In this condition, the shear strength is very small comparing with

RTD conditions because of epoxy. It affects to the PFA results because each direction's mode of Hashin failure criteria contains shear stress term. Unlike the RTD condition's results, failure index contribution of shear stress is very large, therefore the other factors is not effective in this case. For example, non-linear elasticity coming from fiber kinking didn't have much effect on failure strength. Because shear nonlinearity model in this work come from test results completely, the solvers give similar results.

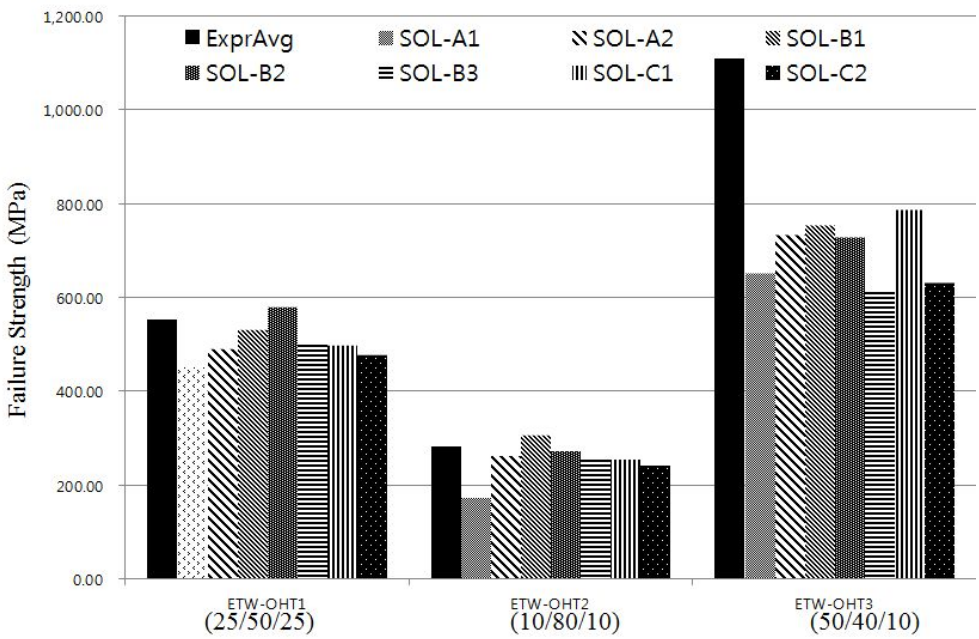

(a) CP150NS/K.015

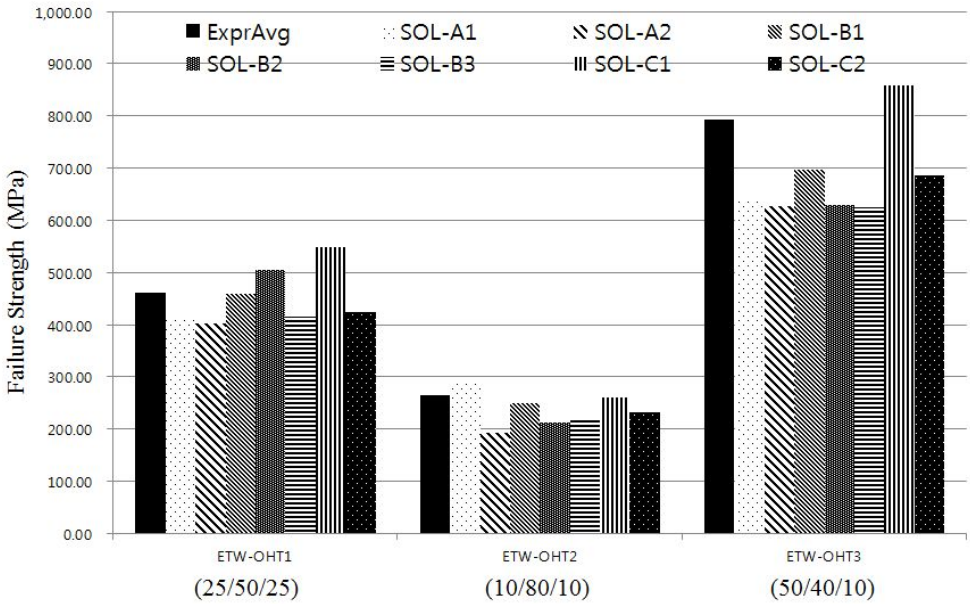

(b) IM7/8552

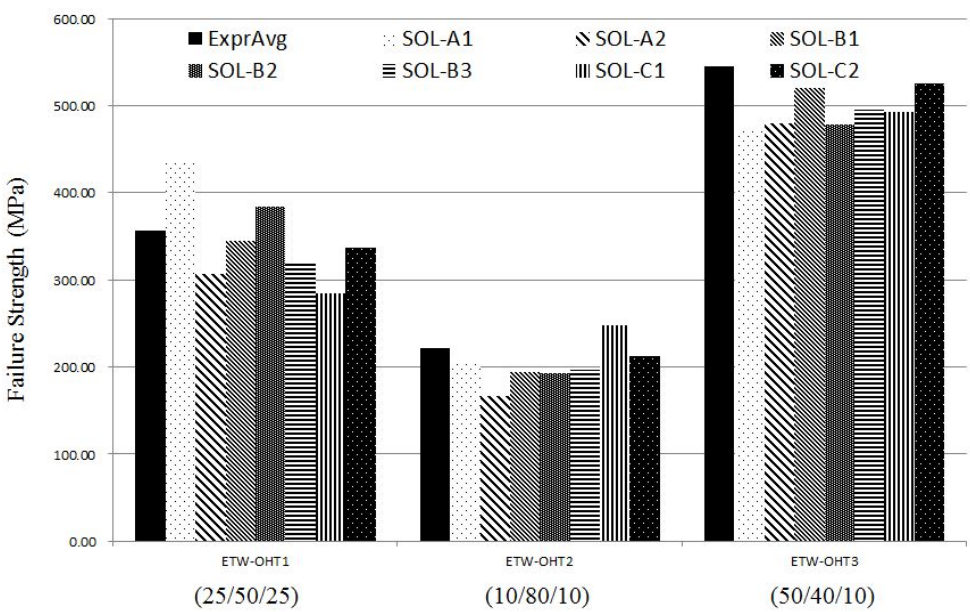

(c) Figure 3 AS4/8552

Figure 4.4 Failure strength under tensile loads on elevated temperature wet condition.

4.3.3 Cold Temperature Dry(CTD) Condition

Figure 4.5-(a) is the failure strength graph for CTD condition of CP150NS/K.015 material. The predicted strengths are accurate. However, micro-mechanics approaches (SOL-C1,SOL-C2) are relatively incorrect because it uses interpolated fiber strength from RTD fiber strength and ETW/RTD longitudinal tensile strength of lamina. For IM7/8552 with CTD conditions is described in Figure 4.5-(b). The pattern of failure strength is similar to CP150NS/K.015 material. In the case of AS4/8552 material, there are no big differences to RTD results as Figure 4.5-(c).

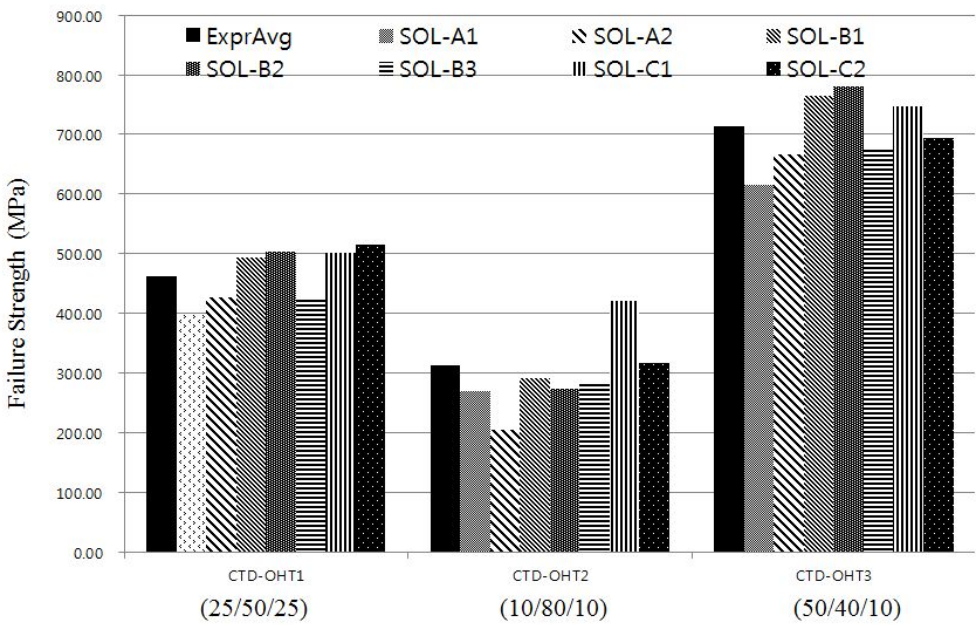

(a) CP150NS/K.015

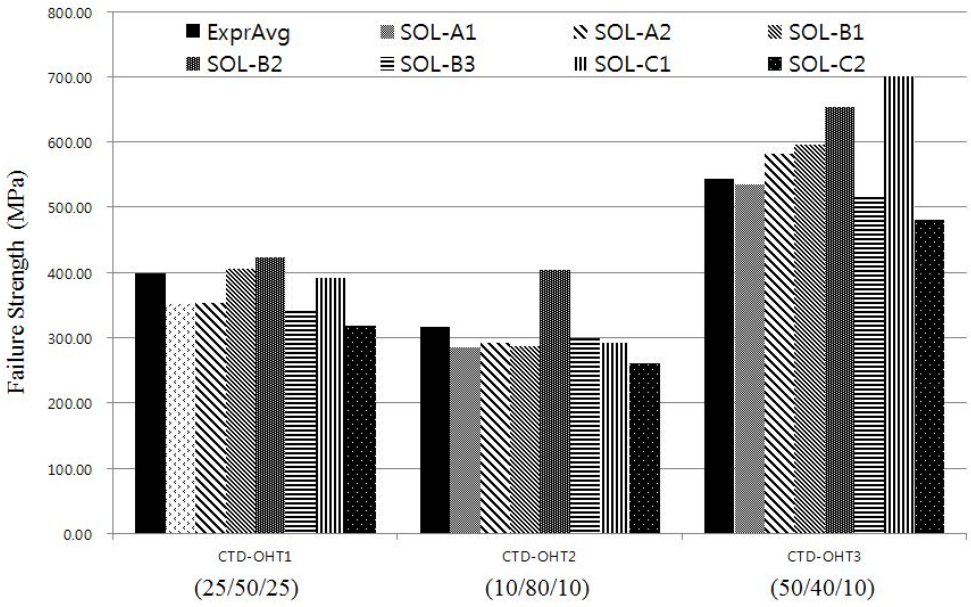

(b) IM7/8552

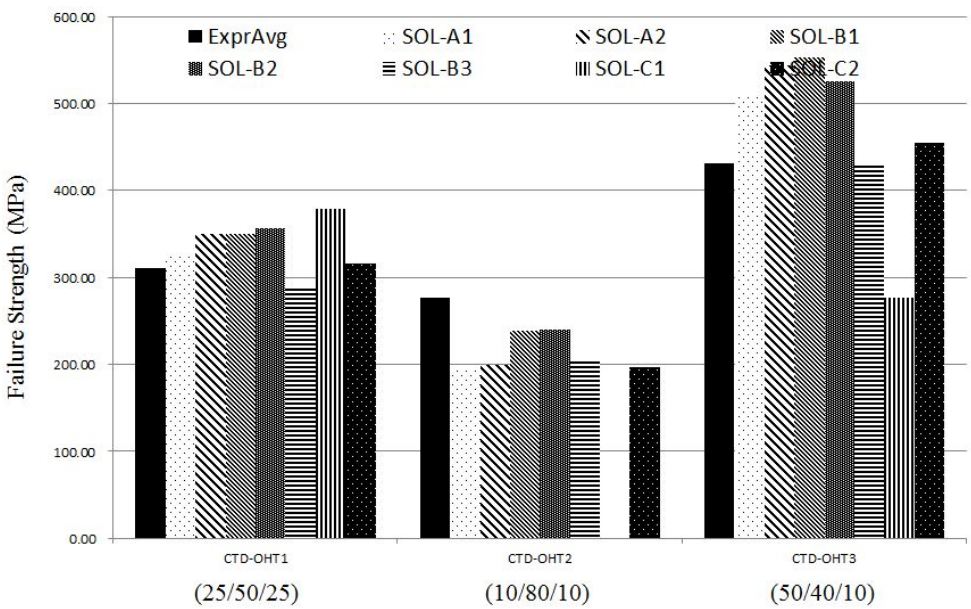

(c) Figure 4 AS4/8552

Figure 4.5 Failure strengths under tensile load on cold temperature dry condition.

4.3.4 Discussion

CTD conditions give lower failure strength than RTD conditions with small difference unexpectedly. Even if their longitudinal failure strength and shear strength of lamina is larger than RTD condition's properties, laminates performance are worse than RTD cases. Because it larger longitudinal modulus and increasing rate of fiber direction modulus, it reaches failure more quickly. It is reason why the failure strength of OHT is smaller than RTD cases.

Open-hole compression(OHC) are tested and simulated as OHT. For this case, there are several differences to tensile case. One is the coupling term of shear and normal direction of Hashin failure criteria removed for fiber failure mode. Another one is elastic modulus will be changed. Therefore, lamina material properties should be surveyed separately. Last one is local buckling should be considered. But in this work, buckling is excluded by change the lay-up and tests conditions. All of the failure modes of laminates tested is containing buckling, therefore the effects can be negligible. However, in the micro-scale, each fiber can be buckled if it reaches critical load. It was refleced in the software setting as increment of fiber direction modulus. Many experimental results suggest the stiffness of fiber will be decreased as compressive load increases. The rate of decrement are assumed as same value to tension test's.

RTD and ETW conditions are used for OHC cases. CTD conditions are excluded because there are no comparable results from experimental tests.

4.4 Open-Hole Compression (OHC) Test Results

4.4.1 Room Temperature Dry(RTD) Condition

Figure 4.6-(a) is the PFA results of RTD condition with compressive external load, for CP150NS/K.015. Evidently, the solvers which use Hashin failure criteria give higher strength than MMF results. Because the failure criteria has no interaction term of shear stress for fiber direction, the initial failure and degradation are simply obtained by the longitudinal tensile strength and stress. It is reason why the methods using Hashin failure criteria overestimate failure strength under compressive loads. In contrast, there are improved results when MMF criterion is used rather than Hashin failure criteria. Figure 4.6-(b) is the results for IM7/8552 using same environment and load conditions. It also predicts over-estimated strength as Hashin failure criterion is used. But MMF results give improved results. Figure 4.6-(c) is AS4/8552 results. It also have similar pattern. For OHC case, it has more accurate results comparing with the other two materials.

For the compressive loads under RTD conditions, all materials gives smaller strength then tensile cases in terms of experiments. However, the simulation results didn't pick up the difference when macro-scale failure criterion are used to describe failure initiation and degradation. MMF failure criteria gives better results consistenly.

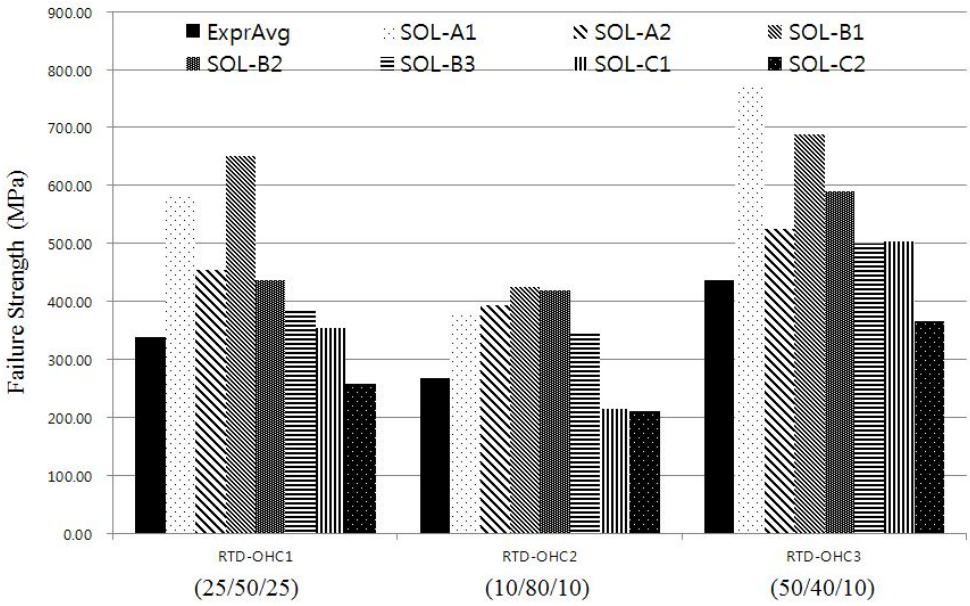

(a) CP150NS/K.015

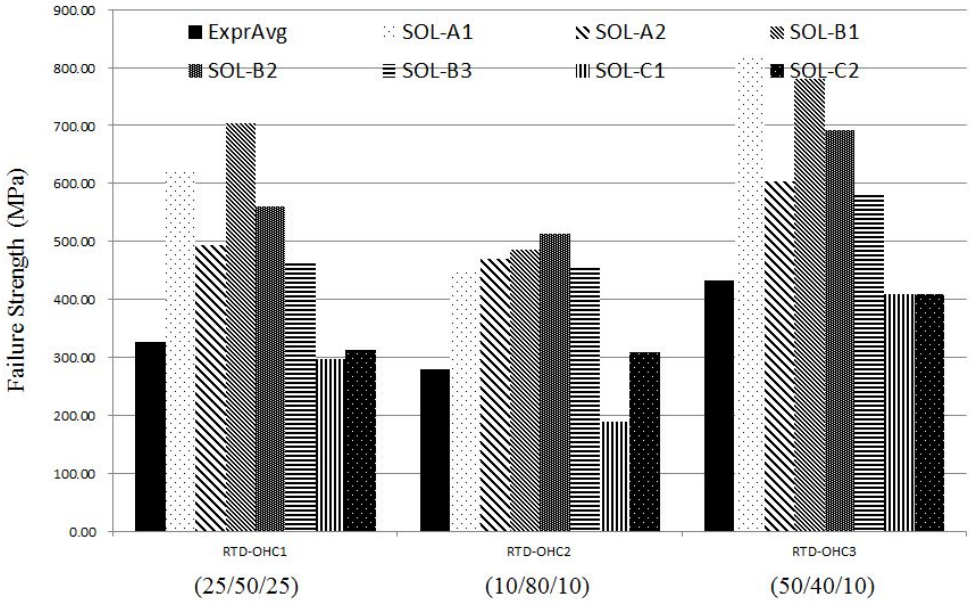

(b) IM7/8552

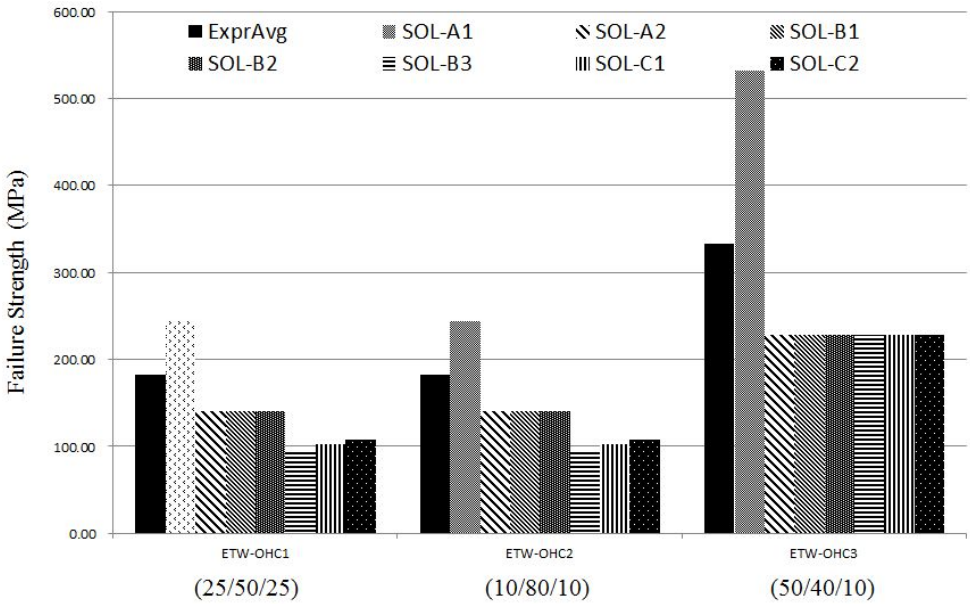

(c) Figure 5 AS4/8552

Figure 4.6 Failure strengths under compressive load on room temperature dry condition.

4.4.2 Elevated Temperature Wet(ETW) Condition

Elevated temperature with compression are tested for each materials such as RTD tests. Figure 4.7-(a) is the PFA results using CP150NS/K.015 material. Except to SOL-A1, most of cases have similar results. In this case, fiber direction strength is small because of compressive loads, and matrix direction and shear direction strength is also small according to lamina test results. Therefore, the failure strength is predicted similarely as a whole. The difference seems to be come from failure criteria. Thus, MMF and Hashin groups give difference results. For the IM7/8552 , the PFA results are described in Figure 4.7-(b). It has similar tendency to CP150NS/K.015. AS4 results are described in the Figure 4.7-(c). it also have similar pattern.

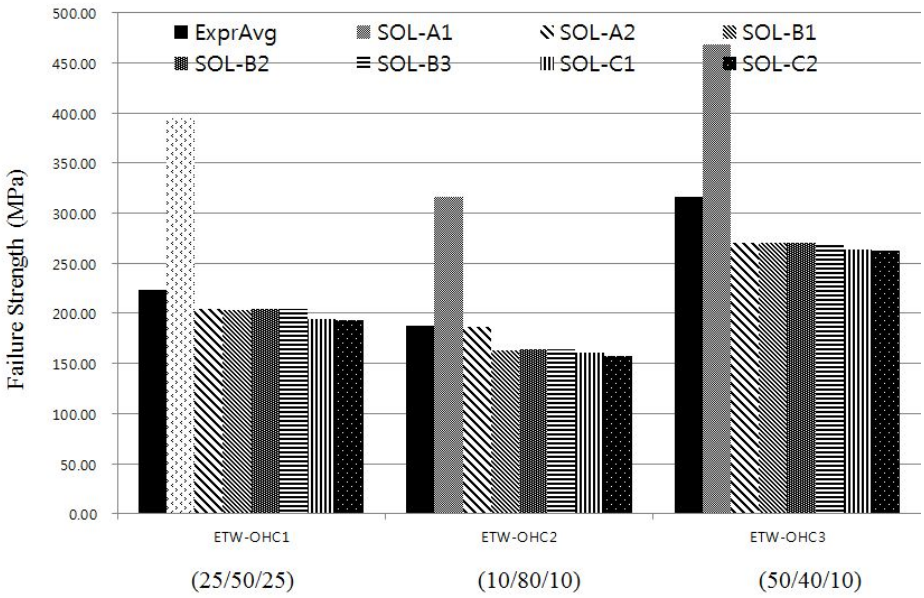

(a) CP150NS/K.015

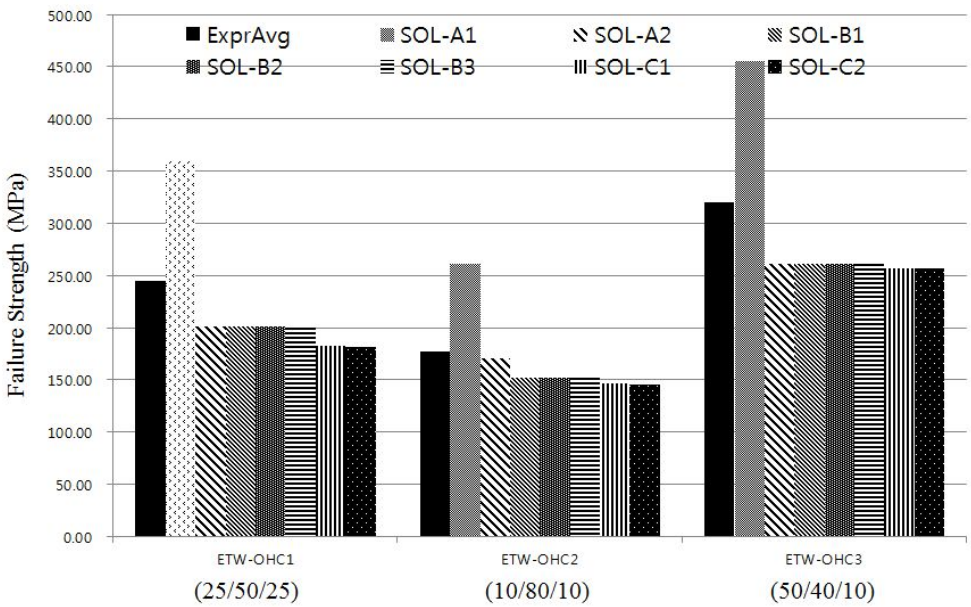

(b) IM7/8552

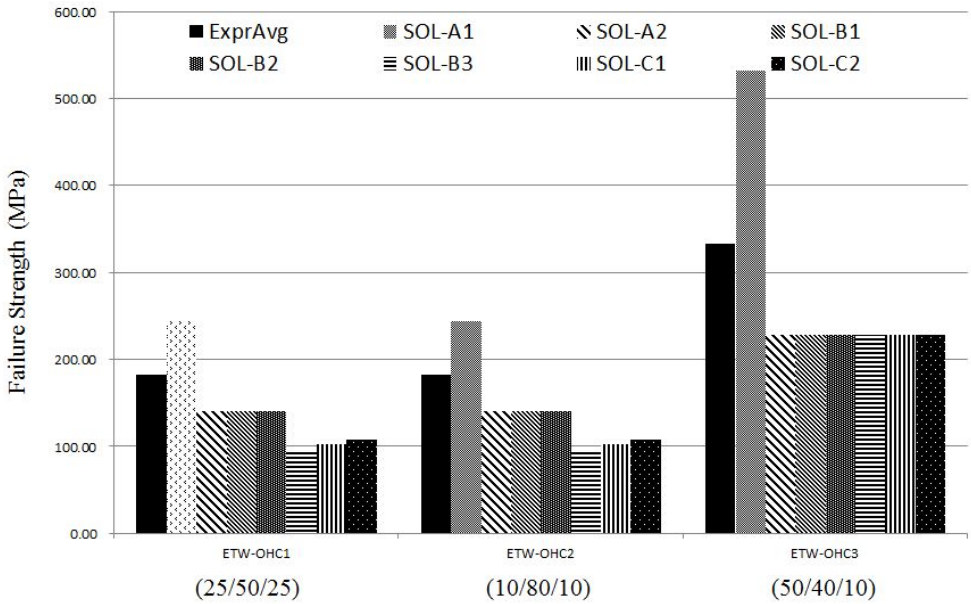

(c) AS4/8552

Figure 4.7 Failure strength under compressive loads on elevated temperature wet condition.

4.4.3 Discussion

As expected, PFA results of ETW under compressive load give much lower strength than RTD. Because not only longitudinal tension, but also transverse and shear direction modulus of each material's lamina is lower than RTD case. Therefore, there are no factor to increase strength for ETW cases. Especially, longitudinal case, the ply is less than 25 percent of the RTD strength. The lamina's characteristic in the laminates results.

4.4 Chapter Summary

In this chapter, open-hole tension and compression tests for various material are performed using commercial and developed software using different combination of the solvers. Room temperature dry, elevated temperature with wet condition and cold temperature dry condition are chosen as environment condition. Three kinds of material, which have carbon fiber and epoxy matrix, are analyzed using the solvers, then the results of PFA were compared. Except several cases, the solver which uses statistically developed degradation model and fully micro-scaled solvers have a good agreement with experimental results.

Concluding Remarks

In this study, novel progressive failure analysis model were developed using improved continuum damage mechanics (CDM) model. The model is stress based non-cumulative damage model with emphasis on the material nonlinearity of the fiber, shear stiffness reductions, the damage contribution of matrix cracks in adjacent layers and the statistical distribution of the fiber strength due to defects. The model is revised using micro mechnics of failure and damage in order to construct fully-micromechanics based PFA procedure. Fiber bundle model are used to obtain the degradation model.

In chapter 2, a PFA solver was developed to predict the nonlinear mechanical behavior of carbon/epoxy laminates under tensile loading by considering the material nonlinearity with a novel CDM model from the statistical results of experiments. A numerical analysis was conducted under unnotched tensile test. Generalized Weibull distribution parameters were configured to determine the damage evolution of a laminate composite. The amount of stiffness degradation was quantified by developing a multi-scale model to determine the parameters.

In chapter 3, a damage evolution model in fiber reinforced composites based on Weibull distribution model was proposed and combined with RVE model including multi-cell. Multi-scale approach for progressive failure analysis was revised to describe

the local load sharing after failure initiation. Representative parameters of the damage variables for the post behaviour of the local failure were derived from statistical results of micro-scale progressive failure analysis.

In chapter 4, Material properties are re-surveyed referring regression model which is suggested in the chapter 2. Even if each material properties are tested using the nonliner elasticity and shear nonlinearity, failure strength highly depends on the failure criteria and post behavior after it reaches unit of failure index. Also, those criteria has a role giving coupling effect of each stress components. PFA were performed about IM7/8552, AS4/8552 and CP150NS/K.015 which is tested by NCAMP and KARI. Open hole tension and compression were solved for room temperature dry, elevated temperature wet and cold temperature dry condition. Analysis results have a good agreements with test results for most of cases.

Reference

1. Ochoa, O. O. and Reddy, J. N., Finite Element Analysis of Composite Laminates. Kluwer Academic Publishers, Dordrecht, The Netherlands, 1992.

2. Krishna Murty, A. V. and Reddy, J. N., Compressive Failure of Laminates and Delamination Buckling: A Review. The Shock and Vibration Digest, 1993; 25: 3-12.

3. Reddy, Y. S. and Reddy, J. N., Three-Dimensional Finite Element Progressive Failure Analysis of Composite Laminates under Axial Compression. Journal of Composite Technology and Research, 1993; 15: 73-87.

4. Singh, S. B., Kumar, A., and Iyengar, N. G. R, Progressive Failure of Symmetrically Laminated Plates under Uni-axial Compression. Structural Engineering and Mechanics, 1997; 5: 433-450.

5. Matzenmiller, A., Lubliner J. and Taylor R.L., A constitutive model for anisotropic damage in fiber-composites. Mechanics of Materials 1995;20: 125-152.

6. Weibull, W., A Statistical distribution Function of Wide Applicability. ASME Journal of Applied Mechanics, 1951;18: 293-297.

7. Creasy, T. S., Modeling Analysis of Tensile Tests of Bundled Filaments with a Bimodal Weibull Survival Function. Journal of Composite Materials, 2002 ;36:183-194.

8. Williams, K. V. and Vaziri, R., Application of a Damage Mechanics Model for Predicting the Impact Response of Composite Materials. Computers & Structures, 2001;79:997-1011.

9. Barbero, E. J. and De Vivo, L., Constitutive model for elastic damage in fiber-reinforced PMC laminate. International Journal of Damage

Mechanics, 2001;10:73-93.

10. Voyiadjis, G. Z., Shojaei, A. and Li, G., A generalized coupled viscoplastic-viscodamage-viscohealing theory for glassy polymers, International Journal of Plasticity, 2012;28:21-45

11. Voyiadjis, G. Z., Shojaei, A. and Li, G., A thermodynamic consistent damage and healing model for self healing materials, International Journal of Plasticity, 2011;27:1025-1044

12. Voyiadjis, G. Z., Shojaei, A., Li, G., & Kattan, P. I., A theory of anisotropic healing and damage mechanics of materials, In Proceedings of the Royal Society of London A: Mathematical, Physical and Engineering Sciences (p. rspa20110326). The Royal Society, 2011

13. Shojaei, A., Sharafi, S. and Li, G., A multiscale theory of self-crack-healing with solid healing agent assisted by shape memory effect, Mechanics of Materials, 2015;81:25-40

14. Shojaei, A., Li, G., Fish, J. and Tan, P. J., Multi-scale constitutive modeling of Ceramic Matrix Composites by Continuum Damage Mechanics, International Journal of Solids and Structures, 2014;51:4068-4081,

15. Shojaei, A. and Li, G., Viscoplasticity analysis of semicrystalline polymers: A multiscale approach within micromechanics framework, International Journal of Plasticity, 2013;42:31-49

16. Curtis, G. J., Milne, J. M. and Reynolds, W. N., Non-Hookean behavior of strong carbon fibers. Nature, 1968; 220:1024-1029.

17. Ishikawa, T., Matsushima, M. and Hayashi, Y., Hardening nonlinear behavior in longitudinal tension of unidirectional carbon composites. Journal of Material Science, 1985; 20: 83.

18. Yokozeki, T., Ogasawara, T. and Ishikawa, T., Effects of fiber nonlinear properties on the compressive strength prediction of unidirectional carbon-fiber composites. Composites Science and

Technology, 2005;65: p. 2140-2147.

19. Wang, H. W., Zhou, H. W., Mishnaevsky, L., et al, Single fibre and multifibre unit cell analysis of strength and cracking of unidirectional composites. Computational Materials Science, 2009;46:810-820

20. Ramberg. Walter and Osgood. William, Description of stress-strain curves by three parameters. NACA TN902, 1943.

21. Shakib, S. M and Li, S., Modified Three-Rail Shear Fixture (ASTMD4255/D4255M) and an Experimental Study of Nonlinear in-Plane Shear Behavior of FRC. Composites Science and Technology, 2009;9:1854-1866.

22. Totry, E., González, C., LLorca, J., et al, Mechanisms of shear deformation in fiber-reinforced polymers: experiments and simulations. International Journal of Fracture, 2009;158:197-209.

23. Kontou, E. and Kallimanis, A., Formulation of the viscoplastic behavior of epoxy glass fiber composites. Journal of Composite Materials, 2005. 39(8): p. 711-721.

24. Flatscher, T., Schuecker, C. and Pettermann, H. E., Prediction of plastic strain accumulation in continuous fiber reinforced laminates by constitutive model. International Journal of Fracture, 2009;158:145-156.

25. Papanicolaou, G. C., Zaoutsos, S. P. and Kontou, E. A., Fiber orientation dependence of continuous carbon/epoxy composites nonlinear viscoelastic behavior. Composite Science of Technology, 2004;64:2535-2580.

26. Lou, Y. C. and Schapery, R. A., Viscoelastic characterization of a nonlinear fiber-reinforced plastic. Journal of Composite Materials, 1971;5:208-242.

27. R.A. Schapery, Nonlinear viscoelastic and viscoplastic constitutive equations based on thermodynamics. Mech Time-Depend Mater,

1997;1:209-249.

28. Pettersson, K. B., Neumeister, J. M., Gamstedt, E. K., et al, Stiffness reduction, creep, and irreversible strains in fiber composites tested in repeated interlaminar shear. Composite Structures, 2006;76:151-212.

29. Giannadakis K. and Varna Jr, Analysis of nonlinear shear stress-strain response of unidirectional GF/EP composite. Composites Part A: Applied Science and Manufacturing, 2014;62:67-76.

30. Weeks C.A. and Sun C.T., Modeling Non-linear Rate-dependent Behavior in fiber-reinforced Composites, Compos. Sci. Technol. 1998;58:603-611.

31. Thiruppukuzhi S.V. and Sun C.T., Testing and modeling high strain rate behavior of polymeric composites, Compos. Part B 1998;29:535-546.

32. Kim, S.J. and Oden, J.T., Finite Element Analysis of a Class of Problems in Finite Elastoplasticity based on the Thermodynamical Theory of Materials of Type N, Compos. Meths. Appl. Mech. Eng. 1985;53: 277-302.

33. Kim, S.J. and Cho, J.Y, Role of matrix in viscoplastic behavior of thermoplastic composites at elevated temperature, AIAA J. 1992;31:2571-2573

34. Kim, J.H., Kim, S.J. and Kim, W.D., A Finite Element Analysis of Damage Propagation during Metal Forming Process, Engineering Fracture Mechanics, 1995; 51: 915-931

35. Kim, S.J. and Kim, J.H., "Finite Element Analysis of Laminated Composite Plate with Multi-Pin Joints Considering Friction", Computers and Structures, 1995;55: 507-514

36. Kim, S.J., and Hwang, J.S., "Progressive Failure Analysis of Pin-Loaded Laminated Composites using Penalty Finite Element Method",

AIAA Journal, 1998; 36:75-80,

37. Kim, J.H. and Kim, S.J., "A Multifrontal Solver Combined with Graph Partitioners", AIAA Journal,1999; 38: 964-970

38. Kim, S.J., Lee, C.S. and Kim, J.H., "Large-Scale Structural Analysis by parallel multifrontal solver through Internet Based PCs", AIAA Journal, 2002;40: 359-367

39. Kim, J.H., Lee, C.S. and Kim, S.J., "High-Performance Domainwise Parallel Direct Solver for Large-Scale Structural Analysis", AIAA Journal, 2005;43: 662-670

40. Park, J.W., Park, S.H. and Kim, S.J., "Optimization With High-Cost Objective Function Evaluations in a Computing Grid and an Application To Simulation-Based Design", International Journal of High Performance Computing Applications, 2009;23:62-83

41. Nuismer, R.J., Predicting the Performance and Failure of Multidirectional Polymeric Matrix Composite Laminates: A Combined Micro-Macro Approach. Advances in Composite Material, 1980. Proc. 3rd Int. Conf. Composite Materials: p. 436.

42. Chen, J. F., Morozov, E. V. and Shankar, K., A combined elastoplastic damage model for progressive failure analysis of composite materials and structures. Composite Structures, 2012;94:3478-3489.

43. Đorđević, I. M., Sekulić, D. R. and Stevanović, M. M., Nonlinear elastic behavior of carbon fibers of different structural and mechanical characteristic. Journal of the Serbian Chemical Society, 2007; 72:513-521.

44. Marlett ,K, Hexcel 8552 IM7 Unidirectional Prepreg 190 gsm & 35% RC Qualification Material Property Data Report,. National Center for Advanced Materials Performance, 2011; Rev. A: p. 1-238.

45. Kun, F., Raischel, F., Hidalgo, R. C., et al., Extensions of Fiber Bundle Models. Modelling Critical and Catastrophic Phenomena in

Geoscience, Lecture Notes in Physics 2006;705: p. 57-92.

46. Phoenix, S. L. and Beyerlein, I. J., Statistical Strength Theory for Fibrous Composite Materials. Comprehensive Composite Materials, 2000;1:chapter 1.19)

47. Van Paepegem, W., De Baere, I. and Degrieck, J., Modelling the nonlinear shear stress-strain response of glass fiber-reinforced composites. Part I: experimental results. Comp Sci Tech, 2006;66:1455-1464.

48. Kim, S. J., Lee, C. S., Yeo, H. J., et al, Direct Numerical Simulation of Composite Structures, Journal of Composite Materials, 2002;36:2765-2785

49. Cho, C., Holmes, J. W. and Barber, J. R., Distribution of matrix cracks in a uniaxial ceramic composite. Journal of the American Ceramic Society, 1992; 75:316-324

50 Tay, T. E. "Characterization and analysis of delamination fracture in composites: an overview of developments from 1990 to 2001." Applied Mechanics Reviews, Vol. 56, No. 1, 2003, pp. 1-32.

51. Hyer, Michael W., and Gabriela F. Wolford. "Progressive failure analysis of internally pressurized noncircular composite cylinders." Proceedings of the 43rd AIAA/ASME/ASCE/AHS/ASC Structures, Structural Dynamics and Materials Conference, 2002

52. Moreton, R. "The effect of gauge length on the tensile strength of RAE carbon fibres." Fibre Science and Technology, Vol. 1, No. 4, 1969, pp. 273-284.

53. Hitchon, J. W., and D. C. Phillips. "The dependence of the strength of carbon fibres on length." Fibre Science and Technology, Vol. 12, No. 3, 1979, pp. 217-233.

54. Tagawa, Tetsuya, and Takashi Miyata. "Size effect on tensile

strength of carbon fibers." Materials Science and Engineering: A, Vol. 238, No. 2, 1997, pp. 336-342.

55. Naito, Kimiyoshi, et al. "The effect of gauge length on tensile strength and Weibull modulus of polyacrylonitrile (PAN)-and pitch-based carbon fibers."Journal of Materials Science, Vol. 47, No. 2, 2012, pp. 632-642.

56. Barbero, Ever J., and Liliana De Vivo. "A constitutive model for elastic damage in fiber-reinforced PMC laminae." International Journal of Damage Mechanics, Vol. 10, No. 1, 2001, pp. 73-93.

57. Xia, Z., T. Okabe, and W. A. Curtin. "Shear-lag versus finite element models for stress transfer in fiber-reinforced composites." Composites Science and Technology, Vol. 62, No. 9, 2002, pp. 1141-1149.

58. Kun, Ferenc, Stefano Zapperi, and Hans J. Herrmann. "Damage in fiber bundle models." The European Physical Journal B-Condensed Matter and Complex Systems, Vol. 17, No. 2, 2000, pp. 269-279.

59. Tay, T. E., V. B. C. Tan, and S. H. N. Tan. "Element-failure: An alternative to material property degradation method for progressive damage in composite structures." Journal of composite materials, Vol. 39, No. 18, 2005, pp. 1659-1675.

60. Tanaka, Fumihiko, et al. "Factors controlling the strength of carbon fibres in tension." Composites Part A: Applied Science and Manufacturing Vol. 57, 2014, pp. 88-94.

61. Marlett, Kristin, Yeow Ng, and John Tomblin. "Hexcel 8552 AS4 Unidirectional Prepreg 190 gsm & 35% RC Qualification Material Property Data Report."National Center for Advanced Materials Performance, Wichita, Kansas. Test Report CAM-RP-2009-015, Rev. A, 2011, pp. 1-278.

62. Sun, X. S., V. B. C. Tan, and T. E. Tay. "Micromechanics-based

progressive failure analysis of fibre-reinforced composites with non-iterative element-failure method." Computers & Structures, Vol. 89, No. 11, 2011, pp. 1103-1116.

63. Abisset, E., F. Daghia, and P. Ladevèze. "On the validation of a damage mesomodel for laminated composites by means of open-hole tensile tests on quasi-isotropic laminates." Composites Part A: Applied Science and Manufacturing, Vol. 42, No. 10, 2011, pp. 1515-1524.

64. Azzi, V. D. and Tsai, S. W. (1965). Anisotropic Strength of Composites, Experimental Mechanics, 5: 283-288.

65. Tsai, S. W. (1965). Strength Characteristics of Composite Materials, NASA Contractor Report, CR-224, National Aeronautics and Space Administration.

66. Tsai, S. W. and Wu, E. M. (1971). A General Theory of Strength for Anisotropic Materials, Journal of Composite Materials, 5: 58-80.

67. Hashin, Z. and Rotem, A. (1973). A Fatigue Failure Criterion for Fiber Reinforced Materials, Journal of Composite Materials, 7: 448-464.

68. Hashin, Z. (1980). Failure Criteria for Unidirectional Fiber Composites, Journal of Applied Mechanics, 47: 329-334.

69. Yamada, S. E. and Sun, C. T. (1978). Analysis of Laminate Strength and Its Distribution, Journal of Composite Materials, 12: 275-284.

70. Chang, F. K., Scott, R. A. and Springer, G. S. (1984). Failure of Composite Laminates Containing Pin Loaded Holes — Method of Solution, Journal of Composite Materials, 18: 255-278.

71. Chang, F. K., Scott, R. A. and Springer, G. S. (1984). Failure Strength of Nonlinearly Elastic Composite Laminates Containing Pin Loaded Holes — Method of Solution, Journal of Composite Materials, 18: 464-477.

72. Chang, F. K. and Chang, K. Y. (1987). A Progressive Damage

Model for Laminated Composites Containing Stress Concentrations, Journal of Composite Materials, 21: 834-855.

73. Hart-Smith, L. J. (1989). A New Approach to Fibrous Composite Laminate Strength Prediction. Eighth DOD/NASA/FAA Conference on Fibrous Composites in Structural Design, NASA CP-3087, Part 2: 663-693.

74. Feng, W. W. (1991). A Failure Criterion for Composite Materials. Journal of Composite Materials, 25: 88-100.

75. Pang, S., Pandian, A. and Bradshaw, R. D. (1992). Modified Tsai-Wu Failure Criterion for Fiber-Reinforced Composite Laminates, Polymer Composites, 13(4): 273-277.

76. Shahid, I. and Chang, F. K. (1993). Failure and Strength of Laminated Composite Plates under Multiple In-Plane Loads, 38th International SAMPE Symposium: 967-977.

77. Shahid, I. and Chang, F. K. (1995). An Accumulative Damage Model for Tensile and Shear Failures of Laminated Composite Plates, Journal of Composite Materials, 29(7): 926-981.

78. Chandler, H. D., Campbell, I. M. D. and Stone, M. A. (1995). An Assessment of Failure Criteria for Fiber Reinforced Composite Laminates. International Journal of Fatigue, 17(7): 513-518.

79 Christensen, R. M. (1997). Stress Based Yield/Failure Criteria for Fiber Composites, International Journal of Solids & Structures, 34(5): 529-543.

80. Deng, S. and Ye, L. (1999). Influence of Fiber-Matrix Adhesion on Mechanical Properties of Graphite/Epoxy Composites: I. Tensile, Flexure, and Fatigue Properties, Journal of Reinforced Plastics and Composites, 18: 1021-1040.

81. Deng, S. and Ye, L. (1999). Influence of Fiber-Matrix Adhesion

on Mechanical Properties of Graphite/Epoxy Composites: II. Interlaminar Fracture and Inplane Shear Behavior, Journal of Reinforced Plastics and Composites, 18: 1041-1057.

82. Deng, S. and Ye, L. (1999). Influence of Fiber-Matrix Adhesion on Mechanical Properties of Graphite/Epoxy Composites: III. Impact and Dynamic Mechanical Properties, Journal of Reinforced Plastics and Composites, 19: 689-703.

83. Kim, K. Y. and Ye, L. (2005). Influence of Matrix and Interface on Transverse Mechanical Properties of CF-PEI Thermoplastic Composites at Elevated Temperatures, Journal of Reinforced Plastics and Composites, 24: 429-445.

84. Hobbiebrunken, T., Hojo, M., Adachi, T., Jong, C. D. and Fiedler, B. (2006). Evaluation of Interfacial Strength in CF/Epoxies Using FEM and In-Situ Experiments, Composites Part A: Applied Science and Manufacturing, 37(12): 2248-2256.

85. Puck, A. and Schürmann, H. (1998). Failure Analysis of FRP Laminates by Means of Physically Based Phenomenological Models, Composites Science and Technology, 58(7):1045-1067.

86. Puck, A. and Schürmann H. (2002). Failure Analysis of FRP Laminates by Means of Physically Based Phenomenological Models, Composites Science and Technology, 62(12-13):1633-1662.3-30 S. K. Ha, K. K. Jin and Y. Huang

87. Mayes, J. S. (1999). Micromechanics Based Failure Analysis of Composite Structural Laminates, Carderock Division, Naval Surface Warfare Center, Ship Structures and Materials Department, NSWCCD-65-TR-1999/15.

88. Mayes, J. S. and Hansen, A. C. (2004). A Comparison of Multicontinuum Theory Based Failure Simulation with Experimental

Results, Composites Science and Technology, 64 (3-4): 517-527.

89. Chaboche, J.-L. and Carrère, N. (2002). Multiscale Structural Analyses Incorporating Damage Mechanics at the Meso- or Micro-Scales, International Symposium on Anisotropic Behavior of Damaged Materials, ABDM-2002, Poland, September 9-22.

90. Laurin, F., Carrère, N. and Maire, J.-F. (2007). A Multiscale Progressive Failure Approach for Composite Laminates Based on Thermodynamical Viscoelastic and Damage Models, Composites Part A: Applied Science and Manufacturing, 38(1): 198-209

91. Hinton, M. J. and Soden, P. D. (1998). Predicting Failure in Composite Laminates: the Background to the Exercise, Composites Science and Technology, 58(7): 1001-1010.

92. Soden, P. D., Hinton, M. J. and Kaddour, A. S. (1998). Lamina Properties, Lay-Up Configurations and Loading Conditions for a Range of Fiber-Reinforced Composite Laminates, Composites Science and Technology, 58(7): 1011-1022.

93. Soden, P. D., Hinton, M. J. and Kaddour, A. S. (1998). A Comparison of the Predictive Capabilities of Current Failure Theories for Composite Laminates, Composites Science and Technology, 58(7): 1225-1254.

94. Hinton, M. J., Kaddour, A. S. and Soden, P. D. (2002). Evaluation of Failure Prediction in Composite Laminates: Background to _Part B ' of the Exercise, Composites Science and Technology, 62(12-13): 1481-1488.

95. Soden, P. D., Hinton, M. J. and Kaddour, A. S. (2002). Biaxial Test Results for Strength and Deformation of a Range of E-Glass and Carbon Fiber Reinforced Composite Laminates: Failure Exercise Benchmark Data, Composites Science and Technology, 62(12-13): 1489-1514.

96. Hinton, M. J., Kaddour, A. S. and Soden, P. D. (2002). A Comparison of the Predictive Capabilities of Current Failure Theories for Composite Laminates, Judged against Experimental Evidence, Composites Science and Technology, 62(12-13): 1725-1797.

97. Hinton, M. J., Kaddour, A. S. and Soden, P. D. (2004). Evaluation of Failure Prediction in Composite Laminates: Background to _Part C ' of the Exercise, Composites Science and Technology, 64(3-4): 321-327

98. Kaddour, A. S., Hinton, M. J. and Soden, P. D. (2004). A Comparison of the Predictive Capabilities of Current Failure Theories for Composite Laminates, Composites Science and Technology, 64(3-4): 449-476.

99. Hinton, M. J., Kaddour, A. S. and Soden, P. D. (2004). A Further Assessment of the Predictive Capabilities of Current Failure Theories for Composite Laminates: Comparison with Experimental Evidence, Composites Science and Technology, 64(3-4): 549-588.

99 Soden, P. D., Kaddour, A. S. and Hinton, M. J. (2004). Recommendations for Designers and Researchers Resulting from the World-Wide Failure Exercise, Composites Science and Technology, 64(3-4): 589-604.

100. Miyano, Y., Nakata, M. and Sekine, N. (2005). Accelerated Testing for Long-Term Durability of FRP Laminates for Marine Use, Journal of Composite Materials, 39: 5-20.

101. Altenbach, H.and Tushtev K. (2001). A New Static Failure Criterion for Isotropic Polymers, Mechanics of Composite Materials, 37(5-6): 475-482.

102. Bowden, P. B. and Jukes, J. A. (1972) The Plastic Flow of Isotropic Polymers, Journal of Material Science, 7: 52-63.

103. Raghava, R. S., Caddell, R. M. and Yeh, G. S. Y. (1973). The

Macroscopic Yield Behavior of Polymers, Journal of Material Science, 8: 225-232.

104. Bauwens, J. C. (1970). Yield Condition and Propagation of Lüders ' Lines in Tension-Torsion Experiments on Poly(Vinyl Chloride), Journal of Polymer Science Part A-2: Polymer Physics, 8(6): 893-901.

105. Camanho, P.P., C.G. Davila, and D.R. Ambur (2001), Numerical Simulation of Delamination Growth in Composite Materials. NASA-TP-211041.

106. Defining the Constitutive Response of Cohesive Elements Using a Traction-Separation Description, Abaqus Analysis User's Manual, Abaqus Version 6.7.

107. Totry, E., González, C. and LLorca, J. (2008). Failure Locus of Fiber-Reinforced Composites under Transverse Compression and Out-of-Plane Shear, Composites Science and Technology, 68(3-4): 829-839.

108. Cuntze, R. G. and Freund, A. (2004). The Predictive Capability of Failure Mode Concept-Based Strength Criteria for Multidirectional Laminates, Composites Science and Technology, 64(3-4): 343-377.

Appendix A

Pre/Post Processor, DIAMOND/IPSAP

Based on the efficient solution algorithm of IPSAP, DIAMOND/IPSAP program is now being developed for pre/post processing and analysis in the Graphic User Interface (GUI). The goal of DIAMOND/IPSAP makes it possible that user can follow the geometry and mesh generation procedure of his structure design faster, more easily and more funny. As a development environment of DIAMOND/IPSAP, OpenGL-based open source program, Open CASCADE is implemented based on Microsoft Visual Studio 2008 and by using Ribbon Pack of Microsoft, the feature of DIAMOND/IPSAP became more brilliant like the name of program. Preprocessing functions to make geometry and mesh has being continuously developed.

A.1 System Configuration

DIAMOND/IPSAP is developed in the base on OOP (Object Oriented Programming) for efficiently maintaining this software and adding the functions. In this section the graphical systems of the object-oriented DIAMOND/IPSAP is described. The user interfaces are implemented using MFC library. The components such as geometries, meshes and load are visualized using the Open CASCADE, including components for 3D surface and solid modeling,

visualization, data exchange and rapid application development.

Open CASCADE Technology is software development platform freely available in open source. It includes components for 3D surface and solid modeling, visualization, data exchange and rapid application development as shown in Table A.1. It can be applied in development of numerical simulation software including CAD/CAM/CAE applications.

The technology has many advantages. Access to high-quality code provides extra stability and robustness for Open CASCADE based solutions and applications. This code can be freely adapted, modified and enriched by necessary function according to particular needs. There is no limitation as to the number of installed copies, meaning greatly reduced cost. Absence of license fees reduces costs of evaluation period, prototyping and piloting projects. A large community of users and customers are constantly testing the software. The increasing quality and robustness of software is ensured by the Initial developer. Open CASCADE provides wide data exchange possibilities, both through neutral formats and directly with CAD systems. This enables an open, long-term viability of the solution based thereupon.

A2 Pre/Post Process Interface

Pre/Post processor for setting PFA was implemented in DIAMOND/IPSAP GUI. It includes auto mesh generation by parametric modelling. The preprocessor have functions for

generating material properties and exporting functions for solvers. Finally, obtained results can be imported in the DIAMOND module. Then their failure index distribution can be confirmed. Figure A.1 is buttons of PFA module. Unit cell model generator contains function to generate RVE model of square and hexagonal array. Generate coupon is the function to generate virtual coupon to test strength and modulus of composite materials.

Table A.1 Object Libraries provided in Open CASCADE

Foundation Classes	Modelling Data	Modelling Algorithms	Visualization	Data Exchange	Application Framework
Kernel Classes Math Utilities	2D Geometry 3D Geometry Geometry Utilities Topology	Construction of Primitives Boolean Operations Fillets and Chamfers Offsets, Drafts Sewing and Sweeps Features Hidden line Removal Geometric Tools Topological Tools	Services Common to 2D and 3D 2D Visualization 3D Visualization	IGES STEP AP203 AP214 Extended data	Data Framework Data Storage Application Desktop

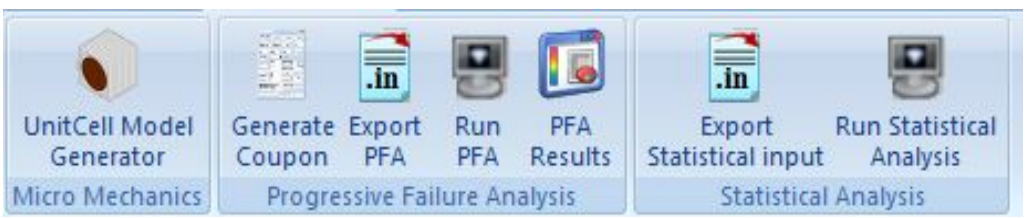

Figure A.1 PFA module interface

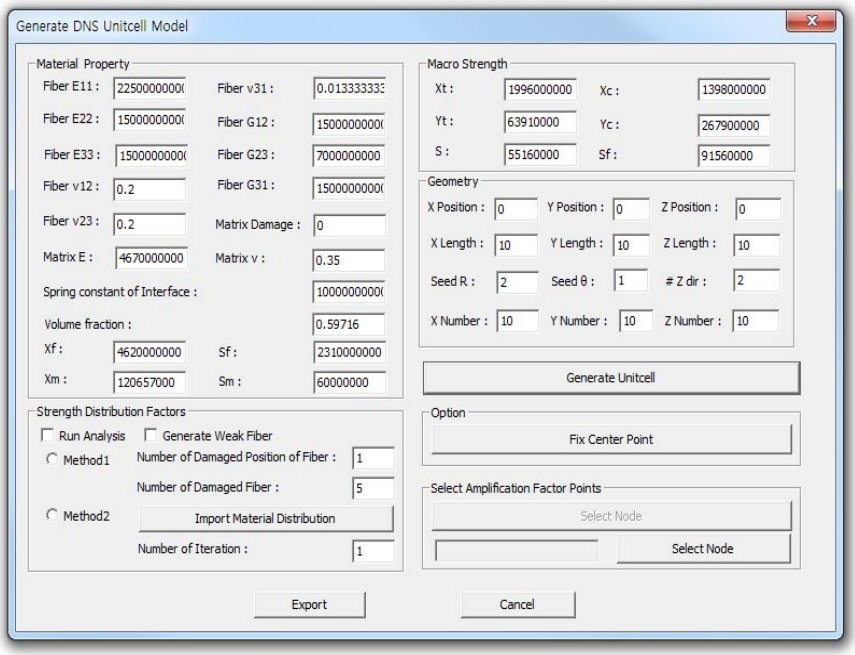

Figure A.2 Unit cell model generator interface

Interface of unit cell generator is described in the Figure A.2. It required inserting constituent properties, namely, fiber and matrix properties. If macro-scale strength exists, it will calculate micro mechanics modification (MMM) to fix micro-scale fiber and matrix failure strength. If method 1 or 2 is chosen, then random fiber strength distribution based on fiber bundle model and their coefficient of variation will be obtained. It can be used as micro-scale model to construct degradation factor.

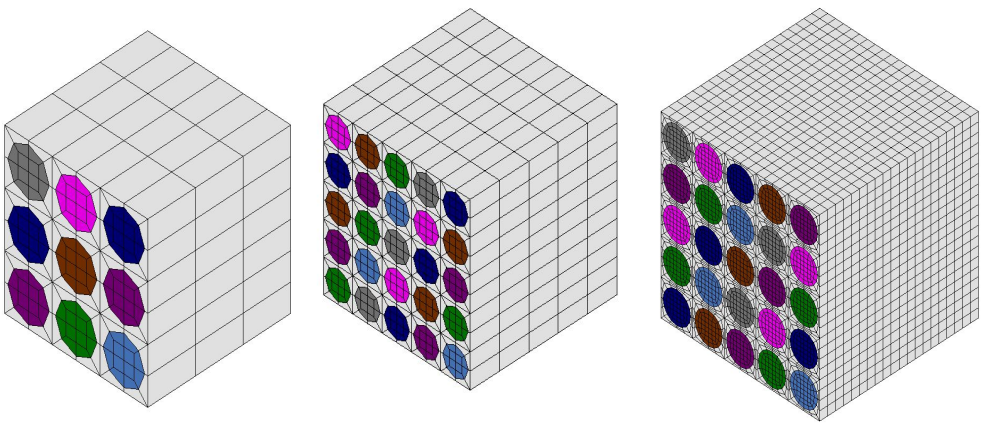

(a) 3X3, coarse mesh (b) 5X5, coarse mesh (c) 5x5, fine mesh
Figure A.3 RVE models according to different number of cluster and mesh density

A3 Coupon Generator

Coupon generator is composed of geometry generator and property generator as Figure A4 and Figure A5. In the geometry generator, unnotched and open-hole virtual coupon can be generated with different size of rectangular and the hole located in the center. Default size is based on ASTM. After giving fixed boundary conditions, displacement step should be chosen. If the step is too large, then it will be not converged. Nonlinear factors are located in geometry dialog, not material properties dialog, because all parameters are dimensionless variables. Nonlinear elasticity, shear nonlinearity and degradation model can be determined using the dialog. Linear material properties for lamina can be determined

using material property dialog. If constituent properties are known, it also can be as input variables, then ply properties is obtained by rule of mixture.

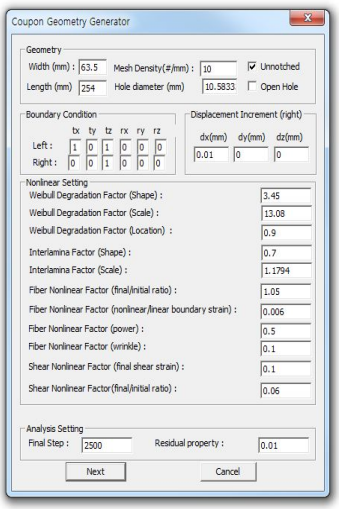

Figure A.4 Coupon geometry dialog

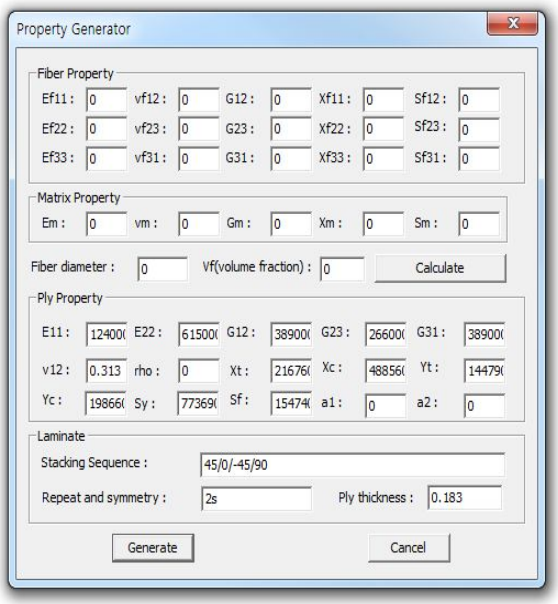

Figure A.5 Material property generator

Appendix B

Progressive Failure Analysis Solver Types

Six kinds of solvers are proposed in this paper, and MSC. Nastran solver also is used to compare with the developed solvers. The solvers are classified in terms of nonlinearity, degradation method, multi-scale method and failure criteria. SOL-A1 is Nastran solver which has linear material, gradual selective stiffness degradation method and Hashin failure criterion. SOL-A2 is the solver which is considering nonlinear elasticity only. SOL-B1~B3 is macro-scale approaches using non-cumulative continuum damage model which is referred in chapter 2. Difference between SOL-B1 and SOL-B2 is whether includes nonlinear elasticity or not. SOL-B3 is considering fiber bundle based degradation model, while it uses Hashin failure criteria which requires macro-scale strength. SOL-C groups don't require macro scale properties. SOL-C1 is the solver includes continuum damage mechanics model referred in chapter 2, while SOL-C2 is constructed considering fiber bundle model as referred in chapter 3.

Each solver's procedure and characteristics are described in Figure B1~B7.

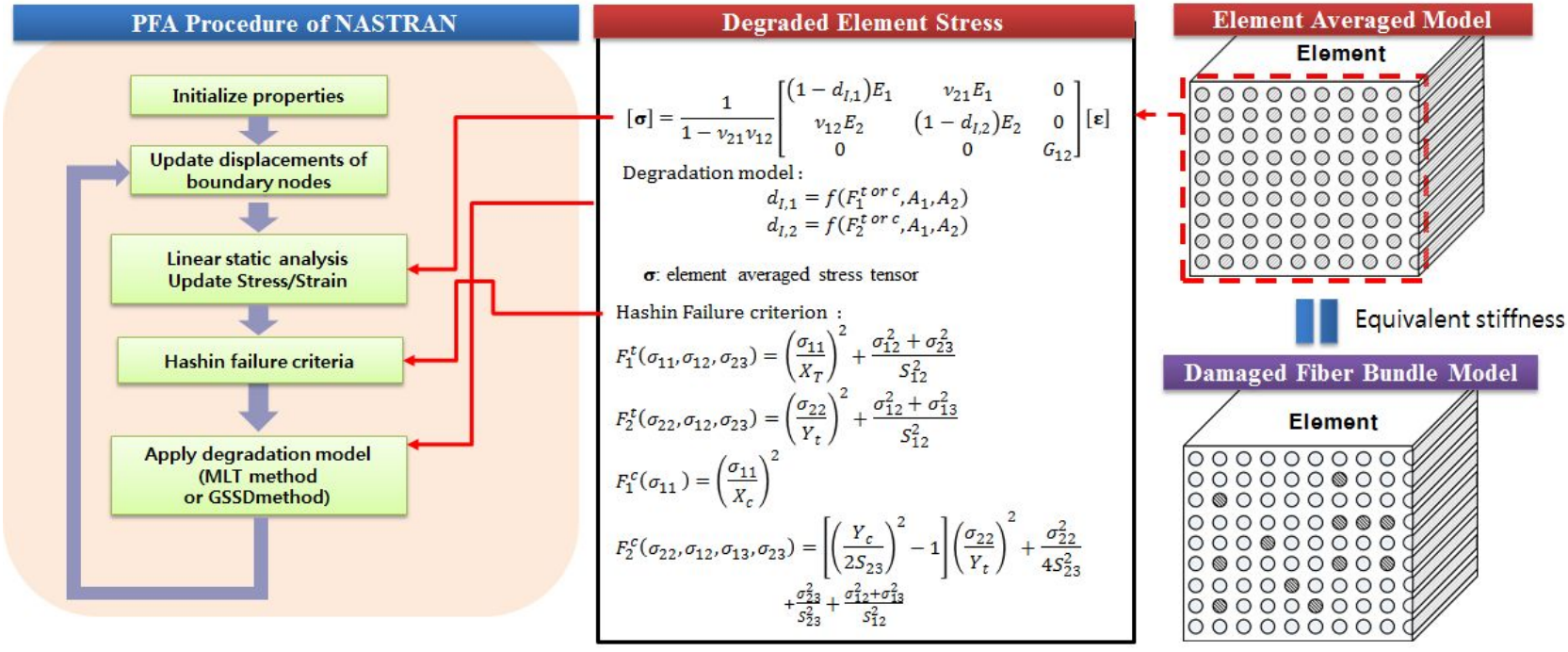

Figure B1 Linear Fiber Modulus, Hashin Failure Criteria, GSSD method (NASTRAN)

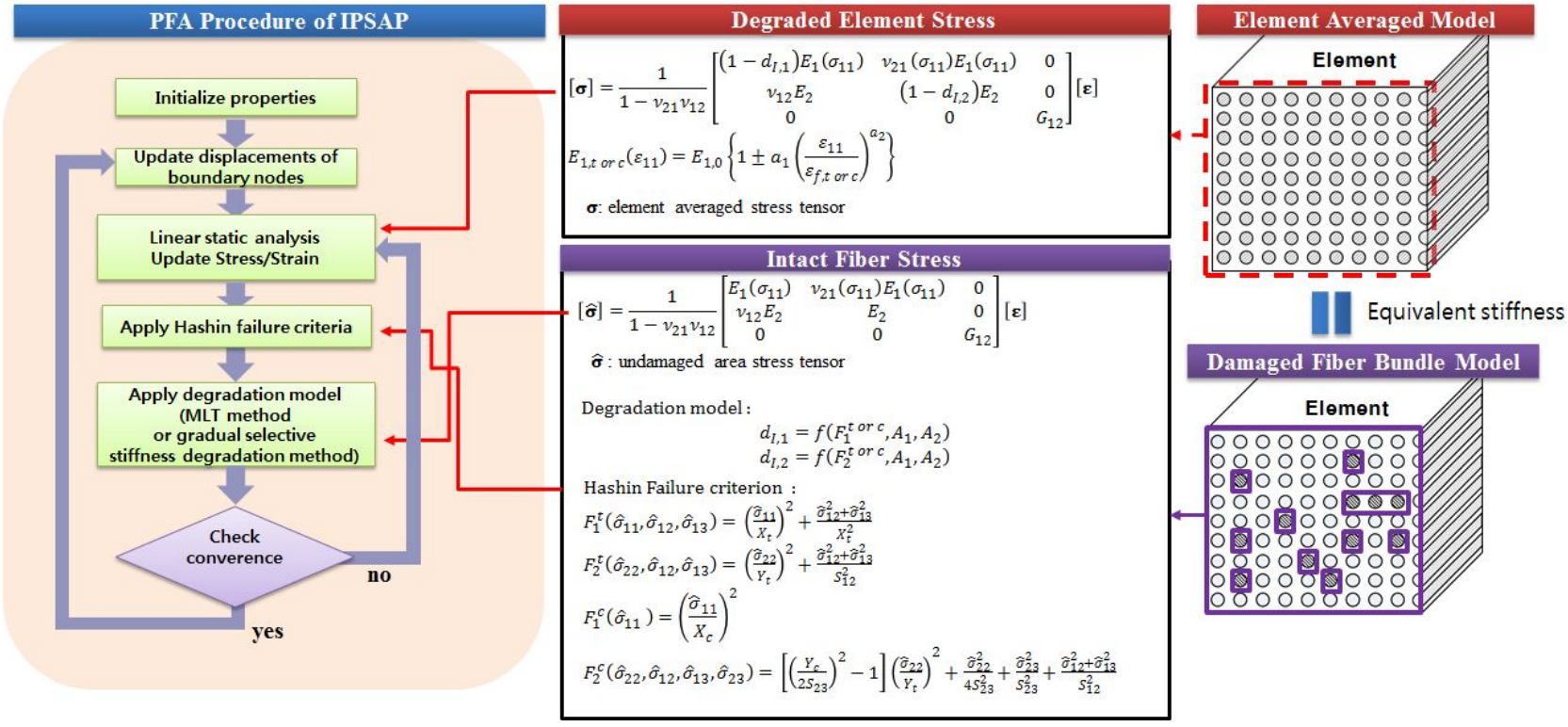

Figure B2 Nonlinear Fiber Modulus, Hashin Failure Criteria, MLT method (IPSAP)

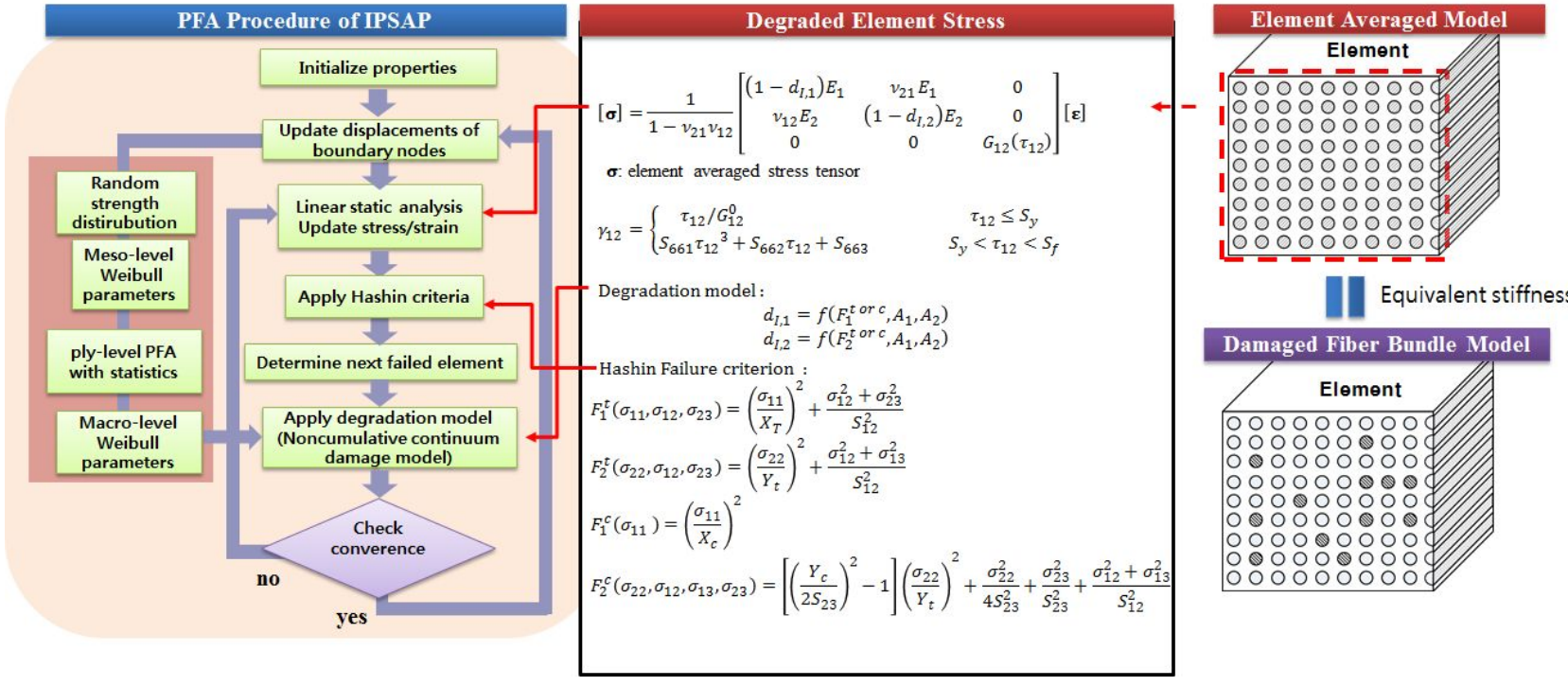

Figure B3 Linear Fiber Modulus, Hashin Criteria, and Degradation from lamina tests (IPSAP)

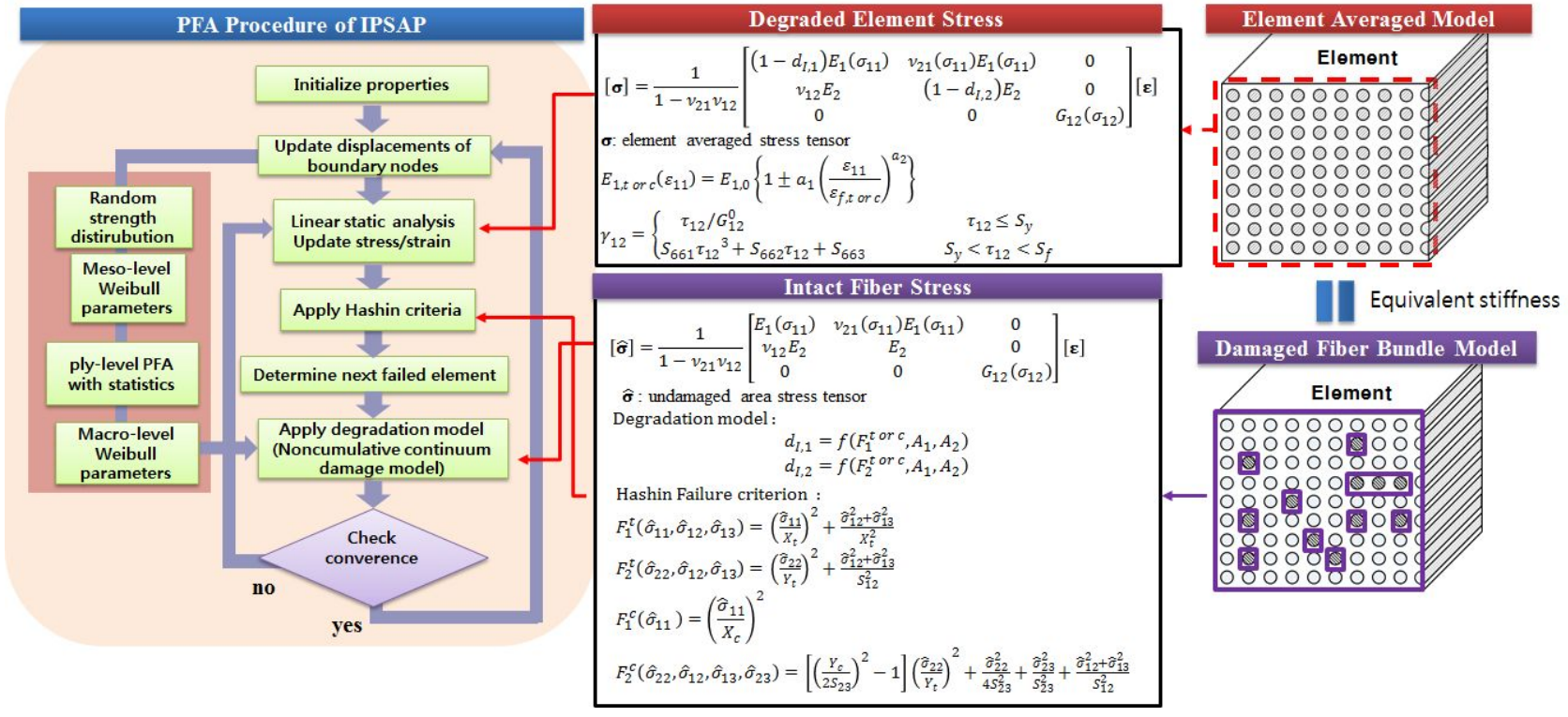

Figure B4 Nonlinear Fiber Modulus, Hashin Criteria, and Degradation from lamina tests (IPSAP)

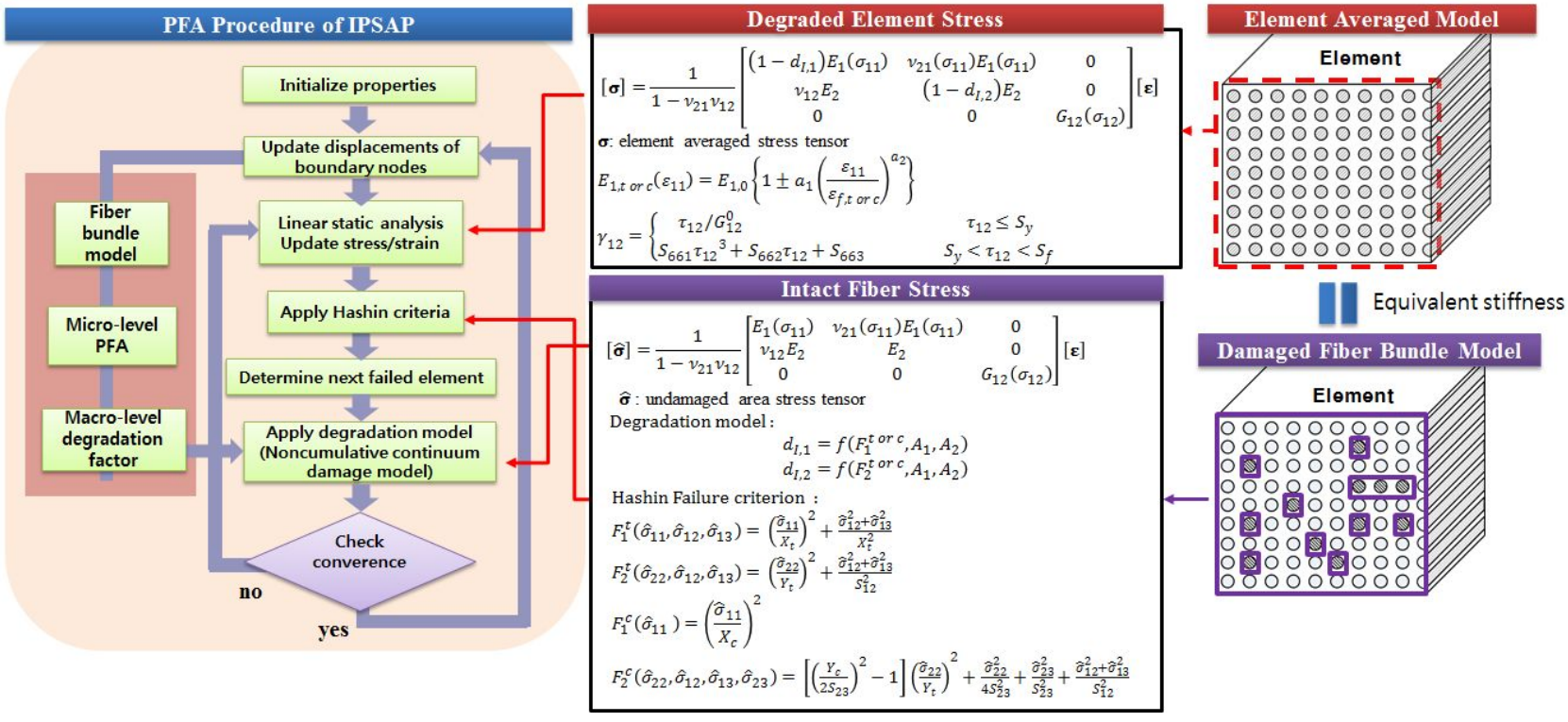

Figure B5 Nonlinear Fiber modulus, Hashin Failure Criteria, Degradation from fiber bundle (IPSAP)

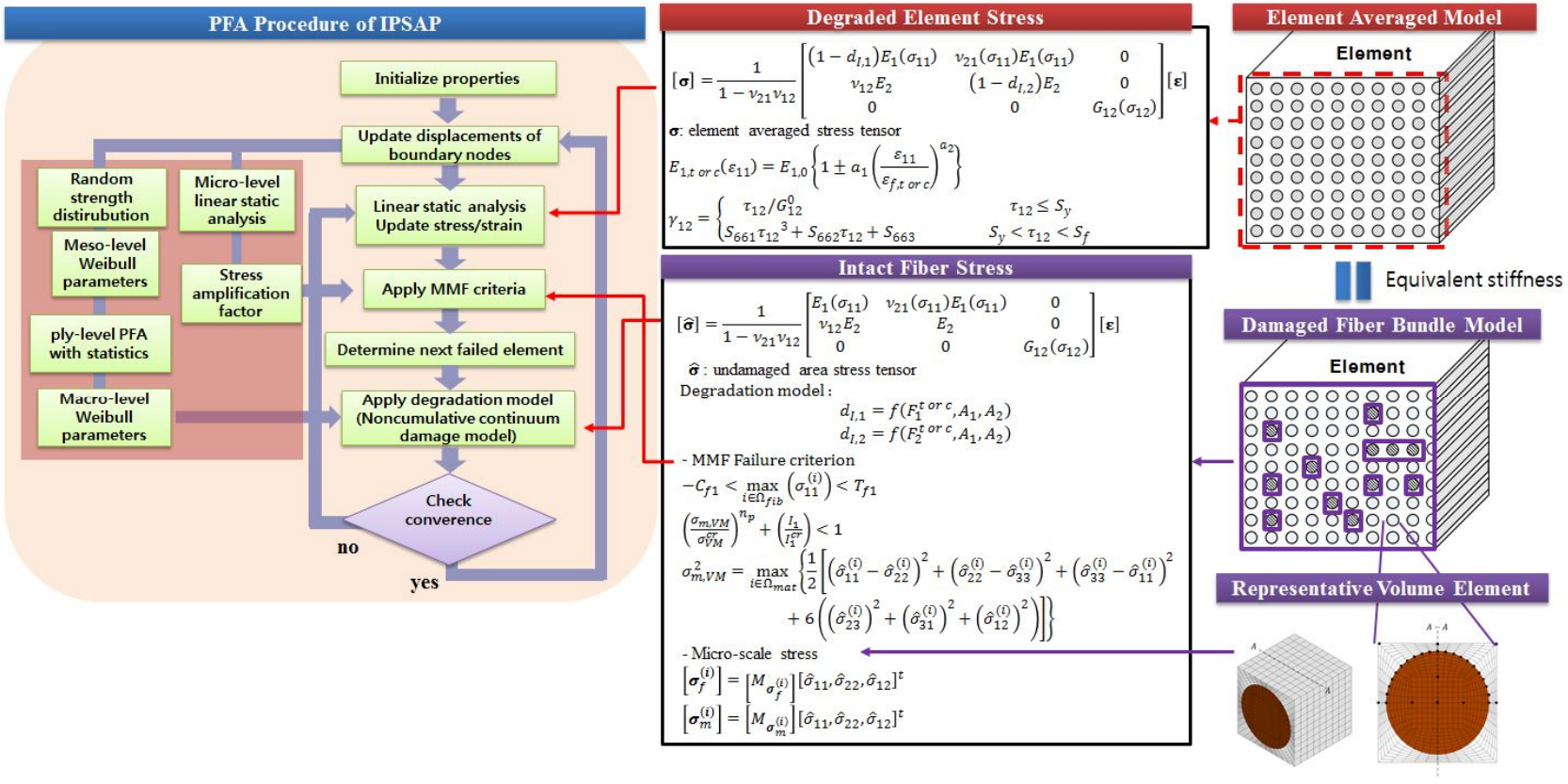

Figure B6 Nonlinear Fiber modulus, MMF Criteria, Degradation from lamina tests (IPSAP)

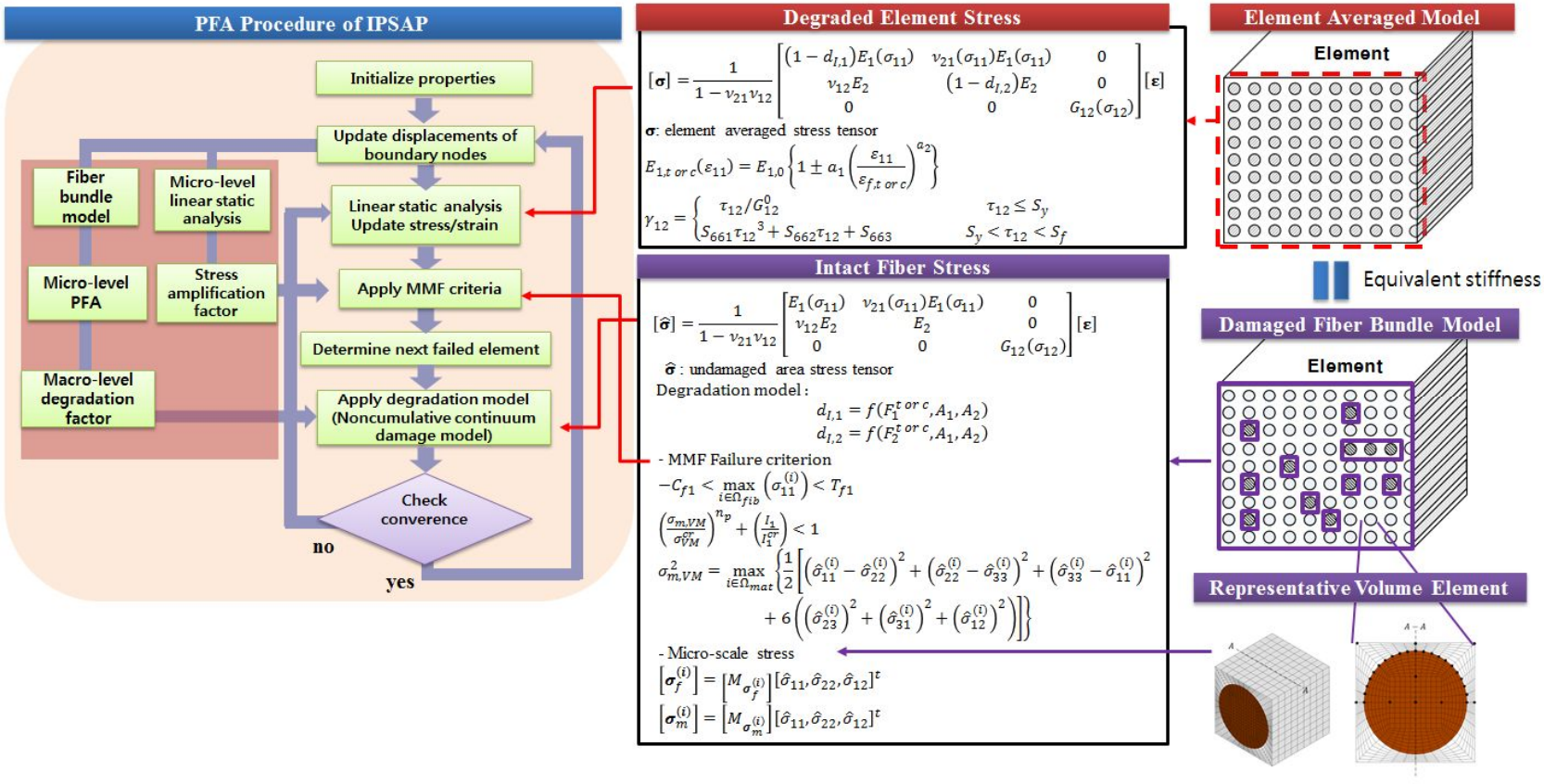

Figure B7 Nonlinear Fiber modulus, MMF Criteria, Degradation from fiber bundle (IPSAP)

국문초록

본 연구에서는 복합재료 적층판의 강도를 보다 정확하게 예측하기 위해 연속체 손상역학을 적용한 멀티 스케일의 점진적 파손해석 기법에 대한 연구를 수행하였다. 비 누적식 연속체 손상역학 식을 Weibull 분포를 기반으로 개발하여, 점진적 파손해석을 모사할 수 있는 강성 저하 파라미터들을 개발하였다. 이 파라미터들은 Tsai-Wu, Hashin 및 미시역학파손(Micro Mechanics of Failure,MMF) 기준에 의해 정의될 수 있도록 응력기반의 식으로 구성되었다. 강성 저하 파라미터들은 섬유강화 복합재료 라미나의 점진적 파손에 대한 통계 해석 결과를 통하여 유도되었다. 손상 모델은 비선형 전단 모델과 결합하여 비선형 해석 절차로 구성되었고, Newton-Raphson 방법으로 솔버가 구성되었다. 새로 제안된 연속체 손상역학 방법을 기존의 점진적 강성 선택 저하(Gradual Selective Stiffness Degradation) 기법과 비교하여 차이를 비교하였다.

또한, 개발된 연속체 손상역학 모델은 미시역학파손 모델과 결합되어 손상의 시작뿐만 아니라 전개에서 미시역학 모델을 고려할 수 있게 하였다. 손상의 시작에 대한 판별은 응력 기반의 미시역학파손 모델을 사용하였으며, 손상 이후의 거동을 모사하기 위해 강성 저하가 고려된 요소 평균응력텐서와 온전한 섬유의 응력텐서를 구분하여 정식화 하였다. 이를 통해 미시역학파손 모델에서 사용되는 응력증폭계수를 초기 파손 이후에도 사용할 수 있게 하여 멀티스케일 해석의 효율성을 증진시켰다. 기존의 대표체적요소로 사용되는 단위 셀 모델을 확장하여 섬유 다발모델에 대한 미시역학 모델을 구성하였다. 이에 대한 미시영역의 파손해석을 수행하여 파단까지의 물성 패턴을 통계적으로 해석하여 대푯값을 추출, 앞서 개발된 강성 저하 파라미터를 결정하는데 사용하였다. 단일 섬유에 대한 시험자료와 섬유 결함 정보를 결합하여 섬유 다발 모델을 구

성하여 Weibull 계수를 유도 하였다. 개발된 점진적 파손해석 모듈은 노치가 없는 시편과 원공이 있는 시편들에 대해 검증되었다. 국내외 복합재료 표준 시험 기관에서 제공하는 재료의 강도와 비교하여 검증을 수행하였다. 3가지 다른 재료 물성에 대해 저온 건조 조건, 올린 온도의 습한 조건 및 상온 건조 조건에서의 3가지 적층 구성에 대한 점진적 파손해석을 수행하였으며, 상용 프로그램 및 시험 결과 값들과 비교・검증하였다.

주요어 : 점진적 파손해석, 연속체 손상역학, 미시역학파손,
멀티스케일 해석, 적층 복합재료
학 번 : 2009-20679